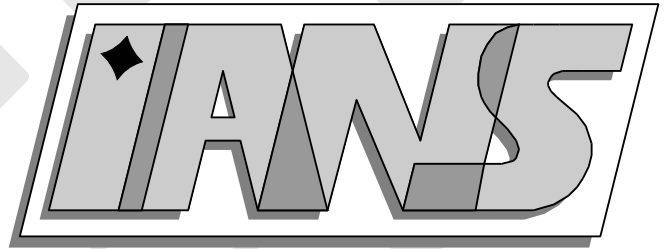


**Universität
Stuttgart**



**Overlapping domain decomposition for multiscale
dynamic contact problems**

Corinna Hager, Patrice Hauret, Patrick Le Tallec, Barbara I. Wohlmuth

**Berichte aus dem Institut für
Angewandte Analysis und Numerische Simulation**

Universität Stuttgart

Overlapping domain decomposition for multiscale
dynamic contact problems

Corinna Hager, Patrice Hauret, Patrick Le Tallec, Barbara I. Wohlmuth

**Berichte aus dem Institut für
Angewandte Analysis und Numerische Simulation**

Preprint 2010/007

Institut für Angewandte Analysis und Numerische Simulation (IANS)
Fakultät Mathematik und Physik
Fachbereich Mathematik
Pfaffenwaldring 57
D-70 569 Stuttgart

E-Mail: ians-preprints@mathematik.uni-stuttgart.de

WWW: <http://preprints.ians.uni-stuttgart.de>

ISSN **1611-4176**

© Alle Rechte vorbehalten. Nachdruck nur mit Genehmigung des Autors.
IANS-Logo: Andreas Klimke. \LaTeX -Style: Winfried Geis, Thomas Merkle.

OVERLAPPING DOMAIN DECOMPOSITION FOR MULTISCALE DYNAMIC CONTACT PROBLEMS

C. HAGER, P. HAURET, P. LE TALLEC, B. I. WOHLMUTH

Abstract. Frictional dynamic contact problems with complex geometries are a challenging task – from the computational as well as from the analytical point of view. A characteristic example of such problems is the simulation of rolling car tires. Within this setting, the additional difficulty occurs that the fine structure of the tire profile has to be resolved accurately enough near the actual contact zone. This is necessary to get a good picture of the evolution of the contact stresses and the temperature during rolling contact.

To be able to reduce the complexity of this kind of contact problem, we employ a non-conforming domain decomposition method in space. This leads to several benefits: Firstly, we are able to resolve details of the surface by a fine mesh and compute the contact conditions only where it is needed. Secondly, the decoupled subproblems can be solved independently of each other which enables us to choose a much finer time scale on the contact zone than on the coarse domain. Hence, a more detailed resolution of the evolution of the contact stress can be achieved. Among other things, we show that the resulting iterative solution scheme is robust with respect to jumps in the material parameters; furthermore, it can be extended to the case of nearly incompressible material by using a stable discretization.

On the fine-meshed subdomain, a frictional contact problem remains to be solved which can very efficiently be done by means of a primal-dual active set strategy. This scheme can be interpreted as a semismooth Newton method applied to a set of nonlinear equations, and the overlapping domain decomposition directly implies an iterative way of solving the resulting tangential problems inexactly. Combined with appropriate stopping criteria for this inner iteration, we obtain a robust and efficient algorithm as can be seen by our numerical examples containing complex three-dimensional geometries, contact and non-linear material laws.

1. Introduction. The numerical simulation of dynamic contact problems plays an important role in many applications in mechanics, like the forming of sheet metal or the rolling of a car tire. Especially the latter application is a challenging task from the point of view of simulation, as the problem usually features a complex threedimensional geometry, incompressible nonlinear elastic materials as well as dynamic effects. In addition, the contact zone is usually quite small compared to the size of the tire but needs to be resolved very accurately to get a good picture of the evolution of the contact stresses and the temperature during rolling contact. This is necessary in order to get information about characteristics such as grip, wear, optimal speed etc. Hence, a fine triangulation is needed near the contact area; but discretizing the whole tire with such fine grid yields a huge system that cannot be treated with today's computer architecture.

In order to be able to perform an accurate simulation of a car tire, there is a huge demand of a sound numerical scheme that combines a suitable multi-scale discretization for the geometry with an efficient solution algorithm for the material nonlinearities and the dynamic contact. Further, the algorithm has to be robust with respect to jumps in the material parameters as well as to be able to deal with nearly incompressible materials. The aim of this work is to design such an algorithm by combining several well-established mathematical methods which are described in the following.

The basic idea of the work is to employ a decomposition of the original structure into several overlapping subdomains which have different grid spacing. The whole d -dimensional structure, with $d \in \{2, 3\}$, is discretized with a relatively coarse mesh that does not resolve the details along the contact boundary, whereas at the contact area, an overlapping patch with a fine triangulation is introduced. An example of such geometry is sketched in Figure 1.1. In order to avoid expensive volume coupling, the transfer between the subdomains is only performed at the inner $(d - 1)$ -dimensional interface. Here, we employ the variationally consistent mortar method (see, e.g., [2, 3]) with dual Lagrange multipliers [58] to enforce the weak continuity of the traces.

The subject of domain decomposition methods is already well-established in the literature; we refer to [44, 51, 55, 56] and the references therein for an overview of the topic. Further, the construction of domain decomposition schemes which are robust with respect to the mesh size as well as jumps in the material parameters has been the topic of several works in the literature (e.g., [4, 26, 43]). In this work, we will make use of the overlapping decomposition in order to obtain an iterative solution scheme whose convergence rate is bounded independently of the mesh size or different material parameters in the subdomains.

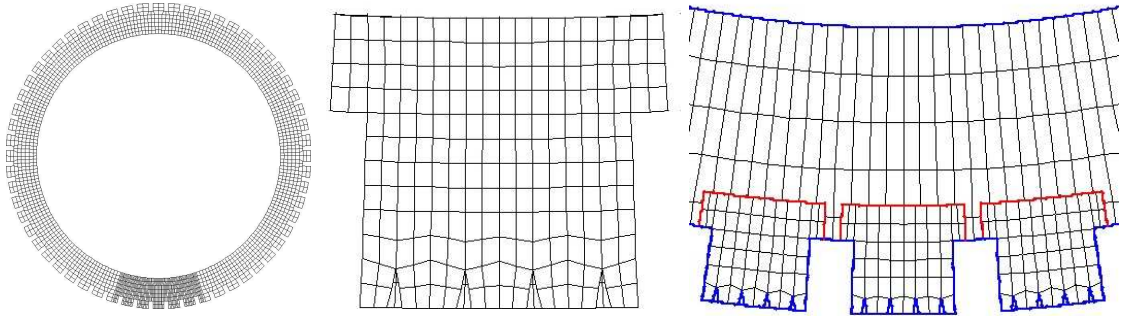


FIGURE 1.1. Sketch of overlapping domain decomposition; left: coarse domain; middle: fine patch resolving the details at the boundary; right: combined geometry with coupling interface.

The next important item is the treatment of the contact inequality constraints (see [20, 42, 47, 57, 60] and the references therein for an overview of the topic). Again, these conditions are enforced in a weak sense using dual Lagrange multipliers. The biorthogonality of the corresponding basis functions leads to the advantage that the consistent segment-to-segment coupling reduces to the structure of a node-to-segment formulation. Hence, the contact constraints can be enforced nodewise, allowing for the application of the primal-dual active set strategy [34, 35, 37]. This scheme can be interpreted as a semismooth Newton method [34] applied to a set of nonlinear equations describing the constitutive equations as well as the contact conditions [1, 16]. Hence, in each Newton step, a linear system has to be solved for the update of the displacements, which can efficiently be done by the iterative subdomain coupling described before. In combination with appropriate stopping criteria for this inner linear iteration (see, e.g., [17, 18, 22]), the superlinear local convergence of the outer Newton method can be conserved.

The incorporation of inertia effects into the formulation makes the simulation of the contact problem even more challenging. Here, we have to take care of the conservation of mechanical energy on the one hand, and of the stability with respect to the impact on the other hand [32, 48, 15]. For this, a local modification of the mass matrix along the potential contact boundary can be employed [28, 29, 41].

Finally, the rubber material of a car tire usually shows an almost incompressible behaviour. The numerical simulation of such materials using lowest order conforming finite elements usually leads to volume locking (see, e.g., [5, 6, 14]). Hence, different discretizations are necessary, e.g., by introducing an additional variable for either the stress or the pressure [8, 9, 39, 40, 52]. In this work, we will employ a generalized Hu–Washizu formulation [14, 46] in order to obtain robustness of the iterative algorithm also for the case of nearly incompressible materials.

Having introduced the main building blocks of our iterative algorithm which is able to tackle the challenging problem of simulating the dynamic contact of a car tire, we turn to the structure of the rest of this work. It is divided into two parts.

Part I is concerned with the case of compressible linear elastic problems and starts with introducing the notation, the governing equations and the fully coupled mortar system in Section 2. Section 3 describes the approximate iterative solution scheme based on overlapping domain decomposition that is used to solve the coupled system efficiently, followed by the analysis of the convergence rate of the iterative method. Section 4 contains several numerical tests for linear elastic problems, confirming the theoretical results. Afterwards, in Section 5, a similar iterative scheme with different coupling conditions at the interface is presented and its convergence behaviour is investigated both theoretically and numerically.

Part II contains the extension of the techniques of the first part to the nonlinear and incompressible case. In Section 6, the subdomain iteration presented in the third section is combined

with a semismooth Newton iteration, which can for example lead to an inexact Newton method. Further, the inequality constraints of frictional contact and their reformulation in terms of a non-linear complementarity function is treated. Section 8 contains several numerical examples in two and three space dimensions with nonconforming geometry at the contact interfaces, illustrating the efficiency and the robustness of the resulting iterative scheme. Finally, in Section 9, it is theoretically and numerically shown that the algorithm can be extended to the case of nearly incompressible material by employing a stable mixed discretization.

Part I - Linear compressible case

2. Setting and problem formulation. This section contains the problem formulation as well as the basic notation for the rest of this part. In Subsection 2.1, the governing equations for the linear problem are stated in their strong and weak form, whereas Subsection 2.2 introduces the spatial discretization, including some properties of trace spaces and mortar operators which will be used in the sequel. The time discretization is sketched in Subsection 2.3, followed by the algebraic Schur complement formulation presented in Subsection 2.4.

2.1. Problem statement. In the following, we consider an elastic body $\Omega \subset \mathbb{R}^d$, where $d \in \{2, 3\}$ denote the number of spatial dimensions. The polyhedral boundary $\partial\Omega$ is partitioned into two nonoverlapping parts Γ_D, Γ_N with $\text{meas}(\Gamma_D) > 0$. On Γ_D , we assume homogeneous Dirichlet boundary conditions for simplicity, whereas a surface load denoted by \mathbf{g}_N acts on the boundary Γ_N where the unit outer normal \mathbf{n} is defined almost everywhere. Then, the strong form of the dynamic linear elasticity problem on Ω subject to the volume load \mathbf{l} reads

$$\begin{aligned} \varrho \ddot{\mathbf{u}} - \text{div } \boldsymbol{\sigma}(\mathbf{u}) &= \mathbf{l}, & \text{in } \Omega, \\ \mathbf{u} &= \mathbf{0}, & \text{on } \Gamma_D, \\ \boldsymbol{\sigma}(\mathbf{u})\mathbf{n} &= \mathbf{g}_N, & \text{on } \Gamma_N. \end{aligned} \tag{2.1}$$

Here, the Cauchy stress $\boldsymbol{\sigma} = \boldsymbol{\sigma}(\mathbf{u})$ is given by $\boldsymbol{\sigma} := \mathbb{C}^{\text{el}}\boldsymbol{\varepsilon}(\mathbf{u})$ with the linearized strain tensor $\boldsymbol{\varepsilon}(\mathbf{u}) := \frac{1}{2}(\nabla\mathbf{u} + \nabla\mathbf{u}^T)$. The Hooke tensor $\mathbb{C}^{\text{el}} = \mathbb{C}^{\text{el}}(\mathbf{x})$ can be defined either in terms of the Lamé parameters λ, μ or with respect to the elasticity module E and the Poisson ratio ν . Further, $\varrho \geq 0$ denotes the density of Ω .

We consider the case that there exists a given subregion $\omega \subset \Omega$, with possibly different material parameters, where a more accurate local resolution is desired. The interface $\partial\omega \cap \Omega$ is denoted by Γ and the domain $\Omega \setminus \bar{\omega}$ by Ξ , as sketched on the left side of Figure 2.1. For simplicity, we assume that $\bar{\Gamma}_D \cap \bar{\Gamma} = \emptyset$.

In the rest of the work, we assume the following boundedness condition of the material parameters on the subdomains Ξ, ω : There exist positive constants c, C independent of E, ν, ϱ as well as constant values $\varrho_\Theta, E_\Theta, \Theta \in \{\Xi, \omega\}$, such that

$$c E_\Theta \|\boldsymbol{\varepsilon}\|^2 \leq \mathbb{C}^{\text{el}}(\mathbf{x})\boldsymbol{\varepsilon} : \boldsymbol{\varepsilon} \leq C E_\Theta \|\boldsymbol{\varepsilon}\|^2, \quad \mathbf{x} \in \Theta, \tag{2.2a}$$

$$c \varrho_\Theta \leq \varrho(\mathbf{x}) \leq C \varrho_\Theta, \quad \mathbf{x} \in \Theta, \tag{2.2b}$$

with (2.2a) holding for all symmetric tensors $\boldsymbol{\varepsilon} \in \mathbb{R}^{d \times d}$. In other words, the material varies only moderately within the subdomains Ξ, ω but can exhibit a large jump along Γ . Furthermore, (2.2a) also implies that the substance is compressible; the case of incompressible material is considered in Section 9.

In order to obtain the variational form of (2.1), we introduce the vector valued function spaces

$$\mathbf{V}(\Theta) := [H^1(\Theta)]^d, \quad \mathbf{V}_0(\Theta) := \{\mathbf{v} \in \mathbf{V}(\Theta) : \mathbf{v}|_{\Gamma_D \cap \partial\Theta} = \mathbf{0}\} \tag{2.3}$$

for $\Theta \in \{\Omega, \Xi, \omega\}$, the abbreviation $\|\cdot\|_{k,\Theta} := \|\cdot\|_{\mathbf{H}^k(\Theta)}$ and the (bi)linear forms

$$m_\Theta(\mathbf{u}, \mathbf{w}) := \int_\Theta \varrho \mathbf{u} \cdot \mathbf{w} \, dx, \tag{2.4a}$$

$$a_\Theta(\mathbf{u}, \mathbf{w}) := \int_\Theta \mathbb{C}^{\text{el}}\boldsymbol{\varepsilon}(\mathbf{u}) : \boldsymbol{\varepsilon}(\mathbf{w}) \, dx, \tag{2.4b}$$

$$f_\Theta(\mathbf{w}) := \int_\Theta \mathbf{l} \cdot \mathbf{w} \, dx + \int_{\Gamma_N \cap \partial\Theta} \mathbf{g}_N \cdot \mathbf{w} \, ds. \tag{2.4c}$$

Further, let $\mathbf{W}_\Gamma := \mathbf{H}^{1/2}(\Gamma)$ be the space of traces on Γ . Then, the weak form of (2.1) can be formulated as two separate problems on the subdomains Ξ, ω , where the continuity of the

displacements at Γ is only enforced weakly by means of a Lagrange multiplier $\zeta_\Gamma \in \mathbf{M}_\Gamma := \mathbf{W}'_\Gamma$. Thus, we obtain the problem: find $(\mathbf{u}|_\Xi, \mathbf{u}|_\omega, \zeta_\Gamma) \in \mathbf{V}_0(\Xi) \times \mathbf{V}_0(\omega) \times \mathbf{M}_\Gamma$ such that for all $t \in (0, T]$

$$\begin{aligned} m_\Xi(\ddot{\mathbf{u}}, \mathbf{w}) + a_\Xi(\mathbf{u}, \mathbf{w}) - \langle \mathbf{w}, \zeta_\Gamma \rangle_\Gamma &= f_\Xi(\mathbf{w}), & \mathbf{w} \in \mathbf{V}_0(\Xi), \\ m_\omega(\ddot{\mathbf{u}}, \mathbf{w}) + a_\omega(\mathbf{u}, \mathbf{w}) + \langle \mathbf{w}, \zeta_\Gamma \rangle_\Gamma &= f_\omega(\mathbf{w}), & \mathbf{w} \in \mathbf{V}_0(\omega), \\ \langle \mathbf{u}|_\omega, \boldsymbol{\mu}_\Gamma \rangle_\Gamma - \langle \mathbf{u}|_\Xi, \boldsymbol{\mu}_\Gamma \rangle_\Gamma &= 0, & \boldsymbol{\mu}_\Gamma \in \mathbf{M}_\Gamma, \end{aligned} \quad (2.5)$$

plus appropriate initial conditions

$$\mathbf{u}|_{t=0} = \mathbf{u}_0, \quad \dot{\mathbf{u}}|_{t=0} = \mathbf{v}_0. \quad (2.6)$$

Above, we have used the duality pairing $\langle \cdot, \cdot \rangle_\Gamma$ on Γ given by $\langle \mathbf{w}, \zeta \rangle_\Gamma = \int_\Gamma \mathbf{w} \cdot \zeta \, ds$. We remark that for the static case, i.e., $\rho = 0$, (2.5) has the structure of a saddle point problem [13], whereas for $\rho > 0$, the continuity conditions (2.5)₃ turn (2.5) into a DAE of index 3 (see [31] for the definition of a DAE and its index). In the latter case, the problem is locally well posed if both initial conditions (2.6) satisfy condition (2.5)₃ [31]. For the static case, we need that the bilinear form $a_\Xi(\cdot, \cdot) + a_\omega(\cdot, \cdot)$ is uniformly coercive for all functions in $\mathbf{V}_0(\Xi) \oplus \mathbf{V}_0(\omega)$ satisfying (2.5)₃ [13, 12]. To verify this, we consider the kernel of (2.4b) for $\Theta \in \{\Xi, \omega\}$, i.e., the space of rigid body modes which is denoted by

$$\mathcal{RB}_\Theta := \{\mathbf{z} \in \mathbf{V}_0(\Theta) : a_\Theta(\mathbf{z}, \mathbf{z}) = 0\}. \quad (2.7)$$

If $\text{meas}(\bar{\Gamma}_D \cap \partial\Theta) > 0$, there are no free rigid body modes on the subdomain Θ and we have $\mathcal{RB}_\Theta = \{\mathbf{0}\}$. For $\text{meas}(\bar{\Gamma}_D \cap \partial\Theta) = 0$, we obtain $\dim(\mathcal{RB}_\Theta) \leq 3$ for $d = 2$ and $\dim(\mathcal{RB}_\Theta) \leq 6$ for $d = 3$. But in this case, the rigid body component on Θ is fixed by the continuity condition (2.5)₃, such that the well-posedness of (2.5) follows from the condition $\text{meas}(\Gamma_D) > 0$ and Korn's inequality.

2.2. Spatial discretization. For the spatial discretization of (2.5), we first triangulate the global domain Ω in terms of a quasi-uniform regular mesh \mathcal{T}^H of simplicial or quadrilateral/ hexahedral elements of size H . We assume that the Dirichlet boundary Γ_D as well as the interface Γ are resolved by this triangulation. On \mathcal{T}^H , we consider lowest order conforming finite element basis functions ϕ_p^H , $p \in \mathcal{N}^H$, with $\mathcal{N}_\Gamma^H \subset \mathcal{N}^H$ denoting the subset of vertices of \mathcal{T}^H on the interface Γ .

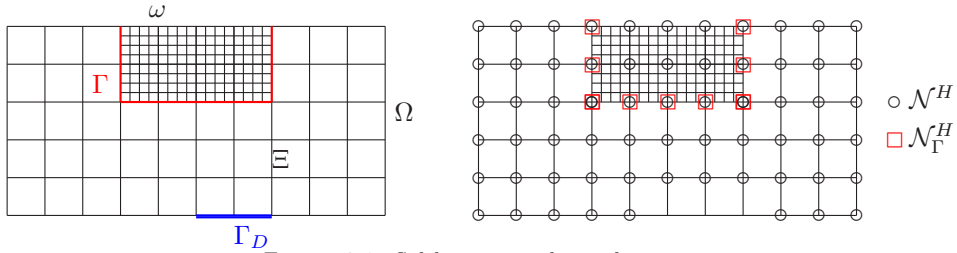


FIGURE 2.1. Subdomains and interfaces

On the patch ω , we introduce a second regular and quasi-uniform discretization \mathcal{T}^h with elements of size $h < H$, the basis functions ϕ_p^h , $p \in \mathcal{N}^h$, and the interface nodes $\mathcal{N}_\Gamma^h \subset \mathcal{N}^h$.

With these triangulations, we can define the following vector valued finite element spaces for the coarse and the fine discretization:

$$\mathbf{V}_\Xi^H := \text{span}\{\phi_p^H|_\Xi\}_{p \in \mathcal{N}^H} \subset \mathbf{V}_0(\Xi), \quad \mathbf{V}_\omega^H := \text{span}\{\phi_p^H|_\omega\}_{p \in \mathcal{N}^H} \subset \mathbf{V}_0(\omega), \quad (2.8a)$$

$$\mathbf{V}^H := \{(\mathbf{v}^H, \mathbf{w}^H) \in \mathbf{V}_\Xi^H \oplus \mathbf{V}_\omega^H : \mathbf{v}^H|_\Gamma = \mathbf{w}^H|_\Gamma\} \subset \mathbf{V}_0(\Omega), \quad (2.8b)$$

$$\mathbf{V}^h = \mathbf{V}_\omega^h := \text{span}\{\phi_p^h\}_{p \in \mathcal{N}^h} \subset \mathbf{V}_0(\omega). \quad (2.8c)$$

where the lower index $_0$ indicating the homogeneous Dirichlet conditions is omitted in (2.8) for ease of notation.

The triangulations \mathcal{T}^m , $m \in \{h, H\}$, induce discretizations \mathcal{G}_Γ^m of the interface Γ , on which we define the trace spaces $\mathbf{W}_\Gamma^m := \mathbf{V}^m|_\Gamma$ spanned by a set of basis functions $\varphi_p^m := \phi_p^m|_\Gamma$, $p \in \mathcal{N}_\Gamma^m$, $m \in \{h, H\}$. With each trace space $\mathbf{W}_\Gamma^m \subset \mathbf{W}_\Gamma$, we associate a Lagrange multiplier space $\mathbf{M}_\Gamma^m \subset \mathbf{M}_\Gamma$ spanned by the basis functions $\{\psi_p^m\}_{p \in \mathcal{N}_\Gamma^m}$. There are several suitable possibilities to define these functions (see [59] and the references therein for more details); in the rest of this work, we are going to use the so-called dual basis functions $\{\psi_p^m\}_{p \in \mathcal{N}_\Gamma^m}$ which are piecewise (bi)linear and satisfy the requirements $\text{supp}(\psi_p^m) = \text{supp}(\varphi_p^m)$ as well as the biorthogonality property

$$\int_\Gamma \psi_p^m \varphi_q^m ds = \delta_{pq} \int_\Gamma \varphi_q^m ds, \quad p, q \in \mathcal{N}_\Gamma^m, \quad m \in \{h, H\}. \quad (2.9)$$

Examples of these dual basis functions for a planar interface Γ and locally uniform triangulations \mathcal{G}_Γ^m are sketched in Figure 2.2.

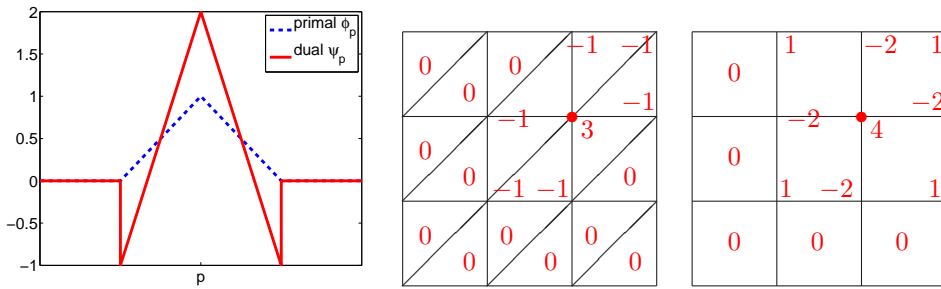


FIGURE 2.2. Example for primal and dual basis functions; left: values of φ_p and ψ_p in 1D; middle: values of ψ_p for triangles in 2D; right: values of ψ_p for quadrilaterals in 2D.

We remark that the above definition of the multiplier spaces yields $\dim(\mathbf{M}_\Gamma^m) = \dim(\mathbf{W}_\Gamma^m)$, i.e., we do not modify the basis functions of \mathbf{M}_Γ^m near the locations where Γ is nondifferentiable. Furthermore, we emphasize that neither the finite element spaces \mathbf{V}_ω^h , \mathbf{V}_ω^H nor the trace spaces \mathbf{W}_Γ^h , \mathbf{W}_Γ^H are assumed to be nested. But even if $\mathbf{W}_\Gamma^H \subset \mathbf{W}_\Gamma^h$ holds, the use of the dual basis functions for the multiplier space yields $\mathbf{M}_\Gamma^H \not\subset \mathbf{M}_\Gamma^h$.

To provide a transfer between the different trace and multiplier spaces on Γ , we introduce the following operators for $l, m \in \{h, H\}$:

$$\begin{aligned} P^{lm} : \mathbf{W}_\Gamma^m &\rightarrow \mathbf{W}_\Gamma^l : \quad \langle P^{lm}(\mathbf{w}_\Gamma^m), \boldsymbol{\mu}_\Gamma^l \rangle_\Gamma = \langle \mathbf{w}_\Gamma^m, \boldsymbol{\mu}_\Gamma^l \rangle_\Gamma, \quad \boldsymbol{\mu}_\Gamma^l \in \mathbf{M}_\Gamma^l, \\ P^{lm*} : \mathbf{M}_\Gamma^m &\rightarrow \mathbf{M}_\Gamma^l : \quad \langle \mathbf{w}_\Gamma^l, P^{lm*}(\boldsymbol{\mu}_\Gamma^m) \rangle_\Gamma = \langle \mathbf{w}_\Gamma^l, \boldsymbol{\mu}_\Gamma^m \rangle_\Gamma, \quad \mathbf{w}_\Gamma^l \in \mathbf{W}_\Gamma^l. \end{aligned} \quad (2.10)$$

The stability properties of the operator P^{lm} defined in (2.10)₁ can be analysed by considering the mortar projection P^l , $l \in \{h, H\}$, with

$$P^l : \mathbf{W}_\Gamma \rightarrow \mathbf{W}_\Gamma^l : \quad \langle P^l(\mathbf{w}_\Gamma), \boldsymbol{\mu}_\Gamma^l \rangle_\Gamma = \langle \mathbf{w}_\Gamma, \boldsymbol{\mu}_\Gamma^l \rangle_\Gamma, \quad \boldsymbol{\mu}_\Gamma^l \in \mathbf{M}_\Gamma^l, \quad (2.11)$$

which satisfies the following

LEMMA 2.1. *The mortar projection P^l , $l \in \{h, H\}$, defined in (2.11) is uniformly continuous with respect to the $\mathbf{L}_2(\Gamma)$ -, the $\mathbf{H}^1(\Gamma)$ - and the $\mathbf{H}^{1/2}(\Gamma)$ -norm.*

Proof. See [59]. \square From Lemma 2.1 and the fact that P^{lm} , $l, m \in \{h, H\}$, is the restriction of P^l to discrete functions in \mathbf{W}_Γ^m , we obtain the $\mathbf{L}_2(\Gamma)$ -, the $\mathbf{H}^{1/2}(\Gamma)$ - and the $\mathbf{H}^1(\Gamma)$ -continuity of P^{lm} with a continuity constant independent of H or h .

Defining the matrices $D_\Gamma^{lm} \in \mathbb{R}^{d|\mathcal{N}_\Gamma^l| \times d|\mathcal{N}_\Gamma^m|}$ which are composed of the $d \times d$ submatrices

$$(D_\Gamma^{lm})_{pq} = \text{Id}_d \cdot \int_\Gamma \psi_p^l \varphi_q^m ds, \quad p \in \mathcal{N}_\Gamma^l, q \in \mathcal{N}_\Gamma^m, \quad (2.12)$$

the algebraic representation of the operators (2.10) can be written as follows:

$$\Pi^{lm} \mathbf{w}_\Gamma^m = (D_\Gamma^l)^{-1} D_\Gamma^{lm} \mathbf{w}_\Gamma^m, \quad (2.13a)$$

$$\Pi^{lm*} \boldsymbol{\mu}_\Gamma^m = (D_\Gamma^l)^{-T} (D_\Gamma^{ml})^T \boldsymbol{\mu}_\Gamma^m. \quad (2.13b)$$

Above and in the following, the discrete functions and the corresponding coefficient vectors are denoted with the same symbol for ease of notation. The extension of the matrices D_Γ^l , $l \in \{h, H\}$, by zero to the vector space \mathbf{V}^h is named $D^{lh} \in \mathbb{R}^{d|\mathcal{N}_\Gamma^l| \times d|\mathcal{N}^h|}$; similarly, the extension of D_Γ^{lH} to the coarse upper space \mathbf{V}_Ξ^H is denoted by D^{lH} .

REMARK 2.2. *Due to the use of the dual basis functions (2.9) for the Lagrange multiplier spaces \mathbf{M}_Γ^l , $l \in \{h, H\}$, the matrices D_Γ^l in (2.12) are diagonal and can easily be inverted.*

In Sections 3 and 5, we will make use of the following assumptions connecting the trace and Lagrange multiplier spaces \mathbf{W}_Γ^m , \mathbf{M}_Γ^m , $m \in \{h, H\}$:

ASSUMPTION 2.3. *There exists a constant $c_p > 0$ independent of h, H such that*

$$\|P^{hH}(\mathbf{w}_\Gamma^H)\|_{l,\Gamma} \geq c_p \|\mathbf{w}_\Gamma^H\|_{l,\Gamma}, \quad \mathbf{w}_\Gamma^H \in \mathbf{W}_\Gamma^H, \quad l \in \left\{0, \frac{1}{2}\right\}. \quad (2.14)$$

ASSUMPTION 2.4. *There exists a constant $c_p^* > 0$ independent of h, H such that for every coarse trace function $\mathbf{w}_\Gamma^H \in \mathbf{W}_\Gamma^H$, there exists a function $\hat{\mathbf{w}}_\Gamma^h \in \mathbf{W}_\Gamma^h$ satisfying*

$$P^{Hh}(\hat{\mathbf{w}}_\Gamma^h) = \mathbf{w}_\Gamma^H \quad \text{and} \quad c_p^* \|\hat{\mathbf{w}}_\Gamma^h\|_{l,\Gamma} \leq \|\mathbf{w}_\Gamma^H\|_{l,\Gamma}, \quad l \in \left\{0, \frac{1}{2}\right\}. \quad (2.15)$$

REMARK 2.5. *Clearly, Assumptions 2.3 and 2.4 can only hold if $\dim(\mathbf{W}_\Gamma^h) \geq \dim(\mathbf{W}_\Gamma^H)$. In the case $\mathbf{W}_\Gamma^H \subseteq \mathbf{W}_\Gamma^h$, both assumptions are trivially satisfied with the constants $c_p = c_p^* = 1$, as P^{hH} is the identity in (2.14) and as the function \mathbf{w}_Γ^H itself can be taken for $\hat{\mathbf{w}}_\Gamma^h$ in (2.15).*

If the trace spaces are not nested, Assumptions 2.3 and 2.4 are not as easy to verify; a possible numerical indicator if they are satisfied is to check whether the matrix

$$Q^{HH} := \Pi^{Hh} \Pi^{hH} \in \mathbb{R}^{d|\mathcal{N}_\Gamma^H| \times d|\mathcal{N}_\Gamma^H|} \quad (2.16)$$

is strictly diagonally dominant with a bound

$$\min_{1 \leq i \leq d|\mathcal{N}_\Gamma^H|} \left(|Q_{ii}^{HH}| - \sum_{j=1, j \neq i}^{d|\mathcal{N}_\Gamma^H|} |Q_{ij}^{HH}| \right) \geq c_0 > 0 \quad (2.17)$$

and c_0 independent of h, H .

From [7, Lemma III.4.2], we obtain that Assumptions 2.3 and 2.4 can be equivalently reformulated as follows:

LEMMA 2.6. (i) *Assumption 2.3 is equivalent to the uniform inf-sup condition of the spaces \mathbf{W}_Γ^H and \mathbf{M}_Γ^h , i.e., there exists a constant $\beta_p > 0$ independent of h, H such that*

$$\inf_{\mathbf{w}_\Gamma^H \in \mathbf{W}_\Gamma^H} \sup_{\boldsymbol{\mu}_\Gamma^h \in \mathbf{M}_\Gamma^h} \frac{\langle \mathbf{w}_\Gamma^H, \boldsymbol{\mu}_\Gamma^h \rangle_\Gamma}{\|\mathbf{w}_\Gamma^H\|_{l,\Gamma} \|\boldsymbol{\mu}_\Gamma^h\|_{-l,\Gamma}} \geq \beta_p, \quad l \in \left\{0, \frac{1}{2}\right\}. \quad (2.18)$$

The constant β_p is related to c_p by the bounds $c_p \beta^h \leq \beta_p \leq c_p$, where β^h is the inf-sup constant of the pairing \mathbf{W}_Γ^h , \mathbf{M}_Γ^h .

(ii) *Assumption 2.4 is equivalent to the uniform inf-sup condition of the spaces \mathbf{M}_Γ^H and \mathbf{W}_Γ^h , i.e., there exists a constant $\beta_p^* > 0$ independent of h, H such that*

$$\inf_{\boldsymbol{\mu}_\Gamma^H \in \mathbf{M}_\Gamma^H} \sup_{\mathbf{w}_\Gamma^h \in \mathbf{W}_\Gamma^h} \frac{\langle \mathbf{w}_\Gamma^h, \boldsymbol{\mu}_\Gamma^H \rangle_\Gamma}{\|\mathbf{w}_\Gamma^h\|_{l,\Gamma} \|\boldsymbol{\mu}_\Gamma^H\|_{-l,\Gamma}} \geq \beta_p^*, \quad l \in \left\{0, \frac{1}{2}\right\}. \quad (2.19)$$

The constant β_p^* is related to c_p^* by the bounds $c_p^* \beta^H \leq \beta_p^* \leq c_p^*$.

Proof. (i) Let Assumption 2.3 hold, which implies $\ker(P^{hH}) = \{\mathbf{0}\}$ and thus

$$\begin{aligned} & \inf_{\mathbf{w}_\Gamma^H \in \mathbf{W}_\Gamma^H} \sup_{\boldsymbol{\mu}_\Gamma^h \in \mathbf{M}_\Gamma^h} \frac{\langle \mathbf{w}_\Gamma^H, \boldsymbol{\mu}_\Gamma^h \rangle_\Gamma}{\|\mathbf{w}_\Gamma^H\|_{l,\Gamma} \|\boldsymbol{\mu}_\Gamma^h\|_{-l,\Gamma}} \\ & \geq \inf_{\mathbf{w}_\Gamma^H \in \mathbf{W}_\Gamma^H} \sup_{\boldsymbol{\mu}_\Gamma^h \in \mathbf{M}_\Gamma^h} \frac{\langle P^{hH}(\mathbf{w}_\Gamma^H), \boldsymbol{\mu}_\Gamma^h \rangle_\Gamma}{c_p^{-1} \|P^{hH}(\mathbf{w}_\Gamma^H)\|_{l,\Gamma} \|\boldsymbol{\mu}_\Gamma^h\|_{-l,\Gamma}} \\ & \geq c_p \inf_{\mathbf{w}_\Gamma^h \in \mathbf{W}_\Gamma^h} \sup_{\boldsymbol{\mu}_\Gamma^h \in \mathbf{M}_\Gamma^h} \frac{\langle \mathbf{w}_\Gamma^h, \boldsymbol{\mu}_\Gamma^h \rangle_\Gamma}{\|\mathbf{w}_\Gamma^h\|_{l,\Gamma} \|\boldsymbol{\mu}_\Gamma^h\|_{-l,\Gamma}} \geq c_p \beta^h, \end{aligned}$$

i.e., there exists $\beta_p \geq c_p \beta^h$ such that (2.18) is satisfied. Conversely, let (2.18) hold. Then we get for any $\mathbf{w}_\Gamma^H \in \mathbf{W}_\Gamma^H$

$$\begin{aligned} \beta_p \|\mathbf{w}_\Gamma^H\|_{l,\Gamma} & \leq \sup_{\boldsymbol{\mu}_\Gamma^h \in \mathbf{M}_\Gamma^h} \frac{\langle P^{hH}(\mathbf{w}_\Gamma^H), \boldsymbol{\mu}_\Gamma^h \rangle_\Gamma}{\|\boldsymbol{\mu}_\Gamma^h\|_{-l,\Gamma}} \\ & \leq \sup_{\boldsymbol{\mu}_\Gamma^h \in \mathbf{M}_\Gamma^h} \frac{\|P^{hH}(\mathbf{w}_\Gamma^H)\|_{l,\Gamma} \|\boldsymbol{\mu}_\Gamma^h\|_{-l,\Gamma}}{\|\boldsymbol{\mu}_\Gamma^h\|_{-l,\Gamma}} = \|P^{hH}(\mathbf{w}_\Gamma^H)\|_{l,\Gamma}, \end{aligned}$$

i.e., (2.14) holds with some $c_p \geq \beta_p$.

(ii) Let Assumption 2.4 hold. Then we get

$$\begin{aligned} & \inf_{\boldsymbol{\mu}_\Gamma^H \in \mathbf{M}_\Gamma^H} \sup_{\mathbf{w}_\Gamma^h \in \mathbf{W}_\Gamma^h} \frac{\langle P^{Hh}(\mathbf{w}_\Gamma^h), \boldsymbol{\mu}_\Gamma^H \rangle_\Gamma}{\|\mathbf{w}_\Gamma^h\|_{l,\Gamma} \|\boldsymbol{\mu}_\Gamma^H\|_{-l,\Gamma}} \\ & \geq \inf_{\boldsymbol{\mu}_\Gamma^H \in \mathbf{M}_\Gamma^H} \sup_{\mathbf{w}_\Gamma^H \in \mathbf{W}_\Gamma^H} \frac{\langle \mathbf{w}_\Gamma^H, \boldsymbol{\mu}_\Gamma^H \rangle_\Gamma}{(c_p^*)^{-1} \|\mathbf{w}_\Gamma^H\|_{l,\Gamma} \|\boldsymbol{\mu}_\Gamma^H\|_{-l,\Gamma}} \geq c_p^* \beta^H, \end{aligned}$$

i.e. there exists $\beta_p^* \geq c_p^* \beta^H$ such that (2.19) is satisfied. Conversely, let (2.19) hold. Decomposing \mathbf{W}_Γ^h orthogonally into $(\mathbf{W}_\Gamma^h)^0 \oplus (\mathbf{W}_\Gamma^h)^\perp$ with

$$\begin{aligned} (\mathbf{W}_\Gamma^h)^0 & := \{ \mathbf{w}_\Gamma^h \in \mathbf{W}_\Gamma^h : \langle \mathbf{w}_\Gamma^h, \boldsymbol{\mu}_\Gamma^H \rangle_\Gamma = 0, \boldsymbol{\mu}_\Gamma^H \in \mathbf{M}_\Gamma^H \}, \\ (\mathbf{W}_\Gamma^h)^\perp & := \{ \mathbf{w}_\Gamma^h \in \mathbf{W}_\Gamma^h : (\mathbf{v}_\Gamma^h, \mathbf{w}_\Gamma^h)_{l,\Gamma} = 0, \mathbf{v}_\Gamma^h \in (\mathbf{W}_\Gamma^h)^0 \}, \end{aligned}$$

we get $\dim(\mathbf{W}_\Gamma^h)^\perp = \dim \mathbf{M}_\Gamma^H$, the inf-sup condition (2.19) implies that P^{Hh} restricted to $(\mathbf{W}_\Gamma^h)^\perp$ is bijective and that the estimate

$$\inf_{\mathbf{w}_\Gamma^h \in (\mathbf{W}_\Gamma^h)^\perp} \sup_{\boldsymbol{\mu}_\Gamma^H \in \mathbf{M}_\Gamma^H} \frac{\langle \mathbf{w}_\Gamma^h, \boldsymbol{\mu}_\Gamma^H \rangle_\Gamma}{\|\mathbf{w}_\Gamma^h\|_{l,\Gamma} \|\boldsymbol{\mu}_\Gamma^H\|_{-l,\Gamma}} \geq \beta_p^*$$

holds. Hence, we get for any $\mathbf{w}_\Gamma^h \in (\mathbf{W}_\Gamma^h)^\perp$

$$\beta_p^* \|\mathbf{w}_\Gamma^h\|_{l,\Gamma} \leq \sup_{\boldsymbol{\mu}_\Gamma^H \in \mathbf{M}_\Gamma^H} \frac{\langle P^{Hh}(\mathbf{w}_\Gamma^h), \boldsymbol{\mu}_\Gamma^H \rangle_\Gamma}{\|\boldsymbol{\mu}_\Gamma^H\|_{-l,\Gamma}} \leq \|P^{Hh}(\mathbf{w}_\Gamma^h)\|_{l,\Gamma},$$

implying that (2.15) holds for some $c_p^* \geq \beta_p^*$. \square

REMARK 2.7. From this lemma, one can easily see that Assumptions 2.3 and 2.4 are equivalent if standard Lagrange multipliers are used, i.e., if $\mathbf{W}_\Gamma^m = \mathbf{M}_\Gamma^m$ holds for $m \in \{h, H\}$.

Using the space discretization described above, we can formulate the equations for the mortar coupled solution between independent grids of the outer domain Ξ and the patch ω , where the continuity of the displacement along Γ is enforced weakly. The number of constraints depends on the choice of the Lagrange multiplier space \mathbf{M}_Γ^m , $m \in \{h, H\}$. In the following, we focus on the case

$m = h$, such that the spatially discrete version of (2.5) reads: find $(\mathbf{u}^H, \mathbf{u}^h, \boldsymbol{\zeta}_\Gamma^h) \in \mathbf{V}_\Xi^H \times \mathbf{V}^h \times \mathbf{M}_\Gamma^h$ such that for all $t \in (0, T)$

$$\begin{aligned} m_\Xi(\ddot{\mathbf{u}}^H, \mathbf{w}^H) + a_\Xi(\mathbf{u}^H, \mathbf{w}^H) - \langle \mathbf{w}^H, \boldsymbol{\zeta}_\Gamma^h \rangle_\Gamma &= f_\Xi(\mathbf{w}^H), & \mathbf{w}^H &\in \mathbf{V}_\Xi^H, \\ m_\omega(\ddot{\mathbf{u}}^h, \mathbf{w}^h) + a_\omega(\mathbf{u}^h, \mathbf{w}^h) + \langle \mathbf{w}^h, \boldsymbol{\zeta}_\Gamma^h \rangle_\Gamma &= f_\omega(\mathbf{w}^h), & \mathbf{w}^h &\in \mathbf{V}^h, \\ \langle \mathbf{u}^h - \mathbf{u}^H, \boldsymbol{\mu}_\Gamma^h \rangle_\Gamma &= 0, & \boldsymbol{\mu}_\Gamma^h &\in \mathbf{M}_\Gamma^h, \end{aligned} \quad (2.20)$$

together with the initial conditions

$$(\mathbf{u}^H, \mathbf{u}^h)|_{t=0} = (\mathbf{u}_0^H, \mathbf{u}_0^h), \quad (\dot{\mathbf{u}}^H, \dot{\mathbf{u}}^h)|_{t=0} = (\mathbf{v}_0^H, \mathbf{v}_0^h). \quad (2.21)$$

We remark that, for the case $\mathbf{W}_\Gamma^H \subset \mathbf{W}_\Gamma^h$, the definition of \mathbf{M}_Γ^h and (2.20)₃ imply that the finite element solution is continuous on the whole domain Ω .

REMARK 2.8. *As stated in [59], it is possible to define the Lagrange multiplier space with respect to a coarser triangulation than \mathcal{G}_Γ^m , $m \in \{h, H\}$; e.g., if \mathcal{G}_Γ^m is obtained from $\mathcal{G}_\Gamma^{m/2}$ by one uniform refinement step, then the mortar problem (2.33) with \mathbf{M}_Γ^m replaced by the multiplier space $\mathbf{M}_\Gamma^{m/2}$ associated with $\mathcal{G}_\Gamma^{m/2}$ still gives a well-defined problem.*

Especially in the case that the trace spaces $\mathbf{W}_\Gamma^H \subset \mathbf{W}_\Gamma^h$ are nested, it is possible to define the Lagrange multiplier with respect to the coarser triangulation \mathcal{G}^H . However, the global continuity of the finite element solution of (2.20) is no longer guaranteed.

The case of a coarse multiplier space \mathbf{M}_Γ^H is considered in more detail in Section 5.

Using standard matrix notation for the mass and stiffness matrices as well as the transfer matrices (2.12), the algebraic version of the discrete mortar system (2.20) reads

$$M_\Xi^H \ddot{\mathbf{u}}^H + A_\Xi^H \mathbf{u}^H - (D^{hH})^T \boldsymbol{\zeta}_\Gamma^h = \mathbf{f}^H, \quad (2.22a)$$

$$M_\omega^h \ddot{\mathbf{u}}^h + A_\omega^h \mathbf{u}^h + (D^{hh})^T \boldsymbol{\zeta}_\Gamma^h = \mathbf{f}^h, \quad (2.22b)$$

$$D^{hh} \mathbf{u}^h - D^{hH} \mathbf{u}^H = \mathbf{0}. \quad (2.22c)$$

2.3. Time discretization. Next, we discretize (2.22) in time by partitioning the time interval $(0, T)$ into equidistant time steps $t_j = j\Delta t$ of step size Δt and considering the implicit trapezoidal rule, i.e., the Newmark scheme with $\gamma = \frac{1}{2}$, $\beta = \frac{1}{4}$ [38]. Furthermore, we introduce the notation

$$\partial_{\Delta t} \mathbf{w}_j := \frac{1}{\Delta t} (\mathbf{w}_j - \mathbf{w}_{j-1}), \quad \mathbf{w}_{j-1/2} := \frac{1}{2} (\mathbf{w}_j + \mathbf{w}_{j-1}). \quad (2.23)$$

With this, we obtain the following problem: find sequences of vectors $(\mathbf{u}_j^H, \mathbf{u}_j^h)_{j=0}^M$, $(\mathbf{v}_j^H, \mathbf{v}_j^h)_{j=0}^M$, $(\boldsymbol{\zeta}_{\Gamma,j}^H)_{j=0}^{M-1}$ satisfying the initial conditions (2.21) as well as

$$M_\Xi^H \partial_{\Delta t} \mathbf{v}_j^H + A_\Xi^H \mathbf{u}_{j-1/2}^H - (D^{hH})^T \boldsymbol{\zeta}_{\Gamma,j}^h = \mathbf{f}_{j-1/2}^H, \quad (2.24a)$$

$$\mathbf{v}_{j-1/2}^H - \partial_{\Delta t} \mathbf{u}_j^H = \mathbf{0}, \quad (2.24b)$$

$$M_\omega^h \partial_{\Delta t} \mathbf{v}_j^h + A_\omega^h \mathbf{u}_{j-1/2}^h + (D^{hh})^T \boldsymbol{\zeta}_{\Gamma,j}^h = \mathbf{f}_{j-1/2}^h, \quad (2.24c)$$

$$\mathbf{v}_{j-1/2}^h - \partial_{\Delta t} \mathbf{u}_j^h = \mathbf{0}, \quad (2.24d)$$

$$D^{hh} \mathbf{u}_j^h - D^{hH} \mathbf{u}_j^H = \mathbf{0}. \quad (2.24e)$$

We emphasize that the continuity of the displacements (2.24e) is enforced at t_j , i.e., at the end of the time step. For conciseness, we denote the corresponding Lagrange multiplier $\boldsymbol{\zeta}_\Gamma^h$ with the time index \cdot_j but think of it as being associated with the intermediate time $t_{j-1/2}$.

The discrete energy at time t_j is the sum of the contributions from the subdomains Ξ , ω given by

$$\begin{aligned} \mathbb{E}_j &= \mathbb{E}_{\Xi,j}^H + \mathbb{E}_{\omega,j}^h := \left(\frac{1}{2} (\mathbf{v}_j^H)^T M_\Xi^H \mathbf{v}_j^H + \frac{1}{2} (\mathbf{u}_j^H)^T A_\Xi^H \mathbf{u}_j^H - (f_j^H)^T \mathbf{u}_j^H \right) \\ &\quad + \left(\frac{1}{2} (\mathbf{v}_j^h)^T M_\omega^h \mathbf{v}_j^h + \frac{1}{2} (\mathbf{u}_j^h)^T A_\omega^h \mathbf{u}_j^h - (f_j^h)^T \mathbf{u}_j^h \right). \end{aligned} \quad (2.25)$$

For time-independent outer loads, the energy is conserved for the discrete system (2.24):

$$\begin{aligned}\mathbb{E}_j - \mathbb{E}_{j-1} &= \Delta t \left((\partial_{\Delta t} \mathbf{v}_j^H)^T M_{\Xi}^H \mathbf{v}_{j-1/2}^H + (\partial_{\Delta t} \mathbf{u}_j^H)^T A_{\Xi}^H \mathbf{u}_{j-1/2}^H - (f^H)^T \partial_{\Delta t} \mathbf{u}_j^H \right) \\ &\quad + \Delta t \left((\partial_{\Delta t} \mathbf{v}_j^h)^T M_{\omega}^h \mathbf{v}_{j-1/2}^h + (\partial_{\Delta t} \mathbf{u}_j^h)^T A_{\omega}^h \mathbf{u}_{j-1/2}^h - (f^h)^T \partial_{\Delta t} \mathbf{u}_j^h \right) \\ &= \Delta t \left((\partial_{\Delta t} \mathbf{u}_j^H)^T (D^{hH})^T \boldsymbol{\zeta}_{\Gamma,j}^h - (\partial_{\Delta t} \mathbf{u}_j^h)^T (D^{hh})^T \boldsymbol{\zeta}_{\Gamma,j}^h \right) = 0,\end{aligned}$$

where we have used (2.24b), (2.24d) as well as (2.24e) for both time steps t_j and t_{j-1} .

2.4. Schur complement formulation. Inserting the relation

$$\mathbf{v}_j^m = -\mathbf{v}_{j-1}^m + 2\partial_{\Delta t} \mathbf{u}_j^m, \quad m \in \{h, H\}, \quad (2.26)$$

into (2.24) and using the notation

$$K^h := \frac{2}{\Delta t^2} M^h + \frac{1}{2} A^h, \quad (2.27a)$$

$$\boldsymbol{\varrho}_{j-1}^h := \mathbf{f}_{j-1/2}^h + \frac{2}{\Delta t} M_{\omega}^h \mathbf{v}_{j-1}^h - A_{\omega}^h \mathbf{u}_{j-1}^h + K_{\omega}^h \mathbf{u}_{j-1}^h, \quad (2.27b)$$

the system to be solved for the displacement at time t_j becomes

$$\begin{pmatrix} K_{\Xi}^H & \mathbf{0} & -(D^{hH})^T \\ \mathbf{0} & K_{\omega}^h & (D^{hh})^T \\ -D^{hH} & D^{hh} & \mathbf{0} \end{pmatrix} \begin{pmatrix} \mathbf{u}_j^H \\ \mathbf{u}_j^h \\ \boldsymbol{\zeta}_{\Gamma,j}^h \end{pmatrix} = \begin{pmatrix} \boldsymbol{\varrho}_{j-1}^H \\ \boldsymbol{\varrho}_{j-1}^h \\ \mathbf{0} \end{pmatrix}. \quad (2.28)$$

As for the continuous case, we shortly look at the well-posedness of the discrete problem (2.28) which is guaranteed if the symmetric matrix

$$\begin{pmatrix} K_{\Xi}^H & \mathbf{0} \\ \mathbf{0} & K_{\omega}^h \end{pmatrix} \quad (2.29)$$

is uniformly coercive on the space

$$\left\{ (\mathbf{w}^H, \mathbf{w}^h) \in (\mathbf{V}_{\Xi}^H \oplus \mathbf{V}^h) : D^{hH} \mathbf{w}^H - D^{hh} \mathbf{w}^h = \mathbf{0} \right\}. \quad (2.30)$$

For $\varrho > 0$, this is always satisfied; otherwise, we need to consider the rigid body modes defined in (2.7). In contrast to Section 2, the functions in (2.30) are in general not globally continuous; however, as any rigid body mode $\mathbf{z} \in \mathcal{RB}_{\Theta}$ is linear, its trace $\text{tr}(\mathbf{z})$ is contained in \mathbf{W}_{Γ}^H as well as in \mathbf{W}_{Γ}^h . This implies that the operator P^{hH} defined in (2.10) restricted to $\text{tr}(\mathcal{RB}_{\Xi})$ is the identity, and $\ker(D^{hH}) \cap \text{tr}(\mathcal{RB}_{\Xi}) = \{\mathbf{0}\}$ holds. With $P^{hh} = \text{Id}$, $\text{meas}(\Gamma_D) > 0$ and the Korn inequalities established in [11], we obtain that the matrix (2.29) is coercive on (2.30) with a constant independent of h, H or the diameters of the subdomains ω, Ξ .

Next, we partition the vectors $(\mathbf{u}^H, \mathbf{u}^h)$ and the matrix (2.29) into its components associated with the nodes on the interface Γ and the inner degrees of freedom by

$$\mathbf{u}^H = \begin{pmatrix} \mathbf{u}_{\Xi}^H \\ \mathbf{u}_{\Gamma}^H \end{pmatrix}, \quad K_{\Xi}^H = \begin{pmatrix} K_{\Xi\Xi}^H & K_{\Xi\Gamma}^H \\ K_{\Gamma\Xi}^H & K_{\Gamma\Gamma}^H \end{pmatrix}, \quad \mathbf{u}^h = \begin{pmatrix} \mathbf{u}_{\Gamma}^h \\ \mathbf{u}_{\omega}^h \end{pmatrix}, \quad K_{\omega}^h = \begin{pmatrix} K_{\Gamma\Gamma}^h & K_{\Gamma\omega}^h \\ K_{\omega\Gamma}^h & K_{\omega\omega}^h \end{pmatrix}.$$

Static condensation of the inner variables yields from (2.28)

$$\mathbf{u}_{\omega,j}^h = (K_{\omega\omega}^h)^{-1} (\boldsymbol{\varrho}_{\omega,j-1}^h - K_{\omega\Gamma}^h \mathbf{u}_{\Gamma,j}^h), \quad (2.31a)$$

$$\mathbf{u}_{\Xi,j}^H = (K_{\Xi\Xi}^H)^{-1} (\boldsymbol{\varrho}_{\Xi,j-1}^H - K_{\Xi\Gamma}^H \mathbf{u}_{\Gamma,j}^H). \quad (2.31b)$$

Hence, by introducing the symmetric positive semi-definite Schur complement matrices $S_{\Xi}^H \in \mathbb{R}^{d|\mathcal{N}_{\Gamma}^H| \times d|\mathcal{N}_{\Gamma}^H|}$, $S_{\omega}^h \in \mathbb{R}^{d|\mathcal{N}_{\Gamma}^h| \times d|\mathcal{N}_{\Gamma}^h|}$ via

$$S_{\Xi}^H := K_{\Gamma\Gamma}^H - K_{\Gamma\Xi}^H (K_{\Xi\Xi}^H)^{-1} K_{\Xi\Gamma}^H, \quad (2.32a)$$

$$S_{\omega}^h := K_{\Gamma\Gamma}^h - K_{\Gamma\omega}^h (K_{\omega\omega}^h)^{-1} K_{\omega\Gamma}^h, \quad (2.32b)$$

we can rewrite (2.28) as

$$\begin{pmatrix} S_{\Xi}^H & \mathbf{0} & -(D_{\Gamma}^{hH})^T \\ \mathbf{0} & S_{\omega}^h & (D_{\Gamma}^{hh})^T \\ -D_{\Gamma}^{hH} & D_{\Gamma}^{hh} & \mathbf{0} \end{pmatrix} \begin{pmatrix} \mathbf{u}_{\Gamma,j}^H \\ \mathbf{u}_{\Gamma,j}^h \\ \zeta_{\Gamma,j}^h \end{pmatrix} = \begin{pmatrix} \bar{\boldsymbol{\varrho}}_{\Xi,j-1}^H \\ \bar{\boldsymbol{\varrho}}_{\omega,j-1}^h \\ \mathbf{0} \end{pmatrix}, \quad (2.33)$$

where the right hand side of (2.33) is given by

$$\bar{\boldsymbol{\varrho}}_{\Xi,j-1}^H := \boldsymbol{\varrho}_{\Gamma,j-1}^H - K_{\Gamma\Xi}^H (K_{\Xi\Xi}^H)^{-1} \boldsymbol{\varrho}_{\Xi,j-1}^H, \quad (2.34a)$$

$$\bar{\boldsymbol{\varrho}}_{\omega,j-1}^h := \boldsymbol{\varrho}_{\Gamma,j-1}^h - K_{\Gamma\omega}^h (K_{\omega\omega}^h)^{-1} \boldsymbol{\varrho}_{\omega,j-1}^h. \quad (2.34b)$$

We remark that the Schur matrices (2.32) are the algebraic representations of discrete linear Dirichlet-to-Neumann maps $\mathcal{S}_{\Xi}^H : \mathbf{W}_{\Gamma}^H \rightarrow (\mathbf{W}_{\Gamma}^H)'$, $\mathcal{S}_{\omega}^h : \mathbf{W}_{\Gamma}^h \rightarrow (\mathbf{W}_{\Gamma}^h)'$ [51].

Instead of solving the fully coupled problem (2.33), we are going to consider an iterative solution scheme that incorporates a coarse mortar problem on \mathbf{V}^H . In Section 3, a corresponding algorithm is derived and theoretically analysed, including a short discussion about estimating the corresponding algebraic error. Numerical results are presented in Section 4.

3. Iterative coupling algorithm. In this section, we derive and investigate an iterative solution scheme for the mortar system (2.33). In Subsection 3.1, the method is introduced and formulated as a block Gauß–Seidel iteration applied to an augmented problem. The error propagation and the convergence rate of the iterative scheme are analysed in Subsections 3.2 and 3.3, followed by a short discussion how its algebraic error can be measured.

3.1. Derivation. We motivate an iterative solution algorithm for the mortar system (2.33) by considering an augmented version of (2.33), with one additional line containing the auxiliary coefficient vector $\boldsymbol{\mu}_{\Gamma}^H \in \mathbb{R}^{d|\mathcal{N}_{\Gamma}^H|}$ which can be interpreted as a coarse Lagrange multiplier in \mathbf{M}_{Γ}^H :

$$\underbrace{\begin{pmatrix} S_{\Xi}^H + S_{\omega}^H & (D_{\Gamma}^{HH})^T & \mathbf{0} & -(D_{\Gamma}^{hH})^T \\ S_{\omega}^H & (D_{\Gamma}^{HH})^T & \mathbf{0} & \mathbf{0} \\ -D_{\Gamma}^{hH} & \mathbf{0} & D_{\Gamma}^{hh} & \mathbf{0} \\ \mathbf{0} & \mathbf{0} & S_{\omega}^h & (D_{\Gamma}^{hh})^T \end{pmatrix}}_{=:\hat{C}_d} \underbrace{\begin{pmatrix} \mathbf{u}_{\Gamma,j}^H \\ \boldsymbol{\mu}_{\Gamma,j}^H \\ \mathbf{u}_{\Gamma,j}^h \\ \zeta_{\Gamma,j}^h \end{pmatrix}}_{=:\hat{\mathbf{z}}_d} = \underbrace{\begin{pmatrix} \bar{\boldsymbol{\varrho}}_{\Xi,j-1}^H + \bar{\boldsymbol{\varrho}}_{\omega,j-1}^H \\ \bar{\boldsymbol{\varrho}}_{\omega,j-1}^h \\ \mathbf{0} \\ \bar{\boldsymbol{\varrho}}_{\omega,j-1}^h \end{pmatrix}}_{=:\hat{\mathbf{F}}_d}. \quad (3.1)$$

In (3.1), we have used the coarse Schur complement matrix $S_{\omega}^H \in \mathbb{R}^{d|\mathcal{N}_{\Gamma}^H| \times d|\mathcal{N}_{\Gamma}^H|}$ and the right hand side $\bar{\boldsymbol{\varrho}}_{\omega,j-1}^h$ which are assumed to be suitable coarse grid approximations of the fine grid quantities S_{ω}^h , $\bar{\boldsymbol{\varrho}}_{\omega,j-1}^h$ defined in (2.32b), (2.34). The exact definition of these approximations is not fixed; however, we require them to comply with the Dirichlet boundary conditions on $\Gamma_D \cap \partial\omega$ and with the rigid body modes in \mathcal{RB}_{ω} , i.e., we assume that

$$S_{\omega}^H \Pi^{Hh} \mathbf{z}_{\Gamma}^h = \mathbf{0} \quad \text{and} \quad (\Pi^{Hh} \mathbf{z}_{\Gamma}^h, \bar{\boldsymbol{\varrho}}_{\omega,j-1}^h) = (\mathbf{z}_{\Gamma}^h, \bar{\boldsymbol{\varrho}}_{\omega,j-1}^h) \quad (3.2)$$

holds for every $\mathbf{z}_{\Gamma}^h \in \text{tr}(\mathcal{RB}_{\omega}) \subset \mathbf{W}_{\Gamma}^h$, where (\cdot, \cdot) denotes the Euclidean scalar product.

For the linear problem we investigate in this part, a natural definition of S_{ω}^H is

$$S_{\omega}^H := K_{\Gamma\Gamma}^H - K_{\Gamma\omega}^H (K_{\omega\omega}^H)^{-1} K_{\omega\Gamma}^H, \quad (3.3)$$

with K_{ω}^H defined as in (2.27a) but assembled with respect to the coarse grid $\mathcal{T}^H|_{\omega}$ instead of \mathcal{T}^h . In Part II, other ways of defining suitable coarse grid approximations will be discussed. We remark that the additional line (3.1)₂ can be interpreted as an auxiliary coarse grid problem on the patch ω with a fixed trace on Γ . A related algorithm with an augmented coarse problem has been investigated in [33].

As the components $(\mathbf{u}_{\Gamma,j}^H, \mathbf{u}_{\Gamma,j}^h, \zeta_{\Gamma,j}^h)$ of the exact solution of (3.1) also solve the mortar system (2.33), any convergent iterative method for the augmented system (3.1) yields an approximation of the solution of (2.33). Hence, we consider the iterative solution of (3.1) by means of a block

Gauß–Seidel scheme according to the splitting $\hat{G}_d = (\hat{G}_d - \hat{K}_d) + \hat{K}_d$, with \hat{K}_d being the upper triangular part of \hat{G}_d , i.e., \hat{K}_d is defined to be zero except for its first row which reads

$$\begin{pmatrix} \mathbf{0} & (D_\Gamma^{HH})^T & \mathbf{0} & -(D_\Gamma^{hH})^T \end{pmatrix}.$$

Given some starting vector $\hat{\mathbf{z}}_d^{(0)}$, the Gauß–Seidel iteration on (3.1) reads for $l \geq 0$:

$$(\hat{G}_d - \hat{K}_d)\delta\hat{\mathbf{z}}_d^{(l)} = \hat{\mathbf{F}}_d - \hat{G}_d\hat{\mathbf{z}}_d^{(l)}, \quad \hat{\mathbf{z}}_d^{(l+1)} = \hat{\mathbf{z}}_d^{(l)} + \delta\hat{\mathbf{z}}_d^{(l)}. \quad (3.4)$$

Equation (3.4) leads to the following system that has to be solved in the l -th iteration step

$$\begin{pmatrix} (S_\Xi^H + S_\omega^H) & \mathbf{0} & \mathbf{0} & \mathbf{0} \\ S_\omega^H & (D_\Gamma^{HH})^T & \mathbf{0} & \mathbf{0} \\ -D_\Gamma^{hH} & \mathbf{0} & D_\Gamma^{hh} & \mathbf{0} \\ \mathbf{0} & \mathbf{0} & S_\omega^h & (D_\Gamma^{hh})^T \end{pmatrix} \begin{pmatrix} \delta\mathbf{u}_{\Gamma,j}^{H,(l)} \\ \delta\boldsymbol{\mu}_{\Gamma,j}^{H,(l)} \\ \delta\mathbf{u}_{\Gamma,j}^{h,(l)} \\ \delta\boldsymbol{\zeta}_{\Gamma,j}^{h,(l)} \end{pmatrix} = \begin{pmatrix} \mathbf{r}_\Xi^{H,(l)} + \mathbf{r}_\omega^{H,(l)} \\ \mathbf{r}_\omega^{H,(l)} \\ \boldsymbol{\nu}_\Gamma^{h,(l)} \\ \mathbf{r}_\omega^{h,(l)} \end{pmatrix}, \quad (3.5)$$

where the residuals on the right hand side of (3.5) are defined in (3.9). One can see that (3.5) is a linear system with a lower block-triangular matrix and can thus be solved by two sequential subproblems on \mathbf{V}^H and \mathbf{V}^h , with the matrix $(S_\Xi^H + S_\omega^H)$ being invertible because of the assumption $\text{meas}(\Gamma_D) > 0$. The corresponding scheme is described in Algorithm 1.

Algorithm 1 Two-way coupling scheme with augmented coarse grid problem

Starting from some initial guess $\hat{\mathbf{z}}_d^{(0)}$, compute sequentially for $l = 0, 1, \dots$

(i) Solve problem on coarse space \mathbf{V}^H with interface load on Γ inherited from fine computation on ω :

$$\begin{pmatrix} (S_\Xi^H + S_\omega^H) & \mathbf{0} \\ S_\omega^H & (D_\Gamma^{HH})^T \end{pmatrix} \begin{pmatrix} \delta\mathbf{u}_{\Gamma,j}^{H,(l)} \\ \delta\boldsymbol{\mu}_{\Gamma,j}^{H,(l)} \end{pmatrix} = \begin{pmatrix} \mathbf{r}_\Xi^{H,(l)} + \mathbf{r}_\omega^{H,(l)} \\ \mathbf{r}_\omega^{H,(l)} \end{pmatrix}. \quad (3.6)$$

(ii) Solve problem on fine space \mathbf{V}^h with weakly imposed trace on Γ inherited from coarse computation on Ω :

$$\begin{pmatrix} S_\omega^h & (D_\Gamma^{hh})^T \\ D_\Gamma^{hH} & \mathbf{0} \end{pmatrix} \begin{pmatrix} \delta\mathbf{u}_{\Gamma,j}^{h,(l)} \\ \delta\boldsymbol{\zeta}_{\Gamma,j}^{h,(l)} \end{pmatrix} = \begin{pmatrix} \mathbf{r}_\omega^{h,(l)} \\ \boldsymbol{\nu}_\Gamma^{h,(l)} \end{pmatrix} + \begin{pmatrix} \mathbf{0} \\ D_\Gamma^{hH}\delta\mathbf{u}_{\Gamma,j}^{H,(l)} \end{pmatrix}. \quad (3.7)$$

(iii) Update the solution vector:

$$\hat{\mathbf{z}}_d^{(l+1)} := \hat{\mathbf{z}}_d^{(l)} + \delta\hat{\mathbf{z}}_d^{(l)}. \quad (3.8)$$

The residuals of (3.6), (3.7) are given by

$$\mathbf{r}_\Xi^{H,(l)} = \bar{\boldsymbol{\varrho}}_{\Xi,j-1}^H - S_\Xi^H \mathbf{u}_{\Gamma,j}^{H,(l)} + (D_\Gamma^{hH})^T \boldsymbol{\zeta}_{\Gamma,j}^{h,(l)}, \quad (3.9a)$$

$$\mathbf{r}_\omega^{H,(l)} = \bar{\boldsymbol{\varrho}}_{\omega,j-1}^H - S_\omega^H \mathbf{u}_{\Gamma,j}^{H,(l)} - (D_\Gamma^{HH})^T \boldsymbol{\mu}_{\Gamma,j}^{H,(l)}, \quad (3.9b)$$

$$\mathbf{r}_\omega^{h,(l)} = \bar{\boldsymbol{\varrho}}_{\omega,j-1}^h - S_\omega^h \mathbf{u}_{\Gamma,j}^{h,(l)} - (D_\Gamma^{hh})^T \boldsymbol{\zeta}_{\Gamma,j}^{h,(l)}, \quad (3.9c)$$

$$\boldsymbol{\nu}_\Gamma^{h,(l)} = D_\Gamma^{hH} \mathbf{u}_{\Gamma,j}^{H,(l)} - D_\Gamma^{hh} \mathbf{u}_{\Gamma,j}^{h,(l)}. \quad (3.9d)$$

REMARK 3.1. After one iteration of Algorithm 1, i.e., for $l \geq 1$, the residuals (3.9b) to (3.9d) vanish.

3.2. Error propagation. In order to analyse the error propagation of Algorithm 1, we are going to reformulate both the mortar system (2.33) and the iteration (3.4) as equations with the only unknown $\mathbf{u}_{\Gamma,j}^H \in \mathbf{W}_{\Gamma}^H$. Introducing the Schur matrix $S_{\omega}^{HhH} \in \mathbb{R}^{d|\mathcal{N}_{\Gamma}^H| \times d|\mathcal{N}_{\Gamma}^H|}$ with

$$S_{\omega}^{HhH} := - \begin{pmatrix} \mathbf{0} & (D_{\Gamma}^{hH})^T \\ D_{\Gamma}^{hh} & \mathbf{0} \end{pmatrix}^{-1} \begin{pmatrix} \mathbf{0} \\ D_{\Gamma}^{hH} \end{pmatrix} = (\Pi^{hH})^T S_{\omega}^h \Pi^{hH}, \quad (3.10)$$

the mortar system (2.33) can be rewritten as a Schur complement system for the coarse trace $\mathbf{u}_{\Gamma,j}^H$:

$$(S_{\Xi}^H + S_{\omega}^{HhH}) \mathbf{u}_{\Gamma,j}^H = \mathbf{g}_{\Gamma,j-1}^H := (\Pi^{hH})^T \bar{\mathbf{e}}_{\omega,j-1}^h + \bar{\mathbf{e}}_{\Xi,j-1}^H. \quad (3.11)$$

REMARK 3.2. *In case that the Lagrange multiplier $\zeta_{\Gamma,j}^h$ is not associated with \mathcal{G}_{Γ}^h but with a coarser triangulation (cf. Remark 2.8), the second equality of (3.10) does not hold, and the Schur complement matrix S_{ω}^{HhH} is defined by the first formula. In the special case that $\mathbf{W}_{\Gamma}^H \subset \mathbf{W}_{\Gamma}^h$ and the multiplier is chosen from \mathbf{M}_{Γ}^H , (3.10) becomes*

$$S_{\omega}^{HhH} := - \begin{pmatrix} \mathbf{0} & (D_{\Gamma}^{HH})^T \\ D_{\Gamma}^{Hh} & \mathbf{0} \end{pmatrix}^{-1} \begin{pmatrix} \mathbf{0} \\ D_{\Gamma}^{HH} \end{pmatrix}.$$

The following lemma shows that the iterative scheme (3.4), which is realized by Algorithm 1, can be reformulated as a fixpoint iteration on $\mathbf{u}_{\Gamma,j}^H$:

LEMMA 3.3. *Let $\hat{\mathbf{z}}_d$ denote the exact solution of the augmented mortar system (3.1), and let $\hat{\mathbf{z}}_d^{(l)}$, $l = 0, 1, \dots$, be the sequence of vectors obtained from Algorithm 1. For $l \geq 1$, the error $\mathbf{e}_{\Gamma}^{H,(l)} := (\mathbf{u}_{\Gamma,j}^{H,(l)} - \mathbf{u}_{\Gamma,j}^H)$ satisfies the relation*

$$\mathbf{e}_{\Gamma}^{H,(l+1)} = \left(\text{Id} - (S_{\Xi}^H + S_{\omega}^H)^{-1} (S_{\Xi}^H + S_{\omega}^{HhH}) \right) \mathbf{e}_{\Gamma}^{H,(l)}. \quad (3.12)$$

Proof. With (3.4) and $\hat{\mathbf{F}}_d = \hat{G}_d \hat{\mathbf{z}}_d$ from (3.1), we get

$$\begin{aligned} (\hat{G}_d - \hat{K}_d) \hat{\mathbf{z}}_d^{(l+1)} &= \hat{\mathbf{F}}_d - \hat{K}_d \hat{\mathbf{z}}_d^{(l)}, \\ (\hat{G}_d - \hat{K}_d) (\hat{\mathbf{z}}_d^{(l+1)} - \hat{\mathbf{z}}_d) &= \hat{G}_d \hat{\mathbf{z}}_d - (\hat{G}_d - \hat{K}_d) \hat{\mathbf{z}}_d - \hat{K}_d \hat{\mathbf{z}}_d^{(l)} = -\hat{K}_d (\hat{\mathbf{z}}_d^{(l)} - \hat{\mathbf{z}}_d). \end{aligned} \quad (3.13)$$

From the definition of \hat{K}_d , we obtain that the right hand side of (3.13) is zero except for its first component which reads

$$\left(-\hat{K}_d (\hat{\mathbf{z}}_d^{(l)} - \hat{\mathbf{z}}_d) \right)_1 = (D_{\Gamma}^{hH})^T (\zeta_{\Gamma,j}^{h,(l)} - \zeta_{\Gamma,j}^h) - (D_{\Gamma}^{HH})^T (\mu_{\Gamma,j}^{H,(l)} - \mu_{\Gamma,j}^H).$$

Using the Schur matrix (3.10), we get

$$S_{\omega}^H \mathbf{e}_{\Gamma}^{H,(l+1)} = -(D_{\Gamma}^{HH})^T (\mu_{\Gamma,j}^{H,(l+1)} - \mu_{\Gamma,j}^H) \quad \text{from (3.13)}_2, \quad (3.14a)$$

$$S_{\omega}^{HhH} \mathbf{e}_{\Gamma}^{H,(l+1)} = -(D_{\Gamma}^{hH})^T (\zeta_{\Gamma,j}^{h,(l+1)} - \zeta_{\Gamma,j}^h) \quad \text{from (3.13)}_{3-4}. \quad (3.14b)$$

For $l \geq 1$, the relations (3.14) also hold for the previous iteration with (l) instead of $(l+1)$. Hence, (3.13)₁ yields

$$\begin{aligned} (S_{\Xi}^H + S_{\omega}^H) \mathbf{e}_{\Gamma}^{H,(l+1)} &= (D_{\Gamma}^{hH})^T (\zeta_{\Gamma,j}^{h,(l)} - \zeta_{\Gamma,j}^h) - (D_{\Gamma}^{HH})^T (\mu_{\Gamma,j}^{H,(l)} - \mu_{\Gamma,j}^H) \\ &= (S_{\omega}^H - S_{\omega}^{HhH}) \mathbf{e}_{\Gamma}^{H,(l)}. \end{aligned}$$

Using the relation

$$(S_{\Xi}^H + S_{\omega}^H)^{-1} (S_{\omega}^H - S_{\omega}^{HhH}) = \text{Id} - (S_{\Xi}^H + S_{\omega}^H)^{-1} (S_{\Xi}^H + S_{\omega}^{HhH}),$$

we finally obtain (3.12). \square

REMARK 3.4. *If the coarse and the fine grid on ω coincide, i.e., $\mathbf{V}^h = \mathbf{V}_\omega^H$ holds with the definitions from (2.8), then we have $S_\omega^{HhH} = S_\omega^H$, and Lemma 3.3 implies that the exact coarse trace $\mathbf{u}_{\Gamma,j}^H$ is obtained after at most two steps. In this case, the definition of Scheme (3.4) yields that the other components of the solution vector $\hat{\mathbf{z}}_d^{(2)}$ coincide with the exact solution $\hat{\mathbf{z}}_d$ of (3.1), too. If the starting vector $\hat{\mathbf{z}}_d^{(0)}$ satisfies $\hat{K}_d \hat{\mathbf{z}}_d^{(0)} = \hat{K}_d \hat{\mathbf{z}}_d$, then the exact solution of (3.1) is already obtained after the first iteration.*

A damped version of (3.12) with a suitable damping parameter $\alpha_l > 0$ yields the error propagation

$$\mathbf{e}_\Gamma^{H,(l+1)} = \left(\text{Id} - \alpha_l (S_\Xi^H + S_\omega^H)^{-1} (S_\Xi^H + S_\omega^{HhH}) \right) \mathbf{e}_\Gamma^{H,(l)}. \quad (3.15)$$

If $\alpha_l = \alpha$ does not depend on l , (3.15) is equivalent to a preconditioned Richardson iteration for the Schur complement system (3.11). But in general, it is more effective to choose α_l in each step according to a conjugate gradient algorithm (see, e.g., [4, 56]).

REMARK 3.5. *From (3.12), one can see that the difference between Algorithm 1 and the classical Dirichlet–Neumann coupling with Ξ as the Neumann subdomain is the additional term of S_ω^H in the factor $(S_\Xi^H + S_\omega^H)^{-1}$. The benefit of this term can be seen in the next subsection, where we analyse the robustness of Algorithm 1 with respect to jumps in the material parameters.*

3.3. Condition number analysis. The convergence properties of the iteration (3.12) or its damped version (3.15) are determined by the condition number of the iteration matrix in (3.12). To this extend, we investigate the spectral equivalence of the matrices S_ω^H and S_ω^{HhH} in Theorem 3.6 below. For its proof, we use the zero extension operators $R_\omega^m : \mathbf{W}_\Gamma^m \rightarrow \mathbf{V}_\omega^m$, $m \in \{h, H\}$, given by

$$R_\omega^m \mathbf{w}_\Gamma^m(p) = \begin{cases} \mathbf{w}_\Gamma^m(p), & p \in \mathcal{N}_\Gamma^m, \\ \mathbf{0}, & \text{else,} \end{cases} \quad (3.16)$$

as well as a projection operator $Z_\omega^m : \mathbf{V}_0(\omega) \rightarrow \mathbf{V}_\omega^m$ which is constructed as the Scott–Zhang operator Z^m introduced in [53] except for a modification on the interface Γ . For convenience, we quote the definition of the Scott–Zhang operator in the interior of ω : Let $\mathbf{v} \in \mathbf{V}_0(\omega)$. For any node $p \in \mathcal{N}^m \setminus \mathcal{N}_\Gamma^m$, one $(d-1)$ -dimensional face σ_p^m with $p \in \bar{\sigma}_p^m$ is chosen and the nodal value of the projected function $Z_\omega^m \mathbf{v}$ at p is given by $\int_{\sigma_p^m} \chi_p^m(\xi) \mathbf{v}(\xi) d\xi$, where χ_p^m is the $L^2(\sigma_p^m)$ -dual function to ϕ_p^m , i.e., $\int_{\sigma_p^m} \chi_p^m(\xi) \phi_q^m(\xi) d\xi = \delta_{pq}$ for any $p, q \in \mathcal{N}^m \setminus \mathcal{N}_\Gamma^m$. If σ_p^m is chosen properly, this operator preserves the homogeneous Dirichlet boundary conditions on Γ_D and allows for the following stability estimates for each element $K \in \mathcal{T}^m$:

$$|Z^m \mathbf{v}|_{1,K} \leq C |\mathbf{v}|_{1,\omega_K}, \quad \mathbf{v} \in \mathbf{H}^1(\omega), \quad (3.17a)$$

$$\|Z^m \mathbf{v}\|_{0,K} \leq C \|\mathbf{v}\|_{0,\omega_K}, \quad \mathbf{v} \in \mathbf{L}^2(\omega). \quad (3.17b)$$

where $\bar{\omega}_K := \bigcup \{\bar{T} : T \in \mathcal{T}^h, \bar{T} \cap \bar{K} \neq \emptyset\}$ is the patch of elements around K .

This operator is now modified at the interface Γ such that the relation $(Z_\omega^m \mathbf{v})|_\Gamma = P^m(\mathbf{v}|_\Gamma)$ holds for any function $\mathbf{v} \in \mathbf{V}_0(\omega)$, where the mortar projection P^m has been defined in (2.11). This can be done by choosing the integration area σ_p^m for any boundary node $p \in \mathcal{N}_\Gamma^m$ to be not only a single face of \mathcal{G}_Γ^m but the support of ϕ_p^m , such that we obtain the relation

$$\int_{\sigma_p^m} \chi_p^m(\xi) \phi_q^m(\xi) d\xi = \int_\Gamma \chi_p^m(\xi) \phi_q^m(\xi) d\xi \quad \Rightarrow \quad \chi_p^m = \left(\int_\Gamma \phi_q^m(\xi) d\xi \right)^{-1} \psi_p^m,$$

with the dual basis functions $\{\psi_p^m\}_{p \in \mathcal{N}_\Gamma^m}$ already introduced in the previous Section. Hence, if we apply Z_ω^m to a discrete function $\mathbf{v}^s \in \mathbf{V}_\omega^s$, $s \in \{h, H\}$, we obtain $(Z_\omega^m \mathbf{v}^s)|_\Gamma = P^{ms}(\mathbf{v}^s|_\Gamma)$ with P^{ms} defined in (2.10). In addition, the $\mathbf{H}^1(\omega)$ -stability estimate (3.17a) still holds for Z_ω^m , $m \in \{h, H\}$

[53]. However, the uniform $\mathbf{L}_2(\omega)$ -stability (3.17b) is not valid in general, which can be seen from the example $\mathbf{v}^h = R_\omega^h \mathbf{w}_\Gamma^h \in \mathbf{V}_\omega^h$ with $\mathbf{w}_\Gamma^h \in \mathbf{W}_\Gamma^h$, leading to the non-uniform estimate

$$\|Z_\omega^H \mathbf{v}^h\|_{0,\omega}^2 \leq CH \|P^H(\mathbf{w}_\Gamma^h)\|_{0,\omega}^2 \leq CH \|\mathbf{w}_\Gamma^h\|_{0,\omega}^2 \leq C \frac{H}{h} \|\mathbf{v}^h\|_{0,\omega}^2. \quad (3.18)$$

However, with $\frac{h}{H} \leq 1$, we obtain the uniform stability estimate

$$\|Z_\omega^h \mathbf{v}^H\|_{0,\omega} \leq C \|\mathbf{v}^H\|_{0,\omega}, \quad \mathbf{v}^H \in \mathbf{V}_\omega^H. \quad (3.19)$$

THEOREM 3.6. *Assume that the material parameters E , ν , and ρ satisfy the estimates (2.2) on ω . Let assumption 2.3 hold. Furthermore, assume that the mass contribution can be bounded by the stiffness term, i.e., that there exists a constant C_{mass} such that $\frac{\rho_\omega}{\Delta t^2} \leq C_{mass} \frac{E_\omega}{h^2}$. Then, there exist constants c^* , C^* independent of the diameter of ω , h , H , Δt and the values E_ω , ρ_ω , such that the following estimates are satisfied for any function $\mathbf{w}_\Gamma^H \in \mathbf{W}_\Gamma^H$:*

$$c^* (\mathbf{w}_\Gamma^H, S_\omega^H \mathbf{w}_\Gamma^H) \leq (\mathbf{w}_\Gamma^H, S_\omega^{HhH} \mathbf{w}_\Gamma^H) \leq C^* (\mathbf{w}_\Gamma^H, S_\omega^H \mathbf{w}_\Gamma^H). \quad (3.20)$$

The constant c^* in (3.20) depends on the value of c_p from Assumption 2.3; further, if $\frac{\rho_\omega}{\Delta t^2} \gg \frac{E_\omega}{h^2}$, c^* can depend on $\frac{h}{H}$.

If the finite element spaces (2.8) satisfy $\mathbf{V}_\omega^H \subset \mathbf{V}^h$ (which implies Assumption 2.3), then the constant C^* in (3.20) can be replaced by one.

Proof. Accordingly to (2.27a), we define the bilinear forms

$$k_\Theta(\mathbf{v}, \mathbf{w}) := \frac{2}{\Delta t^2} m_\Theta(\mathbf{v}, \mathbf{w}) + \frac{1}{2} a_\Theta(\mathbf{v}, \mathbf{w}), \quad \mathbf{v}, \mathbf{w} \in \mathbf{V}_0(\Theta), \quad \Theta \in \{\Xi, \omega\}.$$

Due to the fact that the Schur complement matrices S_ω^H , S_ω^{HhH} defined in (3.3), (3.10) correspond to discrete harmonic extensions onto ω with respect to $k_\omega(\cdot, \cdot)$, we obtain

$$(\mathbf{w}_\Gamma^H, S_\omega^{HhH} \mathbf{w}_\Gamma^H) = \inf_{\mathbf{v}^h \in \mathbf{V}^h} k_\omega(\mathbf{v}^h, \mathbf{v}^h), \quad (\mathbf{w}_\Gamma^H, S_\omega^H \mathbf{w}_\Gamma^H) = \inf_{\mathbf{v}^H \in \mathbf{V}_\omega^H} k_\omega(\mathbf{v}^H, \mathbf{v}^H). \quad (3.21)$$

Thus, we define the values

$$\hat{\mathbf{v}}^h := \arg \inf_{\mathbf{v}^h \in \mathbf{V}^h} k_\omega(\mathbf{v}^h, \mathbf{v}^h), \quad \hat{\mathbf{v}}^H := \arg \inf_{\mathbf{v}^H \in \mathbf{V}_\omega^H} k_\omega(\mathbf{v}^H, \mathbf{v}^H), \quad (3.22)$$

using that the spaces \mathbf{V}^h , \mathbf{V}_ω^H are finite dimensional.

Further, we introduce the seminorms

$$|\mathbf{v}|_{\tilde{\mathbf{V}}(\Theta)} := \inf_{\mathbf{z} \in \mathcal{RB}_\Theta} \|\mathbf{v} + \mathbf{z}\|_{1,\Theta}, \quad \mathbf{v} \in \mathbf{V}(\Theta), \quad (3.23a)$$

$$|\mathbf{w}_\Gamma|_{\tilde{\mathbf{W}}_\Gamma(\Theta)} := \inf_{\mathbf{z} \in \mathcal{RB}_\Theta} \|\mathbf{w}_\Gamma + \text{tr } \mathbf{z}\|_{1/2,\Gamma}, \quad \mathbf{w}_\Gamma \in \mathbf{W}_\Gamma. \quad (3.23b)$$

Then, we get with the stability of Z_ω^h (3.17a), (3.19), the equation $(Z_\omega^h \hat{\mathbf{v}}^H)|_\Gamma = P^{hH}(\mathbf{w}_\Gamma^H)$ as well as the fact that $Z_\omega^h \mathbf{z} = \mathbf{z}$ holds for $\mathbf{z} \in \mathcal{RB}_\omega$, following from $\mathcal{RB}_\omega \subset \mathbf{V}^h \cap (\mathbf{V}_\omega^H)$:

$$\begin{aligned} k_\omega(\hat{\mathbf{v}}^h, \hat{\mathbf{v}}^h) &\leq k_\omega(Z_\omega^h \hat{\mathbf{v}}^H, Z_\omega^h \hat{\mathbf{v}}^H) \\ &\leq C \left(E_\omega |Z_\omega^h \hat{\mathbf{v}}^H|_{\tilde{\mathbf{V}}(\omega)}^2 + \frac{\rho_\omega}{\Delta t^2} \|Z_\omega^h \hat{\mathbf{v}}^H\|_{0,\omega}^2 \right) \\ &\leq C \left(E_\omega |\hat{\mathbf{v}}^H|_{\tilde{\mathbf{V}}(\omega)}^2 + \frac{\rho_\omega}{\Delta t^2} \|\hat{\mathbf{v}}^H\|_{0,\omega}^2 \right) \\ &\leq C^* k_\omega(\hat{\mathbf{v}}^H, \hat{\mathbf{v}}^H). \end{aligned} \quad (3.24)$$

For the other direction, we need to correct the boundary values

$$(Z_\omega^H \hat{\mathbf{v}}^h)|_\Gamma = P^{Hh} P^{hH}(\mathbf{w}_\Gamma^H)$$

using the zero extension operator R_ω^H defined in (3.16). With this, we obtain

$$\begin{aligned}
k_\omega(\hat{\mathbf{v}}^H, \hat{\mathbf{v}}^H) &\leq k_\omega\left(Z_\omega^H \hat{\mathbf{v}}^h + R_\omega^H(\text{Id} - P^{Hh} P^{hH}) \mathbf{w}_\Gamma^H, Z_\omega^H \hat{\mathbf{v}}^h + R_\omega^H(\text{Id} - P^{Hh} P^{hH}) \mathbf{w}_\Gamma^H\right) \\
&\leq C\left(E_\omega |Z_\omega^H \hat{\mathbf{v}}^h|_{\mathbf{V}(\omega)}^2 + \frac{\rho_\omega}{\Delta t^2} \|Z_\omega^H \hat{\mathbf{v}}^h\|_{0,\omega}^2\right) \\
&\quad + C\left(E_\omega |R_\omega^H(\text{Id} - P^{Hh} P^{hH}) \mathbf{w}_\Gamma^H|_{1,\omega}^2 + \frac{\rho_\omega}{\Delta t^2} \|R_\omega^H(\text{Id} - P^{Hh} P^{hH}) \mathbf{w}_\Gamma^H\|_{0,\omega}^2\right).
\end{aligned} \tag{3.25}$$

For the last term in (3.25), we use the uniform continuity of the mortar operators P^{Hh} , P^{hH} as well as Assumption 2.3 for $l = 0$ to arrive at

$$\begin{aligned}
\|R_\omega^H(\text{Id} - P^{Hh} P^{hH}) \mathbf{w}_\Gamma^H\|_{0,\omega}^2 &\leq CH \|(\text{Id} - P^{Hh} P^{hH}) \mathbf{w}_\Gamma^H\|_{0,\Gamma}^2 \\
&\leq CH \|\mathbf{w}_\Gamma^H\|_{0,\Gamma}^2 \leq Cc_p^{-2} H \|P^{hH}(\mathbf{w}_\Gamma^H)\|_{0,\Gamma}^2 \\
&\leq Cc_p^{-2} \frac{H}{h} \|R_\omega^h P^{hH}(\mathbf{w}_\Gamma^H)\|_{0,\omega}^2 \leq Cc_p^{-2} \frac{H}{h} \|\hat{\mathbf{v}}_\Gamma^h\|_{0,\omega}^2.
\end{aligned}$$

The second-to-last term in (3.25) can be bounded using the discrete inequalities stated in, e.g., [61], as well as Assumption 2.3 for $l = \frac{1}{2}$:

$$\begin{aligned}
&|R_\omega^H(\text{Id} - P^{Hh} P^{hH}) \mathbf{w}_\Gamma^H|_{1,\omega}^2 \\
&\leq CH^{d-2} \sum_{e \in \mathcal{G}_\Gamma^H} \sum_{p,q \in \mathcal{N}_\Gamma^H \cap \bar{e}} \left(((\text{Id} - P^{Hh} P^{hH}) \mathbf{w}_\Gamma^H)(p) - ((\text{Id} - P^{Hh} P^{hH}) \mathbf{w}_\Gamma^H)(q) \right)^2 \\
&\leq CH^{d-2} \sum_{p \in \mathcal{N}_\Gamma^H} ((\text{Id} - P^{Hh} P^{hH}) \mathbf{w}_\Gamma^H)^2(p) \\
&\leq CH^{-1} \|(\text{Id} - P^{Hh} P^{hH}) \mathbf{w}_\Gamma^H\|_{0,\Gamma}^2 \leq C |\mathbf{w}_\Gamma^H|_{\overline{\mathbf{W}}_\Gamma(\omega)}^2 \\
&\leq Cc_p^{-2} |P^{hH}(\mathbf{w}_\Gamma^H)|_{\overline{\mathbf{W}}_\Gamma(\omega)}^2 \leq Cc_p^{-2} |\hat{\mathbf{v}}^h|_{\mathbf{V}(\omega)}^2.
\end{aligned} \tag{3.26}$$

For the inequality (3.26), we have used the approximation properties of the continuous mortar projections P^h , P^H defined in (2.11) to show that for any rigid body motion $\mathbf{z} \in \text{tr}(\mathcal{RB}_\omega)$, we get

$$\begin{aligned}
&\|(\text{Id} - P^{Hh} P^{hH}) \mathbf{w}_\Gamma^H\|_{0,\Gamma}^2 \\
&= \|(\text{Id} - P^H + P^H - P^H P^h)(\mathbf{w}_\Gamma^H + \mathbf{z})\|_{0,\Gamma}^2 \\
&\leq \|(\text{Id} - P^H)(\mathbf{w}_\Gamma^H + \mathbf{z})\|_{0,\Gamma}^2 + \|P^H(\text{Id} - P^h)(\mathbf{w}_\Gamma^H + \mathbf{z})\|_{0,\Gamma}^2 \\
&\leq CH \|\mathbf{w}_\Gamma^H + \mathbf{z}\|_{1/2,\Gamma}^2.
\end{aligned}$$

Combining the above results with the stability estimates (3.17a), (3.18) of Z_ω^H , we obtain from (3.25)

$$k_\omega(\hat{\mathbf{v}}^H, \hat{\mathbf{v}}^H) \leq Cc_p \left(E_\omega |\hat{\mathbf{v}}^h|_{\mathbf{V}(\omega)}^2 + \frac{\rho_\omega}{\Delta t^2} \frac{H}{h} \|\hat{\mathbf{v}}^h\|_{0,\omega}^2 \right) \leq \frac{1}{c^*} k_\omega(\hat{\mathbf{v}}^h, \hat{\mathbf{v}}^h), \tag{3.27}$$

with a constant c^* that is independent of h , H , Δt and the material parameters but depends on c_p and can depend on $\frac{h}{H}$ if the mass contribution is dominant.

Using (3.21), we obtain (3.20).

Finally, we prove that the constant C^* in (3.20) can be replaced by one if the finite element spaces $\mathbf{V}_\omega^H \subset \mathbf{V}^h$ are nested. For this, we need to show the inequality

$$(\mathbf{w}_\Gamma^H, (S_\omega^H - S_\omega^{HhH}) \mathbf{w}_\Gamma^H) \geq 0. \tag{3.28}$$

The nestedness of $\mathbf{W}_\Gamma^H \subset \mathbf{W}_\Gamma^h$ implies that P^{hH} is the identity. Observing that

$$\left\{ \mathbf{w}^H \in \mathbf{V}_\omega^H : \mathbf{w}^H|_\Gamma = \mathbf{w}_\Gamma^H \right\} \subset \left\{ \mathbf{w}^h \in \mathbf{V}^h : \mathbf{w}^h|_\Gamma = P^{hH}(\mathbf{w}_\Gamma^H) \right\},$$

we find

$$(\mathbf{w}_\Gamma^H, (S_\omega^H - S_\omega^{HhH})\mathbf{w}_\Gamma^H) = \inf_{\substack{\mathbf{w}^H \in \mathbf{V}_\omega^H \\ \mathbf{w}^H|_\Gamma = \mathbf{w}_\Gamma^H}} k_\omega(\mathbf{w}^H, \mathbf{w}^H) - \inf_{\substack{\mathbf{w}^h \in \mathbf{V}^h \\ \mathbf{w}^h|_\Gamma = P^{hH}(\mathbf{w}_\Gamma^H)}} k_\omega(\mathbf{w}^h, \mathbf{w}^h) \geq 0.$$

□

Thus, if the assumptions of Theorem 3.6 are satisfied, the condition number of the iteration matrix in (3.12) is bounded by

$$\kappa \left((S_\Xi^H + S_\omega^H)^{-1} (S_\Xi^H + S_\omega^{HhH}) \right) \leq \frac{\max(1, C^*)}{\min(1, c^*)}. \quad (3.29)$$

with the constants c^* , C^* from Theorem 3.6. Furthermore, the iterates of (3.15) converge to the solution $\mathbf{u}_{\Gamma, j}^H$ of (3.11) if the damping parameter α_l is chosen within the set $0 < \alpha_{\min} \leq \alpha_l < \frac{2}{C^*}$ for some fixed value of α_{\min} (see, e.g., [56]). Hence, if the finite element spaces $\mathbf{V}_\omega^H \subset \mathbf{V}^h$ are nested, Theorem 3.6 implies the convergence of (3.15) for $\alpha_l = 1$, i.e., the convergence of Algorithm 1.

REMARK 3.7. *The dependence of the convergence rate on the ratio H/h for dominating mass contribution can be seen from the numerical results in Section 4.3; furthermore, they are in agreement with the theoretical estimates on the spectrum of discrete Dirichlet-to-Neumann operators recently presented in [61].*

REMARK 3.8. *Algorithm 1 can also be defined with a Lagrange multiplier space \mathbf{M}_Γ^{h*} associated with a coarser triangulation $\mathcal{G}^{h*} \subset \mathcal{G}^h$ (cf. Remarks 2.8 and 3.2). The results of Lemma 3.3 and Theorem 3.6 can be transferred onto this case, provided that the spaces \mathbf{W}_Γ^H and \mathbf{M}_Γ^{h*} satisfy a uniform inf-sup condition. The latter is trivially fulfilled for the special case $\mathbf{W}_\Gamma^H \subset \mathbf{W}_\Gamma^h$ and $\mathbf{M}_\Gamma^{h*} = \mathbf{M}_\Gamma^H$.*

The disadvantage of Theorem 3.6 is the need for Assumption 2.3 if the trace spaces are not nested. In the following, we state a variant of Theorem 3.6 that replaces Assumption 2.3 by a stronger restriction on the material parameters on the subdomains.

LEMMA 3.9. *Assume that the material parameters E , ν , ϱ satisfy the estimate (2.2) and in addition $E_\omega \leq C_{\text{par}} E_\Xi$, $\varrho_\omega \leq C_{\text{par}} \varrho_\Xi$, for some given value of C_{par} . Then, there exist a constant c_{par}^* independent of the diameter of ω , h or H such that the following estimate is satisfied for any function $\mathbf{w}_\Gamma^H \in \mathbf{W}_\Gamma^H$:*

$$c_{\text{par}}^* (\mathbf{w}_\Gamma^H, (S_\Xi^H + S_\omega^H)\mathbf{w}_\Gamma^H) \leq (\mathbf{w}_\Gamma^H, (S_\Xi^H + S_\omega^{HhH})\mathbf{w}_\Gamma^H). \quad (3.30)$$

Proof. In the proof of Theorem 3.6, we have used Assumption 2.3 for the upper bound of the last two terms in (3.25). If this assumption is not satisfied, we can bound these terms by their counterparts on Ξ . For this, we define

$$\check{\mathbf{v}}^H := \arg \inf_{\substack{\mathbf{v}^H \in \mathbf{V}_\Xi^H \\ \mathbf{v}^H|_\Gamma = \mathbf{w}_\Gamma^H}} k_\Xi(\mathbf{v}^H, \mathbf{v}^H).$$

For the mass term in (3.25), we obtain

$$\|R_\omega^H (\text{Id} - P^{Hh} P^{hH})\mathbf{w}_\Gamma^H\|_{0, \omega}^2 \leq CH \|\mathbf{w}_\Gamma^H\|_{0, \Gamma}^2 \leq C \|R_\Xi^H \mathbf{w}_\Gamma^H\|_{0, \Xi}^2 \leq C \|\check{\mathbf{v}}^H\|_{0, \Xi}^2.$$

For the stiffness term, we obtain from the proof of (3.26)

$$|R^H (\text{Id} - P^{Hh} P^{hH})\mathbf{w}_\Gamma^H|_{1, \omega}^2 \leq C |\mathbf{w}_\Gamma^H|_{\overline{\mathbf{W}}_\Gamma(\Xi)}^2.$$

With (3.25), the above estimates and the assumptions on the material parameters, we obtain

$$\begin{aligned} \inf_{\substack{\mathbf{v}^H \in \mathbf{V}_\omega^H \\ \mathbf{v}^H|_\Gamma = \mathbf{w}_\Gamma^H}} k_\omega(\mathbf{v}^H, \mathbf{v}^H) &\leq C k_\omega(\hat{\mathbf{v}}^h, \hat{\mathbf{v}}^h) + C \left(E_\omega |\mathbf{w}_\Gamma^H|_{\overline{\mathbf{W}}_\Gamma(\Xi)}^2 + \frac{\varrho_\omega}{\Delta t^2} \|\mathbf{w}_\Gamma^H\|_{\mathbf{L}_2(\Xi)}^2 \right) \\ &\leq C k_\omega(\hat{\mathbf{v}}^h, \hat{\mathbf{v}}^h) + CC_{\text{par}} k_\omega(\check{\mathbf{v}}^H, \check{\mathbf{v}}^H), \end{aligned}$$

and (3.30) follows with c_{par}^* independent of h, H but dependent of the ratio C_{par} of the material parameters. \square

However, in the unfavorable case that the material parameters satisfy $E_\omega \gg E_\Xi$ or $\varrho_\omega \gg \varrho_\Xi$ and Assumption 2.3 is not satisfied, both Theorem 3.6 and Lemma 3.9 do not provide a uniform bound for the condition number of (3.29). Concerning the trace spaces $\mathbf{W}_\Gamma^H, \mathbf{W}_\Gamma^h$, this means that there exist some ‘‘high frequency’’ components $\mathbf{w}_\Gamma^H \in \mathbf{W}_\Gamma^H$ that are strongly damped or even annihilated by the mortar operator Π^{hH} . As Π^{hH} is present in the exact mortar system (3.11) but not in the preconditioning matrix $(S_\Xi^H + S_\omega^H)$, these frequencies can spoil the good convergence of Algorithm 1, as a numerical example in Section 4.5 shows.

A possible remedy in the above sketched situation is to define the auxiliary coarse grid operator S_ω^H in a different way such that these spurious frequencies are damped. This can for example be done by replacing S_ω^H in (3.1) and (3.12) by the nonsymmetric matrix $S_\omega^H Q^{HH}$ with $Q^{HH} = \Pi^{Hh} \Pi^{hH}$ (cf. (2.16)). This additional factor is likely to have a damping effect on the high frequency components of \mathbf{W}_Γ^H . Furthermore, if the trace spaces $\mathbf{W}_\Gamma^H \subset \mathbf{W}_\Gamma^h$ are nested and Theorem 3.6 can be applied, Q^{HH} is the identity on \mathbf{W}_Γ^H . The numerical performance of the thus modified nonsymmetric version of Algorithm 1 is investigated in Section 4.5.

3.4. Stopping criteria. In this subsection, we state a measure of the algebraic error introduced by solving (3.1) by means of the iterative scheme (3.4).

As the residuals (3.9b) to (3.9d) vanish for $l \geq 1$, the only nonzero component of the residual vector is (3.9a) which can be written as

$$\mathbf{r}_\Xi^{H,(l)} = \left(-\hat{K}_d \delta \hat{\mathbf{z}}_d^{(l-1)} \right)_1 = (D_\Gamma^{hH})^T \delta \boldsymbol{\zeta}_{\Gamma,j}^{h,(l-1)} - (D_\Gamma^{HH})^T \delta \boldsymbol{\mu}_{\Gamma,j}^{H,(l-1)}. \quad (3.31)$$

As the energy norm of this residual given by

$$\left((S_\Xi^H + S_\omega^{HhH})^{-1} \mathbf{r}_\Xi^{H,(l)}, \mathbf{r}_\Xi^{H,(l)} \right)$$

is too expensive to compute, it is approximated by the value

$$\left((S_\Xi^H + S_\omega^H)^{-1} \mathbf{r}_\Xi^{H,(l)}, \mathbf{r}_\Xi^{H,(l)} \right) = \left(\delta \mathbf{u}_{\Gamma,j}^{H,(l)}, \mathbf{r}_\Xi^{H,(l)} \right), \quad (3.32)$$

where the last equality follows from (3.6) for $l \geq 1$. Thus, we propose to use the following relative algebraic error estimator for $l \geq 1$:

$$(\eta_{\text{alg}}^{(l)})^2 := \frac{\left(\delta \mathbf{u}_{\Gamma,j}^{H,(l)}, \mathbf{r}_\Xi^{H,(l)} \right)}{\left(\mathbf{u}_{\Gamma,j}^{H,(l)}, (S_\Xi^H + S_\omega^H) \mathbf{u}_{\Gamma,j}^{H,(l)} \right)}. \quad (3.33)$$

As (3.33) is a norm of the error between the approximate solution of (3.1) by means of Algorithm 1 and the exact mortar solution, it can be used to define a stopping criterion for the iterative process (see also Section 8).

REMARK 3.10. *In order to compute the denominator of (3.33) without solving a Schur complement problem in each step, one can use the relation*

$$(S_\Xi^H + S_\omega^H) \mathbf{u}_{\Gamma,j}^{H,(l)} = (S_\Xi^H + S_\omega^H) \mathbf{u}_{\Gamma,j}^{H,(0)} + \mathbf{r}_\omega^{H,(0)} + \sum_{k=0}^{l-1} \mathbf{r}_\Xi^{H,(k)}.$$

4. Numerical results.

4.1. Geometry and parameters. For the first numerical tests, we consider the domain $\Omega = [0, 2] \times [0, 1]$ which is split into the patch $\omega = [0.5, 1.5] \times [0, 0.5]$ and the upper domain $\Xi = \Omega \setminus \bar{\omega}$. Both subdomains are initially discretized by quadrilaterals of size $H = h = 0.125$; afterwards, we perform L additional refinements of the fine grid on ω . The resulting grid for

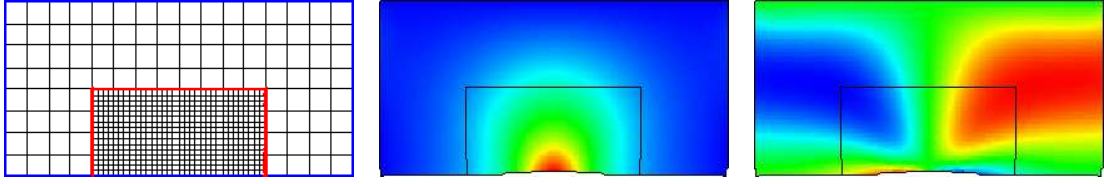


FIGURE 4.1. First example; left: grid for $L = 2$; middle: effective stress; right: pressure.

$L = 2$ is depicted on the left side of Figure 4.1. Hence, we have nested finite element spaces $\mathbf{V}^H|_\omega \subset \mathbf{V}^h$ such that both Assumptions 2.3 and 2.4 are satisfied with $c_p = c_p^* = 1$.

Furthermore, the nestedness of the triangulations $\mathcal{G}_\Gamma^H, \mathcal{G}_\Gamma^h$ implies that Algorithm 1 is well defined even if the Lagrange multiplier ζ_Γ is chosen from \mathbf{M}_Γ^H (cf. Remarks 2.8, 3.2 and 3.8). Hence, both possibilities \mathbf{M}_Γ^h and \mathbf{M}_Γ^H as spaces for the Lagrange multiplier will be tested in the following. We remark that in the latter case, the finite element solution of (2.22) will not be globally continuous.

REMARK 4.1. As stated in Section 2, each node of the interface Γ is associated with a degree of freedom for the Lagrange multiplier, i.e., there are no modifications due to cross points.

On the discretized domain Ω , we solve the equations of linear static elasticity with the constant elasticity module $E_\Xi = E_\omega = 100$ and the Poisson's ratio $\nu = 0.3$, corresponding to the Lamé parameters $\mu = \frac{E}{2(1+\nu)} \approx 38.5$, $\lambda = \frac{E\nu}{(1+\nu)(1-2\nu)} \approx 57.7$. The coarse matrix S_ω^H and the right hand side \bar{q}_j^H are assembled as in (3.3) and (2.27b), (2.34) with h replaced by H , respectively, and the starting vector is taken to be $\mathbf{0}$. Thus, all computations with $L = 0$ yield the exact mortar solution after one iteration and are not presented in the following.

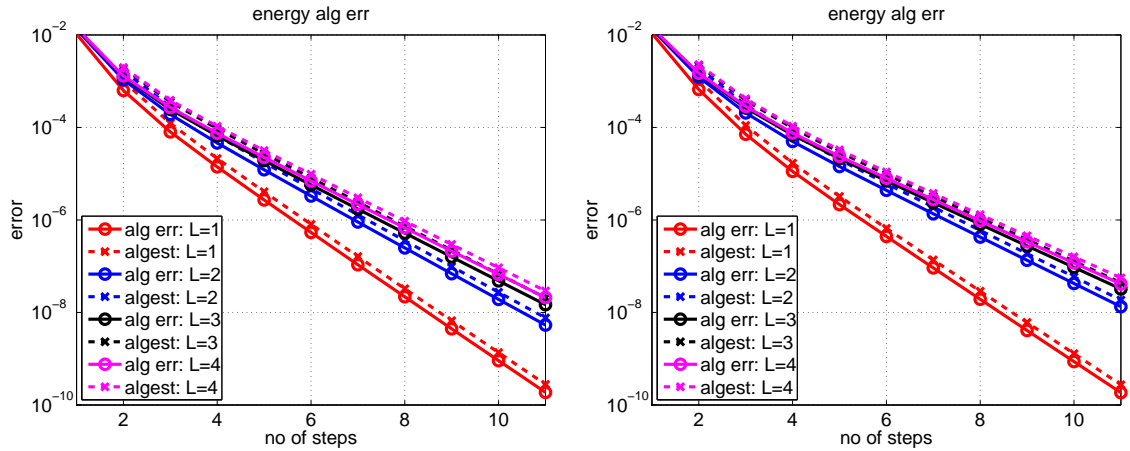


FIGURE 4.2. True $e_{\text{alg}}^{(l)}$ and estimated $\eta_{\text{alg}}^{(l)}$ relative algebraic energy error for Algorithm 1 with $L \in \{1, 2, 3, 4\}$ and $E_\omega = E_\Xi$ with respect to l ; left: \mathbf{M}_Γ^h ; right: \mathbf{M}_Γ^H .

4.2. Algebraic error decrease for static case. For the first set of tests, we set $\varrho = 0$ and $\mathbf{l} = \mathbf{0}$; further, we enforce homogeneous Dirichlet conditions on the upper boundary, homogeneous Neumann boundary conditions on the left and right side and a surface load of $\mathbf{g}_N = 10^6 \cdot \max(0.25 - |x_1 - 1|, 0)$ at the bottom. The effective stress and the pressure of the corresponding mortar solution are depicted in Figure 4.1.

In order to investigate the decrease of the algebraic error for Algorithm 1 with respect to the number of iterations, the difference between the approximations $(\mathbf{u}^{H,(l)}, \mathbf{u}^{h,(l)})$ obtained by Algorithm 1 and the solution $(\mathbf{u}^H, \mathbf{u}^h)$ of the discrete mortar system (2.33) is measured with

respect to the relative energy norm by computing

$$\left(e_{\text{alg}}^{(l)}\right)^2 := \frac{(\mathbf{u}^{H,(l)} - \mathbf{u}^H)^T A_{\Xi}^H (\mathbf{u}^{H,(l)} - \mathbf{u}^H) + (\mathbf{u}^{h,(l)} - \mathbf{u}^h)^T A_{\omega}^h (\mathbf{u}^{h,(l)} - \mathbf{u}^h)}{(\mathbf{u}^H)^T A_{\Xi}^H \mathbf{u}^H + (\mathbf{u}^h)^T A_{\omega}^h \mathbf{u}^h}. \quad (4.1)$$

The results for this relative algebraic error and the corresponding estimator (3.33) are shown in Figure 4.2. There and in the rest of this subsection, the left picture usually shows the results for the Lagrange multiplier ζ_{Γ}^h associated with \mathbf{M}_{Γ}^h , whereas the right plot contains the corresponding outcomes for the case \mathbf{M}_{Γ}^H . One can see that the decay rate with respect to the number of iterations is the same for the true and the estimated algebraic error and that the difference between them is very small, indicating that η_{alg} is well suited to measure the algebraic energy error due to the iterative solution of the coupled system.

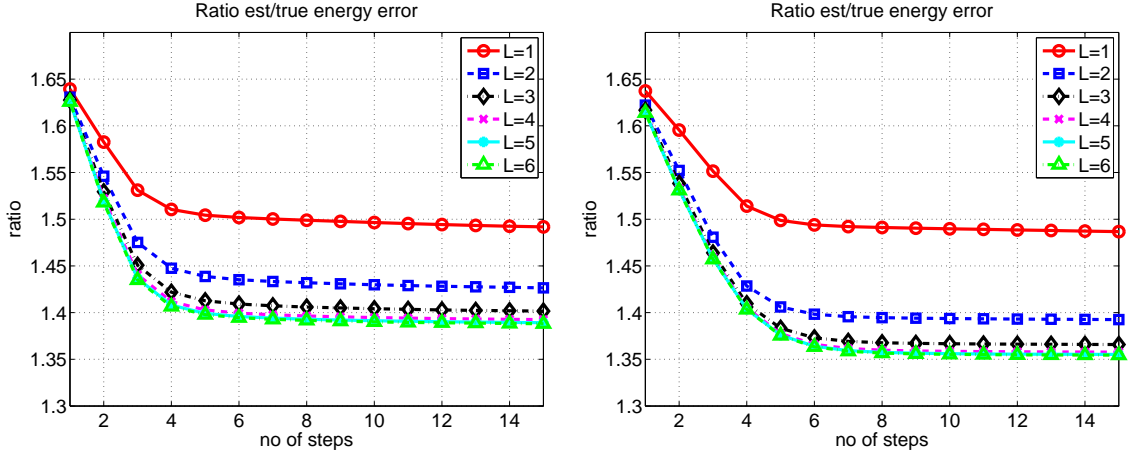


FIGURE 4.3. Ratio estimated/true relative algebraic energy error $\eta_{\text{alg}}^{(l)}/e_{\text{alg}}^{(l)}$ for Algorithm 1 with $L \in \{1, \dots, 6\}$ and $E_{\omega} = E_{\Xi}$ with respect to l ; left: \mathbf{M}_{Γ}^h ; right: \mathbf{M}_{Γ}^H .

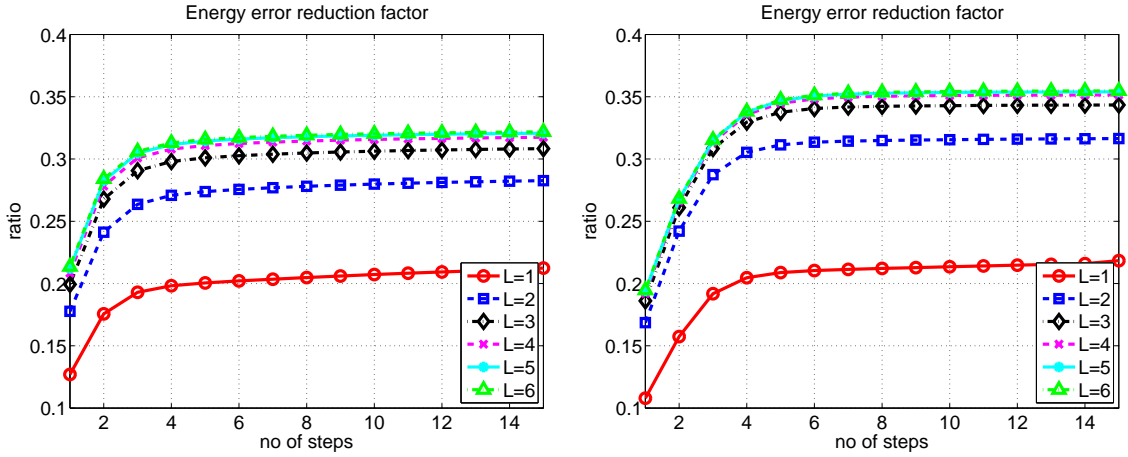


FIGURE 4.4. Mean algebraic energy error reduction factor $e_{\text{alg}}^{(l+1)}/e_{\text{alg}}^{(l)}$ in one step of Algorithm 1 for $L \in \{1, \dots, 6\}$ and $E_{\omega} = E_{\Xi}$ with respect to l ; left: \mathbf{M}_{Γ}^h ; right: \mathbf{M}_{Γ}^H .

Next, we investigate the dependence of the algebraic error reduction on the ratio $H/h = 2^L$. In Figure 4.3, the effectivity index $\eta_{\text{alg}}^{(l)}/e_{\text{alg}}^{(l)}$ of the estimated and the true relative algebraic energy error is displayed with respect to l for different values of L . One can observe that the ratio is always below 1.65, decreases for increasing L and l and converges to a limit of around 1.4 for the

case \mathbf{M}_Γ^h and a slightly lower limit for \mathbf{M}_Γ^H . This indicates the adequacy of the error measure (3.33).

Figure 4.4 features the reduction factor of the relative algebraic error $e_{\text{alg}}^{(l+1)}/e_{\text{alg}}^{(l)}$ in the l -th step of Algorithm 1. The algorithm converges best for small values of L , but the reduction factor is limited from above by around 0.35 independently of L and l , with slightly better results for the fine Lagrange multiplier.

REMARK 4.2. From (3.12), one can see that for $l \rightarrow \infty$, the error in the coarse trace $\mathbf{e}_\Gamma^{H,(l)} = (\mathbf{u}_\Gamma^{H,(l)} - \mathbf{u}_\Gamma^H)$ converges to an eigenvector \mathbf{v}_Γ^H of the iteration matrix in (3.12) corresponding to the largest eigenvalue λ_{\max} such that $\mathbf{v}_\Gamma^H \cdot \mathbf{e}_\Gamma^{H,(0)} \neq 0$. Thus, the error reduction factor $e_{\text{alg}}^{(l+1)}/e_{\text{alg}}^{(l)}$ becomes

$$\frac{e_{\text{alg}}^{(l+1)}}{e_{\text{alg}}^{(l)}} = \frac{\left(\mathbf{e}_\Gamma^{H,(l+1)}, (S_0^H + \bar{S}_\omega^h) \mathbf{e}_\Gamma^{H,(l+1)} \right)}{\left(\mathbf{e}_\Gamma^{H,(l)}, (S_0^H + \bar{S}_\omega^h) \mathbf{e}_\Gamma^{H,(l)} \right)} \rightarrow \lambda_{\max}^2.$$

Hence, the results depicted in Figures 4.4 and 4.7 allow for an estimate of the largest eigenvalue of the iteration matrix in (3.12).

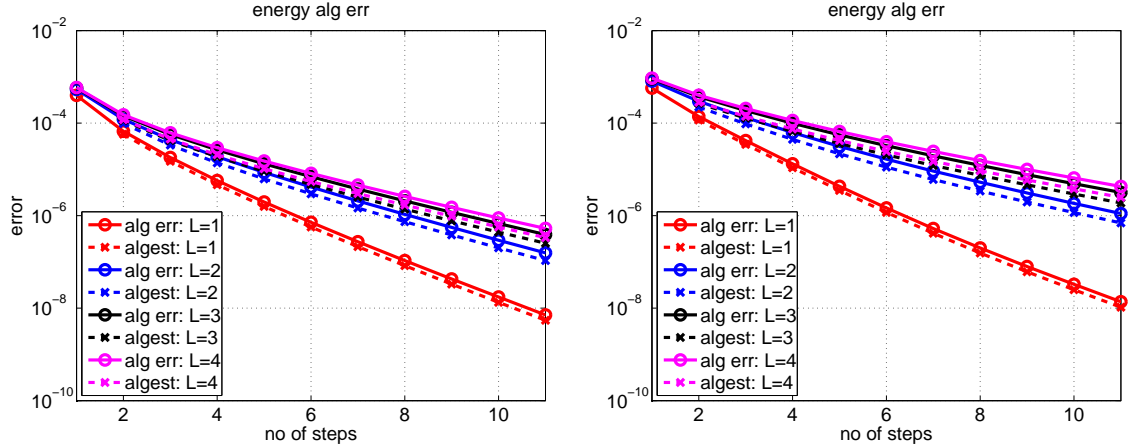


FIGURE 4.5. True $e_{\text{alg}}^{(l)}$ and estimated $\eta_{\text{alg}}^{(l)}$ relative algebraic energy error for $L \in \{1, 2, 3, 4\}$ and $E_\omega = 10^5 \cdot E_\Xi$ with respect to l ; left: \mathbf{M}_Γ^h ; right: \mathbf{M}_Γ^H .

Next, we test the convergence behavior of Algorithm 1 if the material parameters are piecewise constant on Ξ , ω but have a jump in between. For this, we increase the elastic module E_ω on the patch to $E_\omega = 10^{\text{par}} E_\Xi$, $\text{par} \geq 0$. In Figure 4.5, the values of $\eta_{\text{alg}}^{(l)}$ and $e_{\text{alg}}^{(l)}$ are shown for $L \in \{1, \dots, 4\}$, $\text{par} = 5$ and $E_\Xi = 100$. One can see that the convergence of Algorithm 1 is slower compared to the case $\text{par} = 0$ depicted in Figure 4.2; but the error indicator η_{alg} still is very close to the true error e_{alg} and decays with the same rate.

In Figures 4.6 and 4.7, we have fixed $L = 2$ and show the effectivity index $\eta_{\text{alg}}^{(l)}/e_{\text{alg}}^{(l)}$ as well as the error reduction factor $e_{\text{alg}}^{(l+1)}/e_{\text{alg}}^{(l)}$, respectively, for $\text{par} \in \{0, \dots, 5\}$. The results in Figure 4.6 show that for $\text{par} \geq 1$, the indicator η_{alg} slightly underestimates the error e_{alg} . Furthermore, the ratios are bounded with respect to the size of the jump in the material parameters and converge to a limit value of between 0.6 and 0.7. Although the error reduction factor depicted in Figure 4.7 degrades for $\text{par} > 0$, it is bounded in the limit case for $\text{par} \rightarrow \infty$ by around 0.55 for the case \mathbf{M}_Γ^h and 0.6 for \mathbf{M}_Γ^H . Hence, Algorithm 1 is stable with respect to jumps in the coefficients, in accordance with the theoretical results of Theorem 3.6 for the case $\varrho_\omega = 0$.

4.3. Algebraic error decrease for dynamic case. Next, we consider a dynamic setting by choosing $\Delta t = 10^{-3}$ and piecewise constant material parameters $E_\Xi = 100$, $\varrho_\Xi = 0.01$ and

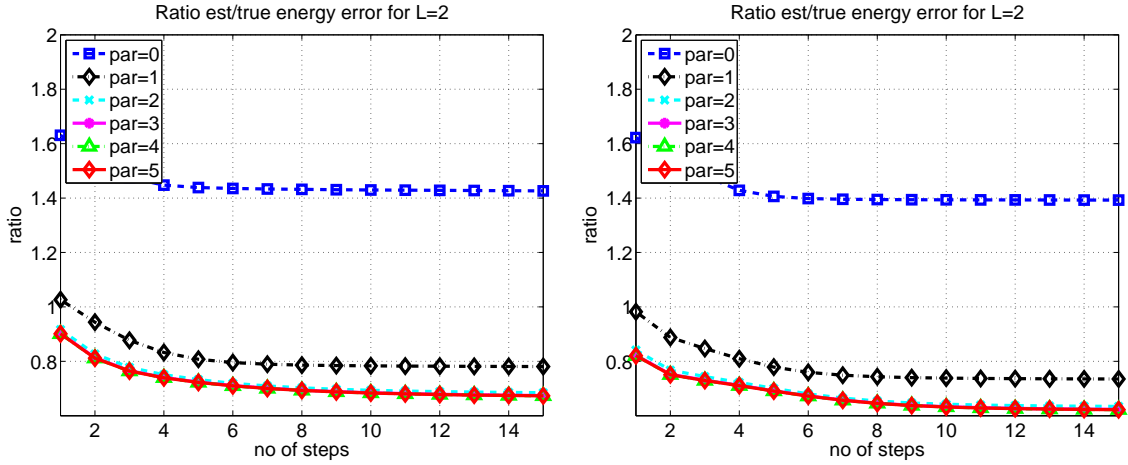


FIGURE 4.6. Ratio estimated/true relative algebraic energy error $\eta_{alg}^{(l)}/e_{alg}^{(l)}$ for Algorithm 1 with $L = 2$ and $E_\omega = 10^{par} E_\Xi$, $par \in \{0, \dots, 5\}$, with respect to l ; left: \mathbf{M}_Γ^h ; right: \mathbf{M}_Γ^H .

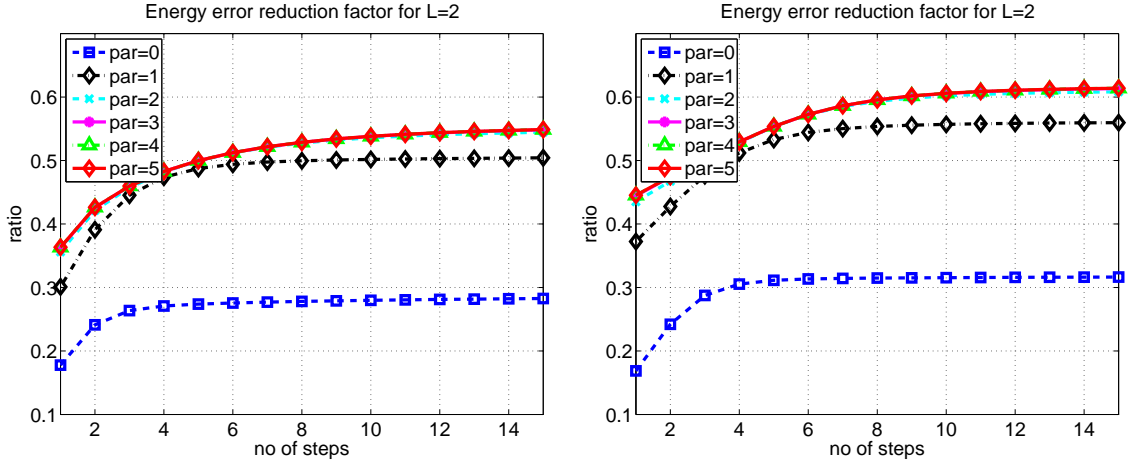


FIGURE 4.7. Mean algebraic energy error reduction factor $e_{alg}^{(l+1)}/e_{alg}^{(l)}$ in one step of Algorithm 1 for $L = 2$ and $E_\omega = 10^{par} E_\Xi$, $par \in \{0, \dots, 5\}$, with respect to l ; left: \mathbf{M}_Γ^h ; right: \mathbf{M}_Γ^H .

$E_\omega = 10^{par_E} \cdot E_\Xi$, $\varrho_\omega = 10^{par_\varrho} \cdot \varrho_\Xi$. The parameters are chosen such that the mass and the stiffness part are approximately equilibrated because of $\frac{E_\Xi}{H^2} \approx 10^4 = \frac{\varrho_\Xi}{\Delta t^2}$. We impose homogeneous Dirichlet boundary conditions on the top, the Neumann compression forces

$$\mathbf{g}_N = f(\text{par}_\varrho) \cdot \max(0, 0.25 - r), \quad \text{with } r^2 = (0.5 - x_1)^2,$$

$$f(\text{par}_\varrho) = 10^{2 + \min(-2, \text{par}_\varrho) + \delta_{\text{par}_\varrho > 0} + \max(3, \min(0, 0.5(\text{par}_\varrho - \text{par}_E))},$$

on the bottom and homogeneous Neumann conditions elsewhere. Both the volume load and the initial velocity are set to zero. As the results for the different multiplier spaces are very similar, we only consider the case of \mathbf{M}_Γ^h in the rest of this section.

In Tables 4.1 and 4.2, the algebraic error reduction rates of Algorithm 1 are summarized for $L \in \{2, 4\}$ and $\text{par}_E, \text{par}_\varrho \in \{-4, -2, 0, 2, 4, 6\}$. One can see that for fixed $L = \log_2(H/h)$, the error reduction factor is bounded from above by $(1 - 2^{-L})$ independently of the ratio of the grid sizes or the material parameters E_ω and ϱ_ω . However, for large values of ϱ_ω , this L -dependent convergence rate is actually reached, in accordance with the theoretical results of Theorem 3.6.

$\text{par}_E \setminus \text{par}_\rho$	-4	-2	0	2	4	6
-4	0.0001	0.0037	0.2572	0.7357	0.7498	0.7500
-2	0.0034	0.0052	0.2449	0.7352	0.7498	0.7500
0	0.2311	0.2315	0.2792	0.6933	0.7498	0.7500
2	0.5441	0.5442	0.5473	0.5568	0.7065	0.7495
4	0.5462	0.5463	0.5516	0.5568	0.5624	0.7066
6	0.5462	0.5464	0.5516	0.5560	0.5558	0.5624

TABLE 4.1

Asymptotic error reduction rates $e_{\text{alg}}^{(l+1)}/e_{\text{alg}}^{(l)}$ for $L = 2$ and different values of $E_\omega = 10^{\text{par}_E} E_\Xi$, $\rho_\omega = 10^{\text{par}_\rho} \rho_\Xi$ with $\text{par}_\rho, \text{par}_E \in \{-4, -2, 0, 2, 4, 6\}$.

$\text{par}_E \setminus \text{par}_\rho$	-4	-2	0	2	4	6
-4	0.0001	0.0043	0.3210	0.9196	0.9373	0.9375
-2	0.0039	0.0059	0.2887	0.9177	0.9373	0.9375
0	0.2617	0.2621	0.3159	0.8144	0.9373	0.9375
2	0.6063	0.6063	0.6095	0.6240	0.8298	0.9355
4	0.6090	0.6091	0.6139	0.6193	0.6302	0.8300
6	0.6091	0.6091	0.6138	0.6195	0.6194	0.6303

TABLE 4.2

Asymptotic error reduction rates $e_{\text{alg}}^{(l+1)}/e_{\text{alg}}^{(l)}$ for $L = 4$ and different values of $E_\omega = 10^{\text{par}_E} E_\Xi$, $\rho_\omega = 10^{\text{par}_\rho} \rho_\Xi$ with $\text{par}_\rho, \text{par}_E \in \{-4, -2, 0, 2, 4, 6\}$.

Algorithm 2 Dirichlet–Neumann coupling

Starting from some initial guess $\hat{\mathbf{z}}^{(0)} := \left(\mathbf{u}_{\Gamma,j}^{H,(0)}, \mathbf{u}_{\Gamma,j}^{h,(0)}, \boldsymbol{\zeta}_{\Gamma,j}^{h,(0)} \right)$, compute sequentially for $l = 0, 1, \dots$

(i) Solve problem on coarse space $\mathbf{V}^H|_\Xi$ with boundary load on Γ inherited from fine computation on ω :

$$S_\Xi^H \delta \mathbf{u}_{\Gamma,j}^{H,(l)} = \bar{\boldsymbol{\rho}}_{\Xi,j-1}^H - S_\Xi^H \mathbf{u}_{\Gamma,j}^{H,(l)} + (D^{hH})^T \boldsymbol{\zeta}_{\Gamma,j}^{h,(l)},$$

(ii) Solve problem on fine space \mathbf{V}^h with weakly imposed trace on Γ inherited from coarse computation on Ω :

$$\begin{pmatrix} S_\omega^h & (D^{hh})^T \\ D^{hh} & \mathbf{0} \end{pmatrix} \begin{pmatrix} \delta \mathbf{u}_{\Gamma,j}^{h,(l)} \\ \delta \boldsymbol{\zeta}_{\Gamma,j}^{h,(l)} \end{pmatrix} = \begin{pmatrix} \mathbf{r}_\omega^{h,(l)} \\ \boldsymbol{\nu}_\Gamma^{h,(l)} \end{pmatrix} + \begin{pmatrix} \mathbf{0} \\ D^{hH} \delta \mathbf{u}_{\Gamma,j}^{H,(l)} \end{pmatrix},$$

(iii) Update the solution vector:

$$\hat{\mathbf{z}}^{(l+1)} := \hat{\mathbf{z}}^{(l)} + \delta \hat{\mathbf{z}}^{(l)}.$$

The residuals $\mathbf{r}_\omega^{h,(l)}$, $\boldsymbol{\nu}_\Gamma^{h,(l)}$ are defined in (3.9c), (3.9d).

4.4. Comparison with classical Dirichlet–Neumann algorithm. In this subsection, we compare the performance of Algorithm 1 with that of a Dirichlet–Neumann coupling on the subdomains ω (Dirichlet) and Ξ (Neumann). This well-known algorithm (see, e.g., [4, 10, 50, 51]) can be implemented as stated in Algorithm 2. The left picture of Figure 4.8 shows the error decay of the relative algebraic energy error $e_{\text{alg}}^{(l)}$ for the static test setting from Subsection 4.2 with $L = 0$, different material coefficients $E_\omega = 10^{\text{par}} E_\Xi$, $\text{par} \in \{0, \dots, 5\}$, and suitable damping parameters α such that the algorithm converges. The right picture displays the quantity $(1 - e_{\text{alg}}^{(l+1)})/e_{\text{alg}}^{(l)}$, again for different material parameters. We remark that the results for $L \in \{0, 1, 2, 3, 4\}$ are overall

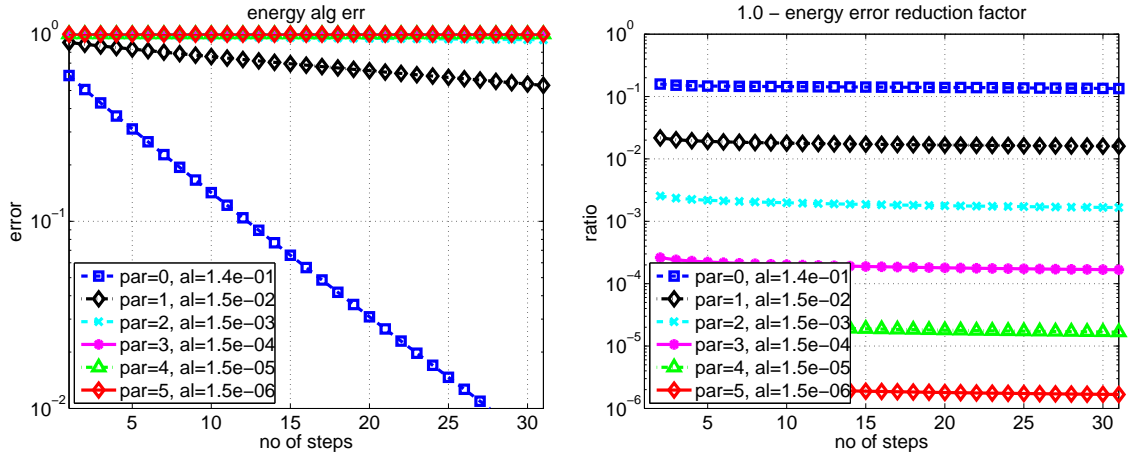


FIGURE 4.8. *Rel. alg. energy error* $e_{alg}^{(l)}$ for Dirichlet–Neumann coupling with $\varrho = 0$, $E_\omega = 10^{par} E_\Xi$, $par \in \{0, \dots, 5\}$ with respect to l ; left: $e_{alg}^{(l)}$; right: $(1 - e_{alg}^{(l+1)}) / e_{alg}^{(l)}$.

independent of L and are hence omitted in Figure 4.8. One can observe that a strong damping is necessary to ensure the convergence of the Dirichlet–Neumann algorithm, that its convergence rate is strongly dependent of the jump in the material parameters, and that its performance is much worse than that of Algorithm 1 even for the case $par = 0$.

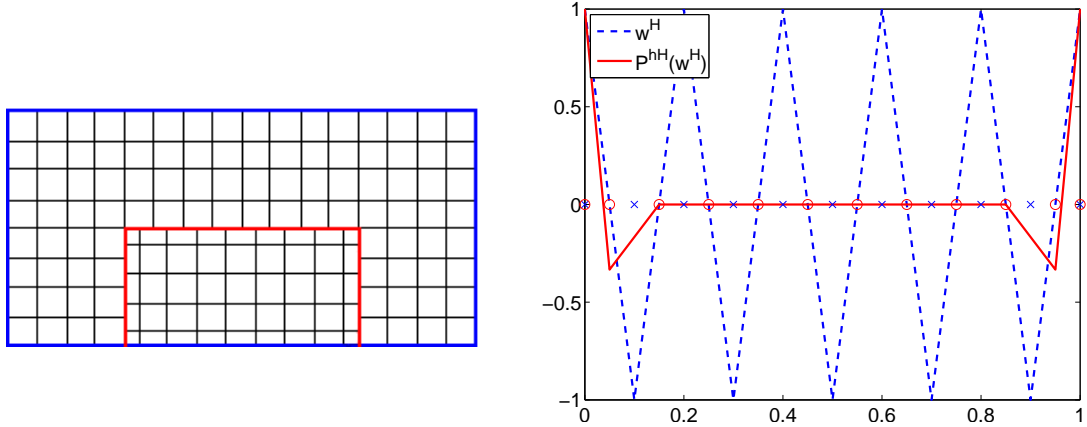


FIGURE 4.9. *Triangulation of Ω with nonnested trace spaces*; left: \mathcal{T}^H and \mathcal{T}^h ; right: trace function $\mathbf{w}^H \in \mathbf{W}_\Gamma^H$ and corresponding image $P^{hH}(\mathbf{w}^H) \in \mathbf{W}_\Gamma^h$ with $\|P^{hH}(\mathbf{w}^H)\|_{1/2,\Gamma} = c_p(H)\|\mathbf{w}^H\|_{1/2,\Gamma}$ and $c_p(H) \rightarrow 0$ for $H \rightarrow 0$.

4.5. Algebraic error for nonnested trace spaces. Next, we investigate the case that the finite element and trace spaces are not nested. For this, we consider the same domains Ω , ω as described in Section 4.1 but now choose a different triangulation \mathcal{T}^h on ω , as depicted on the left of Figure 4.9. One can see that $\mathbf{W}_\Gamma^H \not\subset \mathbf{W}_\Gamma^h$; furthermore, there exist functions $\mathbf{w}^H \in \mathbf{W}_\Gamma^H$, like the one sketched on the right of Figure 4.9, such that (2.14) only holds for $c_p(H)$ depending on H and $c_p(H) \rightarrow 0$ for $H \rightarrow 0$. Hence, Assumption 2.3 is not satisfied for this discretization.

First, we test the performance of Algorithm 1 for these nonnested trace spaces of grid size $h = H = 2^{-3-R_H}$, $R_H \in \{0, 1, 2, 3\}$, for the static case, i.e., we set $\varrho = 0$ and take the problem setting from Subsection 4.2. In Figure 4.10, the convergence for a high jump in the elasticity module $E_\omega = 10^5 E_\Xi$ is shown. One can see that the error reduction is considerably slower compared to the case of nested trace spaces and converges for $H \rightarrow 0$ to a value close to one; furthermore, the

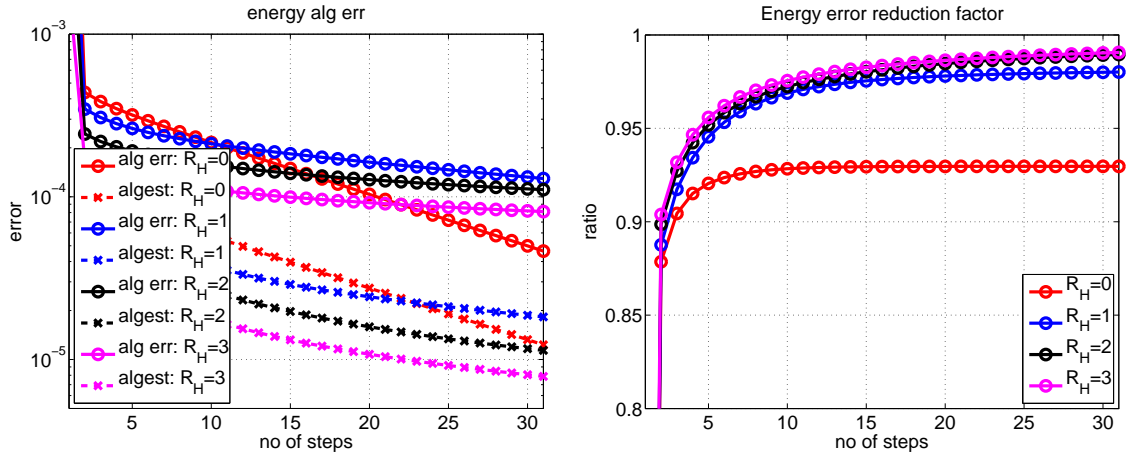


FIGURE 4.10. Performance of Algorithm 1 for $E_\omega = 10^5 E_\Xi$ and $R_H \in \{0, 1, 2, 3\}$; left: true $e_{alg}^{(l)}$ and estimated $\eta_{alg}^{(l)}$ relative algebraic energy error; right: error reduction factor $e_{alg}^{(l+1)}/e_{alg}^{(l)}$.

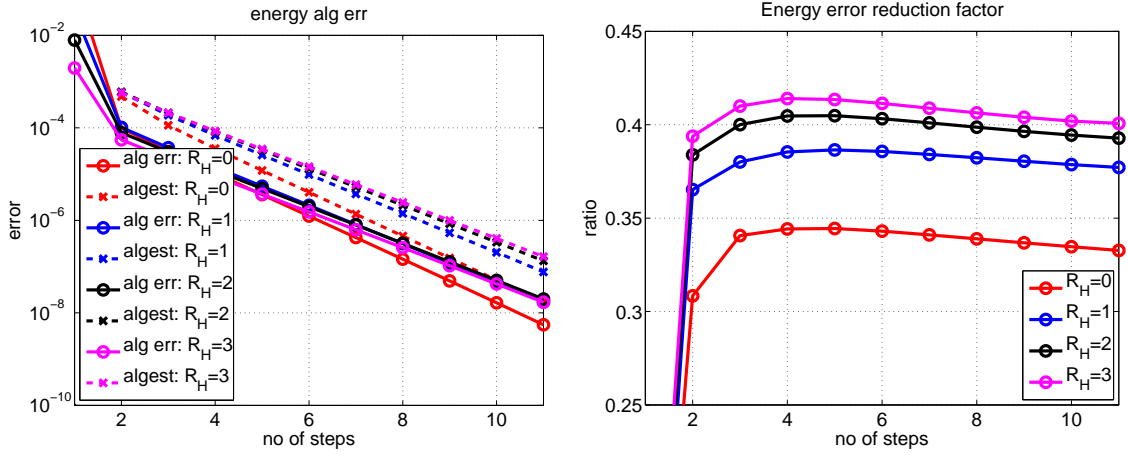


FIGURE 4.11. Performance of modified Algorithm 1 for $E_\omega = 10^5 E_\Xi$ and $R_H \in \{0, 1, 2, 3\}$; left: true $e_{alg}^{(l)}$ and estimated $\eta_{alg}^{(l)}$ relative algebraic energy error; right: error reduction factor $e_{alg}^{(l+1)}/e_{alg}^{(l)}$.

left picture shows that the algebraic error estimator (3.33) strongly underestimates the true value.

Hence, we try to achieve a better convergence rate by using the nonsymmetric modification of Algorithm 1 stated on page 22, i.e., we replace the Schur matrix S_ω^H by the matrix $S_\omega^H Q^{HH}$ with $Q^{HH} = \Pi^{Hh} \Pi^{hH}$. For the example considered here, this modification indeed improves the convergence, as the results of Figures 4.11 and 4.12 show. The former figure demonstrates that the error decay of the modified version is comparable to the results of Algorithm 1 for nested spaces (cf. Figure 4.2 and 4.4). In Figure 4.12, we have fixed $R_H = 3$ and compare the error reduction factors for the original and modified algorithm for different material parameters. One can observe that the nonsymmetric version of Algorithm 1 shown on the right side gives much better results than the unmodified algorithm depicted on the left side.

Next, we apply the algorithm to the dynamic problem setting of Subsection 4.3 and test different combinations for the material parameters $E_\omega = 10^{\text{par}_E} E_\Xi$, $\varrho_\omega = 10^{\text{par}_\varrho} \varrho_\Xi$ with $\text{par}_\varrho, \text{par}_E \in \{0, 2, 4, 6\}$. The asymptotic error reduction rates for $R_H \in \{1, 3\}$ are given in Tables 4.3 and 4.4; the results for the unmodified algorithm are summarized on the left side of the table, and those for the modified version are given on the right side. One can observe that the performance of Algorithm 1 degrades if at least one of the two ratios E_ω/E_Ξ , $\varrho_\omega/\varrho_\Xi$ is large, which agrees with

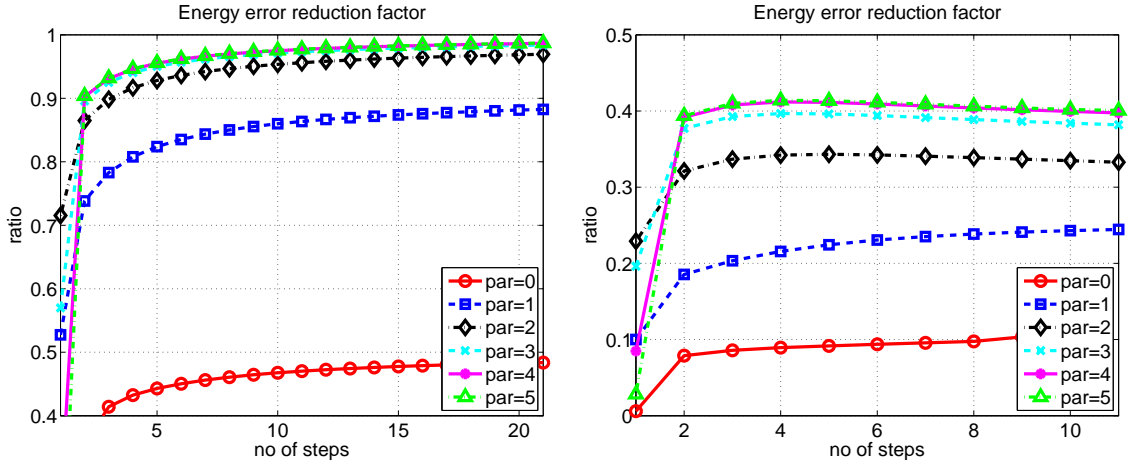


FIGURE 4.12. Error reduction factor of Algorithm 1 for $R_H = 3$ and $E_\omega = 10^{\text{par}} \cdot E_\Xi$, $\text{par} \in \{0, \dots, 5\}$; left: unmodified version; right: modified version.

$\text{par}_E \setminus \text{par}_\varrho$	0	2	4	6	0	2	4	6
0	0.4704	0.8705	0.9700	0.9716	0.1260	0.4101	0.5773	0.5952
2	0.9680	0.9360	0.9651	0.9695	0.3302	0.3455	0.5249	0.5934
4	0.9803	0.9472	0.9457	0.9660	0.3723	0.3737	0.3819	0.5369
6	0.9804	0.9437	0.9459	0.9458	0.4026	0.3301	0.3742	0.3824

TABLE 4.3

Asymptotic error reduction rates $e_{\text{alg}}^{(l+1)}/e_{\text{alg}}^{(l)}$ for $R_H = 1$ and different values of $E_\omega = 10^{\text{par}_E} E_\Xi$, $\varrho_\omega = 10^{\text{par}_\varrho} \varrho_\Xi$ with $\text{par}_\varrho, \text{par}_E \in \{0, 2, 4, 6\}$; left values: unmodified version; right values: modified version.

$\text{par}_E \setminus \text{par}_\varrho$	0	2	4	6	0	2	4	6
0	0.4721	0.8589	0.9677	0.9950	0.1118	0.3347	0.6001	0.5840
2	0.9722	0.9690	0.9801	0.9907	0.3246	0.3185	0.5036	0.5896
4	0.9880	0.9881	0.9853	0.9894	0.3917	0.3861	0.3643	0.4260
6	0.9884	0.9893	0.9874	0.9855	0.4131	0.4020	0.3920	0.3696

TABLE 4.4

Asymptotic error reduction rates $e_{\text{alg}}^{(l+1)}/e_{\text{alg}}^{(l)}$ for $R_H = 3$ and different values of $E_\omega = 10^{\text{par}_E} E_\Xi$, $\varrho_\omega = 10^{\text{par}_\varrho} \varrho_\Xi$ with $\text{par}_\varrho, \text{par}_E \in \{0, 2, 4, 6\}$; left values: unmodified version; right values: modified version.

the results of Lemma 3.9. But the nonsymmetric modification improves the convergence for either case.

5. Alternative coupling algorithm. In this section, we sketch the construction of a different iterative algorithm for the solution of the mortar system (2.33) in case that the Lagrange multiplier is associated with the coarse side \mathcal{G}^H ; then, (2.33) reads

$$\begin{pmatrix} S_\Xi^H & \mathbf{0} & -(D_\Gamma^{HH})^T \\ \mathbf{0} & S_\omega^h & (D_\Gamma^{Hh})^T \\ -D_\Gamma^{HH} & D_\Gamma^{Hh} & \mathbf{0} \end{pmatrix} \begin{pmatrix} \mathbf{u}_{\Gamma,j}^H \\ \mathbf{u}_{\Gamma,j}^h \\ \zeta_{\Gamma,j}^H \end{pmatrix} = \begin{pmatrix} \bar{\varrho}_{\Xi,j-1}^H \\ \bar{\varrho}_{\omega,j-1}^h \\ \mathbf{0} \end{pmatrix}. \quad (5.1)$$

The idea of the algorithm is to obtain an approximation of the Lagrange multiplier ζ_Γ^H from an auxiliary coarse problem, solve a Neumann problem on ω with ζ_Γ^H applied as surface load, and perform the backcoupling via the fine trace \mathbf{u}_Γ^h . For ease of notation, we present this algorithm only for the case that both matrices S_Ξ^H, S_ω^h defined in (2.32) are invertible, which is the case if $\varrho_\Theta > 0$ or $\text{meas}(\Gamma_D \cap \partial\Theta) > 0$ holds for $\Theta \in \{\Xi, \omega\}$. In Subsection 5.5, we describe the modifications

that are necessary to adopt the algorithm and the proofs to the case that one of the matrices is singular.

5.1. Derivation. Analogously to (3.1), we add an additional variable and a further line to the mortar system (5.1):

$$\underbrace{\begin{pmatrix} S_{\Xi}^H & \mathbf{0} & \mathbf{0} & -(D_{\Gamma}^{HH})^T \\ \mathbf{0} & S_{\omega}^H & \mathbf{0} & (D_{\Gamma}^{HH})^T \\ -D_{\Gamma}^{HH} & \mathbf{0} & D_{\Gamma}^{Hh} & \mathbf{0} \\ \mathbf{0} & \mathbf{0} & S_{\omega}^h & (D_{\Gamma}^{Hh})^T \end{pmatrix}}_{=: \hat{G}_n} \underbrace{\begin{pmatrix} \mathbf{u}_{\Gamma,j}^H \\ \mathbf{w}_{\Gamma,j}^H \\ \mathbf{u}_{\Gamma,j}^h \\ \zeta_{\Gamma,j}^H \end{pmatrix}}_{=: \hat{\mathbf{z}}_n} = \underbrace{\begin{pmatrix} \bar{\boldsymbol{\rho}}_{\Xi,j-1}^H \\ \bar{\boldsymbol{\rho}}_{\omega,j-1}^H \\ \mathbf{0} \\ \bar{\boldsymbol{\rho}}_{\omega,j-1}^h \end{pmatrix}}_{=: \hat{\mathbf{F}}_n}. \quad (5.2)$$

This time, the auxiliary variable $\mathbf{w}_{\Gamma}^H \in \mathbb{R}^{d|\mathcal{N}_{\Gamma}^H|}$ can be interpreted as a coarse trace function on Γ . Solving (5.2) iteratively using the splitting $\hat{G}_n = (\hat{G}_n - \hat{K}_n) + \hat{K}_n$ with \hat{K}_n defined to be zero except for its third row which reads

$$\begin{pmatrix} \mathbf{0} & -D_{\Gamma}^{HH} & D_{\Gamma}^{Hh} & \mathbf{0} \end{pmatrix},$$

we obtain the iterative algorithm presented in Algorithm 3.

Algorithm 3 Two-way coupling scheme with Neumann problem on ω

Starting from some initial guess $\hat{\mathbf{z}}_n^{(0)}$, compute sequentially for $l = 0, 1, \dots$

(i) Solve problem on coarse space $\mathbf{V}_{\Xi}^H \oplus \mathbf{V}_{\omega}^H$ with jump in the traces on Γ inherited from fine computation on ω :

$$\begin{pmatrix} S_{\Xi}^H & \mathbf{0} & -(D_{\Gamma}^{HH})^T \\ \mathbf{0} & S_{\omega}^H & (D_{\Gamma}^{HH})^T \\ -D_{\Gamma}^{HH} & D_{\Gamma}^{HH} & \mathbf{0} \end{pmatrix} \begin{pmatrix} \delta \mathbf{u}_{\Gamma,j}^{H,(l)} \\ \delta \mathbf{w}_{\Gamma,j}^{H,(l)} \\ \delta \zeta_{\Gamma,j}^{H,(l)} \end{pmatrix} = \begin{pmatrix} \mathbf{r}_{\Xi}^{H,(l)} \\ \mathbf{r}_{\omega}^{H,(l)} \\ \boldsymbol{\nu}_{\Gamma}^{H,(l)} \end{pmatrix}, \quad (5.3)$$

(ii) Solve problem on fine space \mathbf{V}^h with surface load on Γ inherited from coarse computation on Ω :

$$S_{\omega}^h \delta \mathbf{u}_{\Gamma,j}^{h,(l)} = \mathbf{r}_{\omega}^{h,(l)} - (D_{\Gamma}^{Hh})^T \delta \zeta_{\Gamma,j}^{H,(l)}, \quad (5.4)$$

(iii) Update the solution vector:

$$\hat{\mathbf{z}}_n^{(l+1)} := \hat{\mathbf{z}}_n^{(l)} + \delta \hat{\mathbf{z}}_n^{(l)},$$

The residuals of (5.3), (5.4) are given by

$$\mathbf{r}_{\Xi}^{H,(l)} = \bar{\boldsymbol{\rho}}_{\Xi,j-1}^H - S_{\Xi}^H \mathbf{u}_{\Gamma,j}^{H,(l)} + (D_{\Gamma}^{HH})^T \zeta_{\Gamma,j}^{H,(l)}, \quad (5.5a)$$

$$\mathbf{r}_{\omega}^{H,(l)} = \bar{\boldsymbol{\rho}}_{\omega,j-1}^H - S_{\omega}^H \mathbf{w}_{\Gamma,j}^{H,(l)} - (D_{\Gamma}^{HH})^T \zeta_{\Gamma,j}^{H,(l)}, \quad (5.5b)$$

$$\boldsymbol{\nu}_{\Gamma}^{H,(l)} = D_{\Gamma}^{HH} \mathbf{u}_{\Gamma,j}^{H,(l)} - D_{\Gamma}^{Hh} \mathbf{u}_{\Gamma,j}^{h,(l)}, \quad (5.5c)$$

$$\mathbf{r}_{\omega}^{h,(l)} = \bar{\boldsymbol{\rho}}_{\omega,j-1}^h - S_{\omega}^h \mathbf{u}_{\Gamma,j}^{h,(l)} - (D_{\Gamma}^{Hh})^T \zeta_{\Gamma,j}^{H,(l)}. \quad (5.5d)$$

We remark that the coarse grid problem (5.3) can be condensed to

$$\begin{pmatrix} (S_{\Xi}^H + S_{\omega}^H) & \mathbf{0} \\ S_{\omega}^H & (D_{\Gamma}^{HH})^T \end{pmatrix} \begin{pmatrix} \delta \mathbf{u}_{\Gamma,j}^{H,(l)} \\ \delta \zeta_{\Gamma,j}^{H,(l)} \end{pmatrix} = \begin{pmatrix} \mathbf{r}_{\Xi}^{H,(l)} + \mathbf{r}_{\omega}^{H,(l)} + S_{\omega}^H [\mathbf{u}_{\Gamma,j}^{(l)}] \\ \mathbf{r}_{\omega}^{H,(l)} + S_{\omega}^H [\mathbf{u}_{\Gamma,j}^{(l)}] \end{pmatrix}$$

with $[\mathbf{u}_{\Gamma,j}^{(l)}] := \mathbf{u}_{\Gamma,j}^{H,(l)} - \Pi^{Hh} \mathbf{u}_{\Gamma,j}^{h,(l)}$, yielding the same matrix as the coarse grid problem (3.6) in Algorithm 1.

REMARK 5.1. After one iteration of Algorithm 3, i.e., for $l \geq 1$, the residuals (5.5a), (5.5b), (5.5d) vanish.

5.2. Error propagation. The error propagation of Algorithm 3 can be analysed with the same methods as in Section 3.2. First, we rewrite the mortar system (5.1) as a Schur complement system for $\zeta_{\Gamma,j}^H \in \mathbb{R}^{d|\mathcal{N}_\Gamma^H|}$ (for details on the computation, see [25, 43]):

$$\left((S_\Xi^H)^{-1} + \Pi^{Hh}(S_\omega^h)^{-1}(\Pi^{Hh})^T \right) (D_\Gamma^{HH})^T \zeta_{\Gamma,j}^H = \Pi^{Hh}(S_\omega^h)^{-1} \bar{\rho}_{\omega,j-1}^h - (S_\Xi^H)^{-1} \bar{\rho}_{\Xi,j-1}^H. \quad (5.6)$$

Analogously to Lemma 3.3, we get the following

LEMMA 5.2. Let $\zeta_{\Gamma,j}^H$ denote the exact solution of (5.6) and let $\zeta_{\Gamma,j}^{H,(l)}$, $l = 0, 1, \dots$, be the sequence of vectors obtained from Algorithm 3. For $l \geq 1$, the error $\mathbf{e}^{H,(l)} := (D_\Gamma^{HH})^T (\zeta_{\Gamma,j}^{H,(l)} - \zeta_{\Gamma,j}^H)$ satisfies the relation

$$\mathbf{e}^{H,(l+1)} = \left(Id - \left((S_\Xi^H)^{-1} + (S_\omega^H)^{-1} \right)^{-1} \left((S_\Xi^H)^{-1} + \Pi^{Hh}(S_\omega^h)^{-1}(\Pi^{Hh})^T \right) \right) \mathbf{e}^{H,(l)}. \quad (5.7)$$

Proof. We define the coarse trace function

$$\mathbf{w}_{\Gamma,j}^H := (S_\omega^H)^{-1} \left(\bar{\mathbf{f}}_\omega^H - (D_\Gamma^{HH})^T \zeta_{\Gamma,j}^H \right).$$

From (5.3) and (5.1), we get

$$\begin{pmatrix} S_\Xi^H & \mathbf{0} & -(D_\Gamma^{HH})^T \\ \mathbf{0} & S_\omega^H & (D_\Gamma^{HH})^T \\ -D_\Gamma^{HH} & D_\Gamma^{HH} & \mathbf{0} \end{pmatrix} \begin{pmatrix} \mathbf{u}_{\Gamma,j}^{H,(l+1)} - \mathbf{u}_{\Gamma,j}^H \\ \mathbf{w}_{\Gamma,j}^{H,(l+1)} - \mathbf{w}_{\Gamma,j}^H \\ \zeta_{\Gamma,j}^{H,(l+1)} - \zeta_{\Gamma,j}^H \end{pmatrix} = \begin{pmatrix} \mathbf{0} \\ \mathbf{0} \\ \boldsymbol{\rho}^{H,(l)} \end{pmatrix}, \quad (5.8)$$

with

$$\begin{aligned} \boldsymbol{\rho}^{H,(l)} &= D_\Gamma^{HH} \left(\mathbf{w}_{\Gamma,j}^{H,(l)} - \mathbf{w}_{\Gamma,j}^H - \mathbf{u}_{\Gamma,j}^{H,(l)} + \mathbf{u}_{\Gamma,j}^H \right) + D_\Gamma^{HH} \left(\delta \mathbf{w}_{\Gamma,j}^{H,(l)} - \delta \mathbf{u}_{\Gamma,j}^{H,(l)} \right) \\ &= D_\Gamma^{HH} \left(\mathbf{w}_{\Gamma,j}^{H,(l)} - \mathbf{w}_{\Gamma,j}^H - \mathbf{u}_{\Gamma,j}^{H,(l)} + \mathbf{u}_{\Gamma,j}^H \right) + D_\Gamma^{HH} \mathbf{u}_{\Gamma,j}^{H,(l)} - D_\Gamma^{HH} \mathbf{u}_{\Gamma,j}^{h,(l)} \\ &= D_\Gamma^{HH} \left(\mathbf{w}_{\Gamma,j}^{H,(l)} - \mathbf{w}_{\Gamma,j}^H \right) - D_\Gamma^{Hh} \left(\mathbf{u}_{\Gamma,j}^{h,(l)} - \mathbf{u}_{\Gamma,j}^h \right). \end{aligned}$$

From (5.8), we obtain

$$\begin{aligned} \mathbf{u}_{\Gamma,j}^{H,(l+1)} - \mathbf{u}_{\Gamma,j}^H &= (S_\Xi^H)^{-1} \mathbf{e}^{H,(l+1)}, \\ \mathbf{w}_{\Gamma,j}^{H,(l+1)} - \mathbf{w}_{\Gamma,j}^H &= -(S_\omega^H)^{-1} \mathbf{e}^{H,(l+1)}, \end{aligned}$$

whereas (5.4) and (5.1) yield

$$\mathbf{u}_{\Gamma,j}^{h,(l+1)} - \mathbf{u}_{\Gamma,j}^h = -(S_\omega^h)^{-1} (\Pi^{Hh})^T \mathbf{e}^{H,(l+1)}.$$

For $l \geq 1$, the above relations also hold for the previous iteration with (l) instead of $(l+1)$. Hence, (5.8)₃ gives

$$\begin{aligned} & D_\Gamma^{HH} \left(\mathbf{w}_{\Gamma,j}^{H,(l+1)} - \mathbf{w}_{\Gamma,j}^H \right) - D_\Gamma^{HH} \left(\mathbf{u}_{\Gamma,j}^{H,(l+1)} - \mathbf{u}_{\Gamma,j}^H \right) \\ &= -D_\Gamma^{HH} (S_\omega^H)^{-1} \mathbf{e}^{H,(l+1)} - D_\Gamma^{HH} (S_\Xi^H)^{-1} \mathbf{e}^{H,(l+1)} \\ &= \boldsymbol{\rho}^{H,(l)} = -D_\Gamma^{HH} (S_\omega^H)^{-1} \mathbf{e}^{H,(l)} + D_\Gamma^{Hh} (S_\omega^h)^{-1} (\Pi^{Hh})^T \mathbf{e}^{H,(l)}. \end{aligned}$$

Multiplication with $-(D_\Gamma^{HH})^{-1}$ from the left finally leads to

$$\left((S_\Xi^H)^{-1} + (S_\omega^H)^{-1} \right) \mathbf{e}^{H,(l+1)} = \left((S_\omega^H)^{-1} - \Pi^{Hh} (S_\omega^h)^{-1} (\Pi^{Hh})^T \right) \mathbf{e}^{H,(l)}.$$

□

REMARK 5.3. Again, if the coarse and the fine grid on ω coincide, we get $\Pi^{Hh} = Id$, $(S_\omega^H)^{-1} = (S_\omega^h)^{-1}$, and Lemma 5.2 implies the convergence of Algorithm 3 after at most two steps.

Equation (5.7) illustrates that the difference between Algorithm 3 and a Neumann–Dirichlet coupling with ω as the Neumann subdomain is the additional term of $(S_\omega^H)^{-1}$ in the first factor.

5.3. Condition number analysis. The spectral equivalence of the matrices $(S_\omega^H)^{-1}$ and $\Pi^{Hh}(S_\omega^h)^{-1}(\Pi^{Hh})^T$ is the topic of the following

THEOREM 5.4. *Assume that the material parameters E, ν, ρ satisfy the estimates (2.2) on ω , and let Assumption 2.4 hold. Furthermore, assume that the mass contribution can be bounded by the stiffness term, i.e., that there exists a constant C_{mass} such that $\frac{\rho_\omega}{\Delta t^2} \leq C_{\text{mass}} \frac{E_\omega}{h^2}$. Then, there exists constants c_*, C_* independent of the diameter of ω, h, H and the values E_ω, ρ_ω of (2.2), such that the following estimates are satisfied for any function $\mathbf{f}_\Gamma^H \in (\mathbf{W}_\Gamma^H)'$:*

$$c_* \left((S_\omega^H)^{-1} \mathbf{f}_\Gamma^H, \mathbf{f}_\Gamma^H \right) \leq \left(\Pi^{Hh} (S_\omega^h)^{-1} (\Pi^{Hh})^T \mathbf{f}_\Gamma^H, \mathbf{f}_\Gamma^H \right) \leq C_* \left((S_\omega^H)^{-1} \mathbf{f}_\Gamma^H, \mathbf{f}_\Gamma^H \right). \quad (5.9)$$

The constant c_* in (5.9) depends on the value of c_p^* from Assumption 2.4; further, if $\frac{\rho_\omega}{\Delta t^2} \gg \frac{E_\omega}{h^2}$, C_* can depend on $\frac{H}{h}$.

Proof. Due to the positive definiteness of S_ω^m , $m \in \{h, H\}$, assumed at the beginning of this section, we can define the ‘‘energy’’ trace norm given by

$$\|\mathbf{w}_\Gamma^m\|_{S_\omega^m} := (\mathbf{w}_\Gamma^m, S_\omega^m \mathbf{w}_\Gamma^m)^{1/2}, \quad \mathbf{w}_\Gamma^m \in \mathbf{W}_\Gamma^m. \quad (5.10)$$

Further, we use (5.10) to define a discrete dual norm for functions $\mathbf{f}_\Gamma^m \in (\mathbf{W}_\Gamma^m)'$:

$$\|\mathbf{f}_\Gamma^m\|_{(S_\omega^m)'} := \sup_{\mathbf{w}_\Gamma^m \in \mathbf{W}_\Gamma^m} \frac{(\mathbf{w}_\Gamma^m, \mathbf{f}_\Gamma^m)}{\|\mathbf{w}_\Gamma^m\|_{S_\omega^m}}. \quad (5.11)$$

This norm can be used to express the terms in (5.9), because we have (see, e.g., [21])

$$\|\mathbf{f}_\Gamma^m\|_{(S_\omega^m)'}^2 = ((S_\omega^m)^{-1} \mathbf{f}_\Gamma^m, \mathbf{f}_\Gamma^m).$$

Thus, (5.9) is equivalent to

$$c_* \|\mathbf{f}_\Gamma^H\|_{(S_\omega^H)'}^2 \leq \|(\Pi^{Hh})^T \mathbf{f}_\Gamma^H\|_{(S_\omega^h)'}^2 \leq C_* \|\mathbf{f}_\Gamma^H\|_{(S_\omega^H)'}^2. \quad (5.12)$$

In order to show (5.12), we need the inequalities

$$\|\Pi^{Hh} \mathbf{w}_\Gamma^h\|_{S_\omega^H} \leq \bar{C} \|\mathbf{w}_\Gamma^h\|_{S_\omega^h} \quad \|\hat{\mathbf{w}}_\Gamma^h\|_{S_\omega^h} \leq C_{c_p^*} \|\mathbf{w}_\Gamma^H\|_{S_\omega^H}, \quad (5.13)$$

with the function $\hat{\mathbf{w}}_\Gamma^h$ from Assumption 2.4 and $C_{c_p^*}$ possibly depending on the value c_p^* . The first inequality of (5.13) can be shown exactly as (3.24) in the proof of Theorem 3.6, using the functions $\hat{\mathbf{v}}^h, \hat{\mathbf{v}}^H$ defined in (3.22) and the stability (3.17a), (3.18) of Z_ω^H :

$$\begin{aligned} k_\omega(\hat{\mathbf{v}}^H, \hat{\mathbf{v}}^H) &\leq C \left(E_\omega |Z_\omega^H \hat{\mathbf{v}}^h|_{\hat{\mathbf{V}}(\omega)}^2 + \frac{\rho_\omega}{\Delta t^2} \|Z_\omega^H \hat{\mathbf{v}}^h\|_{0,\omega}^2 \right) \\ &\leq C \left(E_\omega |\hat{\mathbf{v}}^h|_{\hat{\mathbf{V}}(\omega)}^2 + \frac{\rho_\omega}{\Delta t^2} \frac{H}{h} \|\hat{\mathbf{v}}^h\|_{0,\omega}^2 \right) \leq \bar{C} k_\omega(\hat{\mathbf{v}}^h, \hat{\mathbf{v}}^h). \end{aligned}$$

However, if the mass contribution is dominant, \bar{C} depends on the value $\frac{H}{h}$ which comes from the non-uniform estimate (3.18).

For the second part of (5.13), we proceed analogously to the proof of (3.27) but use a different extension operator $T_\omega^h : \mathbf{W}_\Gamma^h \rightarrow \mathbf{V}_\omega^h$ instead of R_ω^h in (3.25). The operator T_ω^h is chosen such that $\hat{\mathbf{w}}_\Gamma^h$ is extended to a strip of width H around Γ , yielding the estimates

$$\|T_\omega^h \hat{\mathbf{w}}_\Gamma^h\|_{0,\omega}^2 \leq CH \|\hat{\mathbf{w}}_\Gamma^h\|_{0,\Gamma}^2, \quad |T_\omega^h \hat{\mathbf{w}}_\Gamma^h|_{1,\omega}^2 \leq CH^{-1} \|\hat{\mathbf{w}}_\Gamma^h\|_{0,\Gamma}^2.$$

With this, we obtain

$$\begin{aligned} k_\omega(\hat{\mathbf{v}}^h, \hat{\mathbf{v}}^h) &\leq C \left(E_\omega |Z_\omega^h \hat{\mathbf{v}}^H|_{\hat{\mathbf{V}}(\omega)}^2 + \frac{\rho_\omega}{\Delta t^2} \|Z_\omega^h \hat{\mathbf{v}}^H\|_{0,\omega}^2 \right) \\ &\quad + C \left(E_\omega |T_\omega^h(\text{Id} - P^{hH} P^{Hh}) \hat{\mathbf{w}}_\Gamma^h|_{1,\omega}^2 + \frac{\rho_\omega}{\Delta t^2} \|T_\omega^h(\text{Id} - P^{hH} P^{Hh}) \hat{\mathbf{w}}_\Gamma^h\|_{0,\omega}^2 \right). \end{aligned} \quad (5.14)$$

The last term in (5.14) can be bounded using Assumption 2.4 for $l = 0$:

$$\begin{aligned} \|T_\omega^h(\text{Id} - P^{hH}P^{Hh})\hat{\mathbf{w}}_\Gamma^h\|_{0,\omega}^2 &\leq CH\|(\text{Id} - P^{hH}P^{Hh})\hat{\mathbf{w}}_\Gamma^h\|_{0,\Gamma}^2 \\ &\leq CH\|\hat{\mathbf{w}}_\Gamma^h\|_{0,\Gamma}^2 \leq C(c_p^*)^{-2}H\|\mathbf{w}_\Gamma^H\|_{0,\Gamma}^2 \\ &\leq C(c_p^*)^{-2}\|R_\omega^H\mathbf{w}_\Gamma^H\|_{0,\omega}^2 \leq C(c_p^*)^{-2}\|\hat{\mathbf{v}}_\Gamma^H\|_{0,\omega}^2, \end{aligned}$$

whereas the second-to-last term in (5.14) is estimated using Assumption 2.4 for $l = \frac{1}{2}$:

$$\begin{aligned} |T_\omega^h(\text{Id} - P^{hH}P^{Hh})\hat{\mathbf{w}}_\Gamma^h|_{1,\omega}^2 &\leq CH^{-1}\|(\text{Id} - P^{hH}P^{Hh})\hat{\mathbf{w}}_\Gamma^h\|_{0,\Gamma}^2 \leq C|\hat{\mathbf{w}}_\Gamma^h|_{\widetilde{\mathbf{W}}_\Gamma(\omega)}^2 \\ &\leq C(c_p^*)^{-2}|\mathbf{w}_\Gamma^H|_{\widetilde{\mathbf{W}}_\Gamma(\omega)}^2 \leq C(c_p^*)^{-2}|\hat{\mathbf{v}}_\Gamma^H|_{\widetilde{\mathbf{V}}(\omega)}^2. \end{aligned} \quad (5.15)$$

The second estimate in (5.15) can be shown analogously to the inequality (3.26).

All together, we obtain the second inequality of (5.13) with a constant $C_{c_p^*}$ independent of the discretization and material parameters but dependent on the constant c_p^* from Assumption 2.4.

With (5.13), (5.12) follows from

$$\begin{aligned} \sup_{\mathbf{w}_\Gamma^h \in \mathbf{W}_\Gamma^h} \frac{(\mathbf{w}_\Gamma^h, (\Pi^{Hh})^T \mathbf{f}_\Gamma^H)}{\|\mathbf{w}_\Gamma^h\|_{S_\omega^h}} &\leq \bar{C}^{-1} \sup_{\mathbf{w}_\Gamma^h \in \mathbf{W}_\Gamma^h} \frac{(\Pi^{Hh} \mathbf{w}_\Gamma^h, \mathbf{f}_\Gamma^H)}{\|\Pi^{Hh} \mathbf{w}_\Gamma^h\|_{S_\omega^H}} \leq C_* \sup_{\mathbf{w}_\Gamma^H \in \mathbf{W}_\Gamma^H} \frac{(\mathbf{w}_\Gamma^H, \mathbf{f}_\Gamma^H)}{\|\mathbf{w}_\Gamma^H\|_{S_\omega^H}}, \\ \sup_{\mathbf{w}_\Gamma^H \in \mathbf{W}_\Gamma^H} \frac{(\mathbf{w}_\Gamma^H, \mathbf{f}_\Gamma^H)}{\|\mathbf{w}_\Gamma^H\|_{S_\omega^H}} &\leq c_*^{-1} \sup_{\hat{\mathbf{w}}_\Gamma^h \in \mathbf{W}_\Gamma^h} \frac{(\Pi^{Hh} \hat{\mathbf{w}}_\Gamma^h, \mathbf{f}_\Gamma^H)}{\|\hat{\mathbf{w}}_\Gamma^h\|_{S_\omega^h}}, \end{aligned}$$

with constants c_* , C_* independent of H , h , Δt and the material parameters, but c_* dependent on the value of c_p^* from Assumption 2.4 and C_* possibly depending on $\frac{H}{h}$ if the mass contribution is dominant. \square Analogously to Lemma 3.9, we provide an alternative version of Theorem 5.4 which does not require Assumption 2.4; the proof can be performed similarly as for Lemma 3.9.

LEMMA 5.5. *Assume that the material parameters E , ν , ϱ satisfy the estimates (2.2) and in addition $E_\Xi \leq c_{par} E_\omega$, $\varrho_\Xi \leq c_{par} \varrho_\omega$ for some constant c_{par} . Then, there exists a constant $c_{par,*}$ independent of the diameter of ω , h , H such that the following estimates are satisfied for any function $\mathbf{f}_\Gamma^H \in (\mathbf{W}_\Gamma^H)'$:*

$$c_{par,*} \left(\left((S_\Xi^H)^{-1} + (S_\omega^H)^{-1} \right) \mathbf{f}_\Gamma^H, \mathbf{f}_\Gamma^H \right) \leq \left(\left((S_\Xi^H)^{-1} + \Pi^{Hh} (S_\omega^h)^{-1} (\Pi^{Hh})^T \right) \mathbf{f}_\Gamma^H, \mathbf{f}_\Gamma^H \right).$$

REMARK 5.6. *For dominating stiffness term, Lemma 3.9 can be applied if the patch ω has a smaller stiffness than the upper domain Ω_Ξ , whereas Lemma 5.5 is useful for the case that E_ω is larger than E_Ξ . This directly relates to the fact that the convergence of a Dirichlet–Neumann coupling is better if the Dirichlet subdomain has a smaller stiffness than the Neumann subdomain.*

5.4. Stopping criteria. For the estimation of the algebraic error, we observe that the only nonzero component of the residual vector for $l \geq 1$ is given by (5.5c). In order to obtain a suitable norm of this residual, we use the relation

$$\boldsymbol{\nu}_\Gamma^{H,(l)} = -D_\Gamma^{HH} \left((S_\Xi^H)^{-1} + (S_\omega^H)^{-1} \right) (D_\Gamma^{HH})^T \delta \boldsymbol{\zeta}_{\Gamma,j}^{H,(l)} \quad (5.16)$$

following from (5.3) to propose the following relative algebraic error estimator for $l \geq 1$:

$$(\eta_{\text{alg},n}^{(l)})^2 := \frac{- \left(\boldsymbol{\nu}_\Gamma^{H,(l)}, \delta \boldsymbol{\zeta}_{\Gamma,j}^{H,(l)} \right)}{\left(D_\Gamma^{HH} \left((S_\Xi^H)^{-1} + (S_\omega^H)^{-1} \right) (D_\Gamma^{HH})^T \boldsymbol{\zeta}_{\Gamma,j}^{H,(l)}, \boldsymbol{\zeta}_{\Gamma,j}^{H,(l)} \right)}. \quad (5.17)$$

The denominator can be simplified using (5.16).

5.5. Extension to singular subproblems. Because of the requirement $\text{meas}(\Gamma_D) > 0$, at most one of the matrices S_{Ξ}^H , S_{ω}^h can be singular. For the case that S_{ω}^h is invertible and S_{Ξ}^H is singular, Algorithm 3 can be performed as given above, (5.7) becomes

$$\mathbf{e}^{H,(l+1)} = \left(\text{Id} - \left(\text{Id} + S_{\Xi}^H (S_{\omega}^H)^{-1} \right)^{-1} \left(\text{Id} + S_{\Xi}^H \Pi^{Hh} (S_{\omega}^h)^{-1} (\Pi^{Hh})^T \right) \right) \mathbf{e}^{H,(l)},$$

and the results of both Theorem 5.4 and Lemma 5.5 still hold.

The case of a singular matrix S_{ω}^h needs somewhat more care; here, we need to decompose the space $\mathbf{V}_0(\omega)$ orthogonally into

$$\mathbf{V}_0(\omega) =: \mathcal{RB}_{\omega} \oplus \mathbf{V}^{\perp}(\omega)$$

and define the discrete subspaces

$$\mathbf{V}_{\omega}^{m,\perp} := \mathbf{V}_{\omega}^m \cap \mathbf{V}^{\perp}(\omega), \quad \mathbf{W}_{\Gamma}^{m,\perp} := (\mathbf{V}_{\omega}^{m,\perp})|_{\Gamma}, \quad m \in \{h, H\}.$$

Then, the patch subproblem (5.4) is only solved on $\mathbf{V}_{\omega}^{h,\perp}$ by means of a suitable pseudo-inverse $(S_{\omega}^h)^{\dagger}$ being the inverse of the restricted operator

$$S_{\omega}^{h,\perp} : \mathbf{W}_{\Gamma}^{h,\perp} \rightarrow \text{im}(S_{\omega}^h) : \mathbf{w}_{\Gamma}^h \mapsto S_{\omega}^h \mathbf{w}_{\Gamma}^h.$$

The missing rigid body modes are determined from the result of the global problem (5.3). We do not specify the technical details of the construction of $(S_{\omega}^h)^{\dagger}$ but refer to [56] and the references therein.

Replacing $(S_{\omega}^h)^{-1}$ and $(S_{\omega}^H)^{-1}$ in (5.7) by the pseudo-inverse matrices, the statement of Lemma 5.2 is still valid. Further, Theorem 5.4 also holds but is restricted to $\mathbf{f}_{\Gamma}^H \in \text{im}(S_{\omega}^h)$. In its proof, the definition (5.10) yields only a seminorm on \mathbf{W}_{Γ}^h but a norm on $\mathbf{W}_{\Gamma}^{h,\perp}$, such that we replace (5.11) by

$$\|\mathbf{f}_{\Gamma}^m\|_{(S_{\omega}^m)'} := \sup_{\mathbf{w}_{\Gamma}^m \in \mathbf{W}_{\Gamma}^{m,\perp}} \frac{(\mathbf{w}_{\Gamma}^m, \mathbf{f}_{\Gamma}^m)}{\|\mathbf{w}_{\Gamma}^m\|_{S_{\omega}^m}}, \quad \mathbf{f}_{\Gamma}^H \in \text{im}(S_{\omega}^h),$$

and use $\mathbf{w}_{\Gamma}^m \in \mathbf{W}_{\Gamma}^{m,\perp}$ instead of \mathbf{W}_{Γ}^m in the rest of the proof.

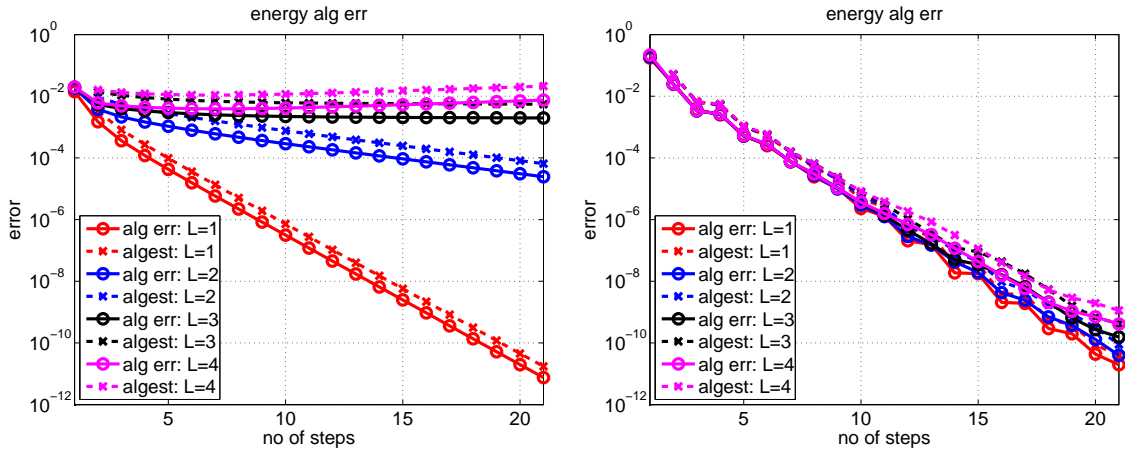


FIGURE 5.1. True $e_{\text{alg}}^{(l)}$ and estimated $\eta_{\text{alg}}^{(l)}$ relative algebraic energy error for Algorithm 3, $E_{\omega} = E_{\Xi}$ and $L \in \{1, 2, 3, 4\}$ with respect to l ; left: $\alpha = 1$; right: damped version with $\alpha = 0.87$.

5.6. Numerical results. In this subsection, the performance of Algorithm 3 and its damped version with a fixed damping factor α is tested numerically. For this, we apply the iterative scheme

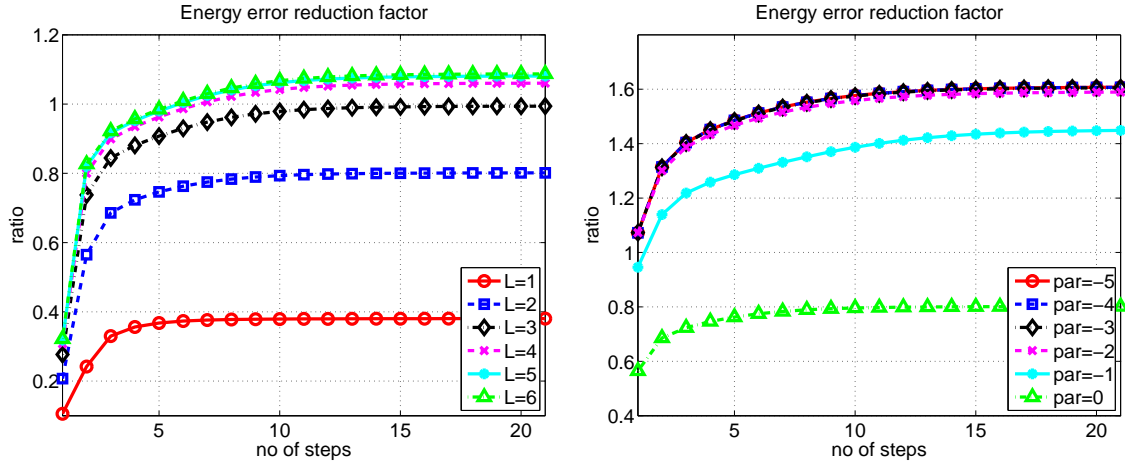


FIGURE 5.2. Error reduction factor $e_{\text{alg}}^{(l+1)}/e_{\text{alg}}^{(l)}$ for Algorithm 3 with respect to l ; left: $E_\omega = E_\Xi$ and $L \in \{1, \dots, 6\}$; right: $L = 2$ and $\text{par} \in \{-5, \dots, 0\}$.

to the test settings described in Sections 4.1 to 4.3 with nested finite element spaces, such that Assumption 2.4 is satisfied. Figure 5.1 shows the true algebraic error (4.1) and its estimated value (5.17) applied to the static problem with $\varrho = 0$ and $E_\omega = E_\Xi$, with no damping on the left and the damping parameter $\alpha = 0.87$ on the right side. In contrast to Algorithm 1, Algorithm 3 does not always converge if the finite element spaces are nested, as can be seen for the case $L \geq 4$. Nevertheless, the right picture in Figure 5.1 indicates that a suitably damped version of Algorithm 3 converges with a rate independent of L .

In Figure 5.2, the error quotient $e_{\text{alg}}^{(l+1)}/e_{\text{alg}}^{(l)}$ is shown for $E_\omega = E_\Xi$, $L \in \{1, \dots, 6\}$ on the left side, and for $L = 2$ and different material parameters $E_\omega = 10^{\text{par}} E_\Xi$, $\text{par} \in \{-5, \dots, 0\}$, on the right side. These results confirm the theoretical estimates of Theorem 5.4 that the largest eigenvalue of the iteration matrix in (5.7) is bounded from above by a value independent of L and par . The results for $\text{par} > 0$ are omitted because the algorithm converges quite fast in this case (cf. Tables 5.1 and 5.2 below). This is in contrast to Algorithm 1, where the speed of convergence is generally better for smaller values of E_ω , corresponding to par being negative.

$\text{par}_E \setminus \text{par}_\varrho$	-4	-2	0	2	4
-4	1.5344	3.3235	2.6359	0.1350	0.0006
-2	1.5914	1.5192	2.3174	0.1349	0.0006
0	0.9387	0.9350	0.7832	0.1286	0.0006
2	0.0565	0.0566	0.0561	0.0174	0.0005
4	0.0007	0.0007	0.0007	0.0005	0.0001

TABLE 5.1

Asymptotic error quotients $e_{\text{alg}}^{(l+1)}/e_{\text{alg}}^{(l)}$ for $L = 2$ and different values of $E_\omega = 10^{\text{par}_E} E_\Xi$, $\varrho_\omega = 10^{\text{par}_\varrho} \varrho_\Xi$ with $\text{par}_\varrho, \text{par}_E \in \{-4, -2, 0, 2, 4\}$.

Next, we consider the dynamic test setting of Subsection 4.3 and vary the material parameters $E_\omega = 10^{\text{par}_E} E_\Xi$, $\varrho_\omega = 10^{\text{par}_\varrho} \varrho_\Xi$. The corresponding error quotients for $L \in \{2, 4\}$ are summarized in Tables 5.1 and 5.2. One can observe that the quotients become worst for $\text{par}_E < \text{par}_\varrho \leq 0$, i.e., if the mass contribution on ω is dominating. Especially for the case $\text{par}_E = -4$, $\text{par}_\varrho = 0$, the error quotient seems to be proportional to $\frac{H}{h} = 2^L$.

In general, Algorithm 3 seems to be less efficient than Algorithm 1, such that we restrict ourselves to the latter one in the second part of this work.

$\text{par}_E \setminus \text{par}_\varrho$	-4	-2	0	2	4
-4	2.0880	10.8152	12.4981	0.6472	0.0035
-2	2.1075	2.0672	7.4568	0.6366	0.0035
0	1.2478	1.2429	1.0654	0.3368	0.0035
2	0.0686	0.0687	0.0686	0.0234	0.0011
4	0.0008	0.0008	0.0009	0.0006	0.0002

TABLE 5.2

Asymptotic error quotients $e_{\text{alg}}^{(l+1)}/e_{\text{alg}}^{(l)}$ for $L = 4$ and different values of $E_\omega = 10^{\text{par}_E} E_\Xi$, $\varrho_\omega = 10^{\text{par}_\varrho} \varrho_\Xi$ with $\text{par}_\varrho, \text{par}_E \in \{-4, -2, 0, 2, 4\}$.

Part II - Nonlinear case

6. Nonlinear setting. In this part, we extend the considerations of Part I to the nonlinear case by incorporating nonlinear effects like, e.g., geometrical or material nonlinearity, plasticity or contact. The latter two features can be described using additional inner or dual variables in addition to the displacement; we refer to Section 6.2 as well as to [30, 35] and the references therein for a possible formulation of the corresponding nonlinear equations.

In Subsection 6.1, the general nonlinear setting is sketched, followed by the conditions of dynamic frictional contact as an example of a nonlinear effect in Subsection 6.2. Possible approximate solution schemes using the overlapping domain decomposition approach are presented in Subsection 7. The following Section 8 contains several numerical examples including complex geometries, contact and nonlinear material laws. Finally, in Section 9, it is shown that the algorithm can be extended to the case of nearly incompressible material by employing a stable mixed discretization.

6.1. General equations. In comparison with the mortar system (2.28), the matrices K_Θ^m , $\Theta \in \{\Xi, \omega\}$, $m \in \{h, H\}$, are now replaced by nonlinear operators $\mathcal{K}_\Theta^m : \mathbf{V}_\Theta^m \rightarrow (\mathbf{V}_\Theta^m)'$. The general nonlinear version of the mortar coupled discrete problem (2.28) reads

$$\begin{pmatrix} \mathcal{K}_\Xi^H(\mathbf{u}_j^H) \\ \mathcal{K}_\omega^h(\mathbf{u}_j^h) \\ D^{hh}\mathbf{u}_j^h - D^{hH}\mathbf{u}_j^H \end{pmatrix} + \begin{pmatrix} -(D^{hH})^T \\ (D^{hh})^T \\ \mathbf{0} \end{pmatrix} \boldsymbol{\zeta}_{\Gamma,j}^h = \mathbf{0}. \quad (6.1)$$

Above, we have included the volume and surface forces as well as the terms from the last time step (2.27b) in the definition of the maps \mathcal{K}_Θ^m , i.e.,

$$\mathcal{K}_\Theta^m(\mathbf{u}_j^m) = \mathcal{K}_\Theta^m(\mathbf{u}_j^m, \mathbf{u}_{j-1}^m, \mathbf{v}_{j-1}^m),$$

but we omit the dependence on the latter two arguments for ease of notation. Further, the exact definition of \mathcal{K}_Θ^m depends on the kind of nonlinearity considered. For example, the Cauchy stress $\boldsymbol{\sigma}$ in (2.1) can be replaced by a nonlinear stress tensor \mathbf{s} . If additionally plastic effects or contact is included, \mathcal{K}_Θ^m also depends on inner plastic or dual contact variables [30]. In Subsection 6.2, we state the conditions of frictional contact as an example for a nonlinear problem with inequality constraints and sketch how these conditions can equivalently be reformulated as a set of semismooth equations. Hence, we assume in the following that (6.1) is a system of semismooth equations, enabling us to apply a generalized form of the Newton method for the solution of (6.1), namely a semismooth Newton method. We refer to [18] and the references therein for an overview of Newton methods and to [23, 24, 34] for the definition of semismoothness.

Similar to (2.33), (6.1) can also be formulated with respect to the interface variables only, by introducing nonlinear Dirichlet-to-Neumann operators $\mathcal{S}_\Theta^m : \mathbf{W}_\Gamma^m \rightarrow (\mathbf{W}_\Gamma^m)'$ defined by

$$\langle \mathcal{S}_\Theta^m \mathbf{u}_\Gamma^m, \mathbf{w}^m |_\Gamma \rangle_\Gamma = (\mathcal{K}_\Theta^m(\mathbf{u}^m), \mathbf{w}^m), \quad \mathbf{w}^m \in \mathbf{V}_\Theta^m, \quad (6.2)$$

where $\mathbf{u}^m \in \mathbf{V}_\Theta^m$ is such that $\mathbf{u}^m|_\Gamma = \mathbf{u}_\Gamma^m$ and

$$(\mathcal{K}_\Theta^m(\mathbf{u}^m), \hat{\mathbf{w}}^m) = 0, \quad \hat{\mathbf{w}}^m \in \mathbf{V}_\Theta^m, \quad \hat{\mathbf{w}}^m|_\Gamma = \mathbf{0}.$$

With this, (6.1) can be written as

$$\begin{pmatrix} \mathcal{S}_{\Xi}^H(\mathbf{u}_{\Gamma,j}^H) \\ \mathcal{S}_{\omega}^h(\mathbf{u}_{\Gamma,j}^h) \\ D_{\Gamma}^{hh}\mathbf{u}_{\Gamma,j}^h - \bar{D}_{\Gamma}^{hH}\mathbf{u}_{\Gamma,j}^H \end{pmatrix} + \begin{pmatrix} -(D_{\Gamma}^{hH})^T \\ (D_{\Gamma}^{hh})^T \\ \mathbf{0} \end{pmatrix} \zeta_{\Gamma,j}^h = \mathbf{0}. \quad (6.3)$$

6.2. Frictional contact. In this subsection, we present the conditions of frictional contact as a characteristic example for a nonlinear semismooth problem. We designate a part $\gamma \subset \Gamma_N$ of the Neumann boundary where the body Ω can come into contact with a fixed obstacle Ω_{obs} ; for the contact of several elastic bodies we refer to, e.g., [36, 37]. On γ , we enforce the Neumann conditions $-\boldsymbol{\sigma}\mathbf{n} = \boldsymbol{\lambda}$, where the contact stress $\boldsymbol{\lambda}$ is a priori unknown and has to be determined by the contact conditions.

As, in general, a detailed resolution of the contact area is desired, it is reasonable to assume that the patch ω is large enough to cover the whole contact boundary, i.e., $\bar{\gamma} \subset \partial\omega$. Further, we assume $\bar{\Gamma} \cap \bar{\gamma} = \emptyset$, $\bar{\Gamma}_D \cap \bar{\gamma} = \emptyset$ for simplicity and denote the set of degrees of freedom of \mathbf{V}_{ω}^m on γ by $\mathcal{N}_{\gamma}^m \subset \mathcal{N}^m$, $m \in \{h, H\}$.

The discrete conditions for normal contact with Coulomb or Tresca friction [42, 47, 60] can be described in terms of the fine scale displacement $\mathbf{u}_{\gamma}^h = (\mathbf{u}_p^h)_{p \in \mathcal{N}_{\gamma}^h}$ and the additional dual variable $\boldsymbol{\lambda}_{\gamma}^h = (\boldsymbol{\lambda}_p^h)_{p \in \mathcal{N}_{\gamma}^h}$. For the discretization of $\boldsymbol{\lambda}_{\gamma}^h$, we employ dual basis functions $\{\psi_p^h\}_{p \in \mathcal{N}_{\gamma}^h}$ which are characterized by a biorthogonality condition similar to (2.9). This allows for a separation of the contact conditions into separate constraints for each contact node $p \in \mathcal{N}_{\gamma}^h$ (see [35, 37] for more details). In order to state these condition, we split the displacement vector \mathbf{u}_p^h into its normal and tangential part according to $u_{p,n}^h := \mathbf{u}_p^h \cdot \mathbf{n}_p$, $\mathbf{u}_{p,t}^h := \mathbf{u}_p^h - u_{p,n}^h \mathbf{n}_p$, where the vector \mathbf{n}_p denotes the discrete unit outer normal of ω at $p \in \mathcal{N}_{\gamma}^h$. Similarly, we define the normal and tangential parts $\lambda_{pn}^h := \boldsymbol{\lambda}_p^h \cdot \mathbf{n}_p$, $\boldsymbol{\lambda}_{p,t}^h := \boldsymbol{\lambda}_p^h - \lambda_{pn}^h \mathbf{n}_p$ of the Lagrange multiplier. The constraints for normal contact employ the initial normal gap $g_{p,n}$ between the node p and the fixed obstacle Ω_{obs} ; taken at the time step t_j , they read

$$u_{p,j,n}^h - g_{p,n} \leq 0, \quad \lambda_{p,j,n}^h \geq 0, \quad \lambda_{p,j,n}^h (u_{p,j,n}^h - g_{p,n}) = 0. \quad (6.4)$$

The first inequality of (6.4) states the non-penetration condition at p , whereas the second one ensures that the force in normal direction is compressive. The last complementarity equation states that contact stresses can only develop if the gap is closed.

The constraints for frictional contact with either Coulomb or Tresca friction are given by

$$\begin{aligned} \|\boldsymbol{\lambda}_{p,j,t}^h\| &\leq g_{p,t} + \mathfrak{F}|\lambda_{p,j,n}^h|, \\ \|\boldsymbol{\lambda}_{p,j,t}^h\| &< g_{p,t} + \mathfrak{F}|\lambda_{p,j,n}^h| \Rightarrow \partial_{\Delta t} \mathbf{u}_{p,j,t}^h = \mathbf{0}, \\ \|\boldsymbol{\lambda}_{p,j,t}^h\| &= g_{p,t} + \mathfrak{F}|\lambda_{p,j,n}^h| \Rightarrow \exists \beta \geq 0 : \boldsymbol{\lambda}_{p,j,t}^h = \beta \partial_{\Delta t} \mathbf{u}_{p,j,t}^h. \end{aligned} \quad (6.5)$$

If the friction coefficient $\mathfrak{F} \geq 0$ is set to zero, the above inequalities describe the case of Tresca friction with the given friction bound $g_{p,t} \geq 0$, whereas for $g_{p,t} = 0$, the Coulomb friction law is obtained.

There are several possibilities to rewrite the inequality constraints (6.4), (6.5) as a set of nonsmooth equations [16, 24, 30, 35]; the form we propose employs the trial values

$$\lambda_{p,j,n}^{h,\text{tr}} := \lambda_{p,j,n}^h + c_n h_p^{-1} (u_{p,j,n}^h - g_{p,n}), \quad (6.6a)$$

$$\boldsymbol{\lambda}_{p,j,t}^{h,\text{tr}} := \boldsymbol{\lambda}_{p,j,t}^h + c_t h_p^{-1} \Delta t \partial_{\Delta t} \mathbf{u}_{p,j,t}^h. \quad (6.6b)$$

with the local mesh size h_p and some fixed constants $c_n, c_t > 0$, as well as the combined friction bound

$$\hat{g}_{p,j,t} := g_{p,t} + \mathfrak{F} \max(0, \lambda_{p,j,n}^{h,\text{tr}}).$$

Then, we can rewrite the contact conditions (6.4), (6.5) as

$$\mathbf{C}_\gamma^h(\mathbf{u}_{\gamma,j}^h, \boldsymbol{\lambda}_{\gamma,j}^h) := \left(C_p^h(\mathbf{u}_{p,j}^h, \boldsymbol{\lambda}_{p,j}^h) \right)_{p \in \mathcal{N}_\gamma^h} = \mathbf{0} \quad (6.7)$$

with

$$C_p^h(\mathbf{u}_{p,j}^h, \boldsymbol{\lambda}_{p,j}^h) := \begin{pmatrix} \lambda_{p,j,n}^h - \max\left(0, \lambda_{p,j,n}^{h,\text{tr}}\right) \\ \max\left(\hat{g}_{p,j,t}, \|\boldsymbol{\lambda}_{p,j,t}^{h,\text{tr}}\|\right) \boldsymbol{\lambda}_{p,j,t}^h - \hat{g}_{p,j,t} \boldsymbol{\lambda}_{p,j,t}^{h,\text{tr}} \end{pmatrix}. \quad (6.8)$$

The scaling with the mesh size h_p in (6.6) is used in order to equilibrate displacements and stresses. We refer to [30, 35] for details.

The evaluation of the max-functions in (6.8) directly leads to a partition of the set \mathcal{N}_γ^h into subsets of active and inactive nodes denoted by $\mathcal{A}_{j,n}^h$, $\mathcal{A}_{j,t}^h$ and $\mathcal{I}_{j,n}^h$, $\mathcal{I}_{j,t}^h$, respectively, and defined via

$$\mathcal{A}_{j,n}^h := \left\{ p \in \mathcal{N}_\gamma^h : \lambda_{p,j,n}^{h,\text{tr}} > 0 \right\}, \quad \mathcal{I}_{j,n}^h := \mathcal{N}_\gamma^h \setminus \mathcal{A}_{j,n}^h, \quad (6.9a)$$

$$\mathcal{A}_{j,t}^h := \left\{ p \in \mathcal{N}_\gamma^h : \|\boldsymbol{\lambda}_{p,j,t}^{h,\text{tr}}\| > \hat{g}_{p,j,t} \right\} \cup \left\{ p \in \mathcal{N}_\gamma^h : \hat{g}_{p,j,t} = 0 \right\}, \quad \mathcal{I}_{j,t}^h := \mathcal{N}_\gamma^h \setminus \mathcal{A}_{j,t}^h. \quad (6.9b)$$

The set $\mathcal{A}_{j,n}^h$ contains all nodes which are in contact with the obstacle at time t_j , whereas $\mathcal{A}_{j,t}^h$ and $\mathcal{I}_{j,t}^h$ represent the slippy and sticky nodes, respectively.

According to the partition (6.9), the complementarity function (6.8) simplifies to

$$C_p^h(\mathbf{u}_{p,j}^h, \boldsymbol{\lambda}_{p,j}^h) = \begin{pmatrix} \begin{cases} \lambda_{p,j,n}^h, & p \in \mathcal{I}_{j,n}^h, \\ c_n h_p^{-1} (g_{p,n} - u_{p,j,n}^h), & p \in \mathcal{A}_{j,n}^h, \end{cases} \\ \begin{cases} -\hat{g}_{p,j,t} c_t h_p^{-1} \Delta t \partial_{\Delta t} \mathbf{u}_{p,j,t}^h, & p \in \mathcal{I}_{j,t}^h, \\ \|\boldsymbol{\lambda}_{p,j,t}^{h,\text{tr}}\| \boldsymbol{\lambda}_{p,j,t}^h - \hat{g}_{p,j,t} \boldsymbol{\lambda}_{p,j,t}^{h,\text{tr}}, & p \in \mathcal{A}_{j,t}^h, \end{cases} \end{pmatrix}. \quad (6.10)$$

We remark that (6.10)_{2,3} can be seen as Dirichlet conditions for the normal or tangential displacement, whereas (6.10)₁ is a Neumann and (6.10)₄ a Robin-type condition.

REMARK 6.1. *As shown in [47], the normal contact conditions (6.4) in combination with the trapezoidal rule can yield an unstable algorithm which is not energy consistent. Hence, if inertia terms are present, it is advisable to change the time discretization of (6.4) like, e.g., described in [15, 48, 49]. As an example, we sketch the approach given in [48] which also restores the energy consistency of the time stepping scheme. It is based on the enforcement of the persistency condition $\lambda_n \frac{d}{dt}(u_n - g_n) = 0$ instead of the complementarity condition $\lambda_n(u_n - g_n) = 0$ and reads*

$$\begin{aligned} u_{p,j-1,n}^h - g_{p,n} < 0 &\Rightarrow \lambda_{p,j,n} = 0, \\ u_{p,j-1,n}^h - g_{p,n} \geq 0 &\Rightarrow \begin{cases} \lambda_{p,j,n} \geq 0, \\ \partial_{\Delta t} u_{p,j,n}^h \leq 0, \\ \partial_{\Delta t} u_{p,j,n}^h \lambda_{p,j,n} = 0. \end{cases} \end{aligned} \quad (6.11)$$

We remark that the persistency condition (6.11) tends to the original non-penetration condition as the time step size Δt goes to zero. It can be included in the semismooth setting (6.7) by replacing (6.8)₁ by

$$\lambda_{p,j,n}^h - \max\left(0, \lambda_{p,j,n}^{h,\text{en}}\right), \quad (6.12)$$

where

$$\lambda_{p,j,n}^{h,\text{en}} := \begin{cases} c_n h_p^{-1} (u_{p,j-1,n} - g_{p,n}) & \text{if } u_{p,j-1,n} - g_{p,n} < 0, \\ \lambda_{p,j,n} + c_n h_p^{-1} \Delta t \partial_{\Delta t} u_{p,j,n} & \text{if } u_{p,j-1,n} - g_{p,n} \geq 0. \end{cases}$$

The fine Dirichlet-to-Neumann operator $\mathcal{S}_\omega^h : \mathbf{W}_\Gamma^h \rightarrow (\mathbf{W}_\Gamma^h)'$ corresponding to the above sketched contact problem is given by

$$\mathcal{S}_\omega^h(\mathbf{u}_{\Gamma,j}^h) = K_{\Gamma\Gamma}^h \mathbf{u}_{\Gamma,j}^h + K_{\Gamma\omega}^h \mathbf{u}_{\omega,j}^h - \boldsymbol{\varrho}_{\Gamma,j-1}^h, \quad (6.13)$$

with $\mathbf{u}_{\omega,j}^h$ being the first component of the solution $(\mathbf{u}_{\omega,j}^h, \boldsymbol{\lambda}_{\gamma,j}^h)$ of

$$K_{\omega\omega}^h \mathbf{u}_{\omega,j}^h + (D_{\gamma\omega}^{hh})^T \boldsymbol{\lambda}_j^h = \boldsymbol{\varrho}_{\omega,j-1}^h - K_{\omega\Gamma}^h \mathbf{u}_{\Gamma,j}^h, \quad (6.14a)$$

$$\mathbf{C}_\gamma^h(\mathbf{u}_{\omega,j}^h, \boldsymbol{\lambda}_{\gamma,j}^h) = \mathbf{0}. \quad (6.14b)$$

The matrix $D_{\gamma\omega}^{hh} \in \mathbb{R}^{d|\mathcal{N}_\gamma^h| \times d|\mathcal{N}_\omega^h|}$ in (6.14a) consists of the entries

$$(D_{\gamma\omega}^{hh})_{pq} := \text{Id}_d \int_\gamma \psi_p^h \phi_q^h ds \in \mathbb{R}^{d \times d}, \quad p \in \mathcal{N}_\gamma^h, q \in \mathcal{N}_\omega^h.$$

REMARK 6.2. *Although Equations (6.14) contain both the displacements \mathbf{u}_j^h and the contact stresses $\boldsymbol{\lambda}_{\gamma,j}^h$ as unknowns, the use of the dual basis functions for the discretization of $\boldsymbol{\lambda}_{\gamma,j}^h$ allows for an easy static condensation in the tangential system of (6.13), such that only a system of the size of the displacement has to be solved. We refer to [35] for details.*

7. Approximate solution schemes. In this section, we transfer the idea of Algorithm 1 to the nonlinear problem (6.1).

7.1. Nested iterations. Because of the nonlinearity, we have to combine two iterative processes: on the one hand, the semismooth Newton loop with iteration index k , on the other hand, the subdomain coupling as presented in Section 3 with iteration index l . These loops can be nested in two different ways:

- (a) kl version: Linearize (6.1) and solve the resulting tangential problem using Algorithm 1.
- (b) lk version: Approximate (6.1) by two separate nonlinear subproblems coupled at the interface Γ and solve each subproblem by an inner semismooth Newton loop.

Both (a) and (b) result in an algorithm with an inner and an outer iteration. The efficiency of these schemes can possibly be increased by replacing the inner iteration by an approximate solver; one can for example perform only a fixed small number of inner iteration steps or use a more sophisticated strategy to avoid oversolving, see, e.g., [17].

First, we consider possibility (a) in more detail. The application of the semismooth Newton scheme to the nonlinear problem (6.1) leads to the following linear system to be solved for the next Newton iterate $(\mathbf{u}_j^{H,(k+1)}, \mathbf{u}_j^{h,(k+1)}, \boldsymbol{\zeta}_{\Gamma,j}^{h,(k+1)})$:

$$\begin{pmatrix} K_{\Xi}^{H,(k)} & \mathbf{0} & -(D^{hH})^T \\ \mathbf{0} & K_{\omega}^{h,(k)} & (D^{hh})^T \\ -D^{hH} & D^{hh} & \mathbf{0} \end{pmatrix} \begin{pmatrix} \mathbf{u}_j^{H,(k+1)} \\ \mathbf{u}_j^{h,(k+1)} \\ \boldsymbol{\zeta}_{\Gamma,j}^{h,(k+1)} \end{pmatrix} = \begin{pmatrix} \mathbf{q}^{H,(k)} \\ \mathbf{q}^{h,(k)} \\ \mathbf{0} \end{pmatrix}, \quad (7.1)$$

with the tangential matrices

$$K_{\Theta}^{m,(k)} := \left(\partial_{\mathbf{u}_j^m} \mathcal{K}_{\Theta}^m \right) (\mathbf{u}_j^{m,(k)}), \quad \Theta \in \{\Xi, \omega\}, \quad m \in \{h, H\}, \quad (7.2)$$

and the right hand side vectors

$$\mathbf{q}^{H,(k)} := K_{\Xi}^{H,(k)} \mathbf{u}_j^{H,(k)} - \mathcal{K}_{\Xi}^H(\mathbf{u}_j^{H,(k)}), \quad (7.3a)$$

$$\mathbf{q}^{h,(k)} := K_{\omega}^{h,(k)} \mathbf{u}_j^{h,(k)} - \mathcal{K}_{\omega}^h(\mathbf{u}_j^{h,(k)}). \quad (7.3b)$$

This linear system has exactly the same structure as (2.28) and can thus be solved inexactly by means of Algorithm 1. For convenience, the resulting nested iteration is summarized in Algorithm

Algorithm 4 Inexact nonlinear two-way coupling scheme

Start from some initial guess $\hat{\mathbf{z}}_d^{(0, l_{\max})}$.

Newton loop: Compute sequentially for $k = 0, 1, \dots$

- (1) Initialize the solution $\hat{\mathbf{z}}_d^{(k+1, 0)} = \hat{\mathbf{z}}_d^{(k, l_{\max})}$. Compute the stiffness matrices $S_{\Xi}^{H, (k)}$, $S_{\omega}^{h, (k)}$ and the right hand side vectors $\bar{\mathbf{q}}_{\Xi}^{H, (k)}$, $\bar{\mathbf{q}}_{\omega}^{h, (k)}$.

Define coarse grid approximations $S_{\omega}^{H, (k)}$, $\bar{\mathbf{q}}_{\omega}^{H, (k)}$ of $S_{\omega}^{h, (k)}$, $\bar{\mathbf{q}}_{\omega}^{h, (k)}$.

- (2) Gauß–Seidel loop: Compute sequentially for $l = 0, 1, \dots$,
 (i) Solve problem on coarse space \mathbf{V}^H with interface load on Γ inherited from fine computation on ω :

$$\begin{pmatrix} (S_{\Xi}^{H, (k)} + S_{\omega}^{H, (k)}) & \mathbf{0} \\ S_{\omega}^{H, (k)} & (D_{\Gamma}^{HH})^T \end{pmatrix} \begin{pmatrix} \delta \mathbf{u}_{\Gamma, j}^{H, (k+1, l)} \\ \delta \boldsymbol{\mu}_{\Gamma, j}^{H, (k+1, l)} \end{pmatrix} = \begin{pmatrix} \mathbf{r}_{\Xi}^{H, (k+1, l)} + \mathbf{r}_{\omega}^{H, (k+1, l)} \\ \mathbf{r}_{\omega}^{H, (k+1, l)} \end{pmatrix}, \quad (7.4)$$

- (ii) Solve problem on fine space \mathbf{V}^h with weakly imposed trace on Γ inherited from coarse computation on Ω :

$$\begin{pmatrix} S_{\omega}^{h, (k)} & (D_{\Gamma}^{hh})^T \\ D_{\Gamma}^{hh} & \mathbf{0} \end{pmatrix} \begin{pmatrix} \delta \mathbf{u}_{\Gamma, j}^{h, (k+1, l)} \\ \delta \boldsymbol{\zeta}_{\Gamma, j}^{h, (k+1, l)} \end{pmatrix} = \begin{pmatrix} \mathbf{r}_{\omega}^{h, (k+1, l)} \\ \boldsymbol{\nu}_{\Gamma}^{h, (k+1, l)} \end{pmatrix} + \begin{pmatrix} \mathbf{0} \\ D_{\Gamma}^{hH} \delta \mathbf{u}_{\Gamma, j}^{H, (k+1, l)} \end{pmatrix}, \quad (7.5)$$

- (iii) Update the solution vector:

$$\hat{\mathbf{z}}_d^{(k+1, l+1)} := \hat{\mathbf{z}}_d^{(k+1, l)} + \delta \hat{\mathbf{z}}_d^{(k+1, l)}, \quad (7.6)$$

The residuals are given by

$$\mathbf{r}_{\Xi}^{H, (k+1, l)} = \bar{\mathbf{q}}_{\Xi}^{H, (k)} - S_{\Xi}^{H, (k)} \mathbf{u}_{\Gamma, j}^{H, (k+1, l)} + (D_{\Gamma}^{hH})^T \boldsymbol{\zeta}_{\Gamma, j}^{h, (k+1, l)}, \quad (7.7a)$$

$$\mathbf{r}_{\omega}^{H, (k+1, l)} = \bar{\mathbf{q}}_{\omega}^{H, (k)} - S_{\omega}^{H, (k)} \mathbf{u}_{\Gamma, j}^{H, (k+1, l)} - (D_{\Gamma}^{HH})^T \boldsymbol{\mu}_{\Gamma, j}^{H, (k+1, l)}, \quad (7.7b)$$

$$\mathbf{r}_{\omega}^{h, (k+1, l)} = \bar{\mathbf{q}}_{\omega}^{h, (k)} - S_{\omega}^{h, (k)} \mathbf{u}_{\Gamma, j}^{h, (k+1, l)} - (D_{\Gamma}^{hh})^T \boldsymbol{\zeta}_{\Gamma, j}^{h, (k+1, l)}, \quad (7.7c)$$

$$\boldsymbol{\nu}_{\Gamma}^{h, (k+1, l)} = D_{\Gamma}^{hH} \mathbf{u}_{\Gamma, j}^{H, (k+1, l)} - D_{\Gamma}^{hh} \mathbf{u}_{\Gamma, j}^{h, (k+1, l)}. \quad (7.7d)$$

- (iv) If $l + 1 = l_{\max}$ or (7.8) is satisfied, set $\hat{\mathbf{z}}_d^{(k+1, l_{\max})} = \hat{\mathbf{z}}_d^{(k+1, l+1)}$ and stop.

- (3) Check convergence of Newton iteration.
-

4, using the notation $\hat{\mathbf{z}}_d$ for the union of all unknowns on the interface Γ (see (3.1)), and with $S_{\Theta}^{m, (k)}$ denoting the Schur complement of the matrix (7.2).

The convergence rate of the inner Gauß–Seidel iteration can be analysed with the results from Section 3. Furthermore, the superlinear local convergence of the outer Newton iteration can be preserved if the norm of the residual of the inner iteration is bounded in terms of the norm of the Newton residual

$$\mathbf{R}^{(k)} := \begin{pmatrix} \mathcal{K}_{\Xi}^H(\mathbf{u}_j^{H, (k)}) - (D^{hH})^T \boldsymbol{\zeta}_{\Gamma, j}^{h, (k)} \\ \mathcal{K}_{\omega}^h(\mathbf{u}_j^{h, (k)}) + (D^{hh})^T \boldsymbol{\zeta}_{\Gamma, j}^{h, (k)} \end{pmatrix}$$

(see, e.g., [17, 18, 22]). For $l \geq 1$, the residual of the inner loop is given by the vector (7.7a), such that the Gauß–Seidel iteration has to be solved until the condition

$$\|\mathbf{r}_{\Xi}^{H, (k+1, l)}\| = \mathcal{O}\left(\|\mathbf{R}^{(k)}\|\right) \quad (7.8)$$

is satisfied.

Second, we look at possibility (b) which can easier be formulated using the trace formulation (6.3). We introduce a coarse nonlinear Dirichlet–to–Neumann map $\mathcal{S}_{\omega}^H : \mathbf{W}_{\Gamma}^H \rightarrow (\mathbf{W}_{\Gamma}^H)'$ and

augment (6.3) with an additional equation:

$$\begin{aligned} & \hat{\mathbf{F}}(\hat{\mathbf{z}}_d) + \hat{D}_d \hat{\mathbf{z}}_d \\ & := \begin{pmatrix} \mathcal{S}_{\Xi}^H(\mathbf{u}_{\Gamma}^H) + \mathcal{S}_{\omega}^H(\mathbf{u}_{\Gamma}^H) \\ \mathcal{S}_{\omega}^H(\mathbf{u}_{\Gamma,j}^H) \\ \mathcal{S}_{\omega}^h(\mathbf{u}_{\Gamma,j}^h) \\ D_{\Gamma}^{hh} \mathbf{u}_{\Gamma,j}^h - D_{\Gamma}^{hH} \mathbf{u}_{\Gamma,j}^H \end{pmatrix} + \begin{pmatrix} (D_{\Gamma}^{HH})^T & -(D_{\Gamma}^{hH})^T \\ (D_{\Gamma}^{HH})^T & \mathbf{0} \\ \mathbf{0} & (D_{\Gamma}^{hh})^T \\ \mathbf{0} & \mathbf{0} \end{pmatrix} \begin{pmatrix} \boldsymbol{\mu}_{\Gamma,j}^H \\ \boldsymbol{\zeta}_{\Gamma,j}^h \end{pmatrix} = \mathbf{0}. \end{aligned} \quad (7.9)$$

Then, a Gauß–Seidel iteration similar to (3.4) is applied to the augmented nonlinear system (7.9). Using the matrix \hat{K}_d already introduced on page 16, the resulting nonlinear fixpoint iteration can be written as

$$\hat{\mathbf{F}}(\hat{\mathbf{z}}_d^{(l+1)}) + (\hat{D}_d - \hat{K}_d) \hat{\mathbf{z}}_d^{(l+1)} = -\hat{K}_d \hat{\mathbf{z}}_d^{(l)}. \quad (7.10)$$

The nonlinear part of (7.10) naturally decouples into two nonlinear problems on the subdomains which can be solved separately by inexact semismooth Newton methods.

In summary, both coupling schemes can be interpreted as the combination of a fixpoint iteration with index l and a semismooth Newton iteration with index k ; possibility (a) is the kl version with the Newton method as outer loop, whereas (b) corresponds to the lk version with the linear iteration as outer loop. However, as a Newton step is, in general, more expensive than a linear fixpoint step due to the reassembly of the stiffness matrix, the former version is likely to be more efficient than the latter one. This conjecture has been confirmed by some simple numerical tests, such that the numerical results presented in Section 8 focus on the variant (a).

REMARK 7.1. *In the special case that the inner iterations of (a) and (b) are both stopped after only one step, the schemes collapse to the same inexact iterative scheme which can be obtained by setting $l_{\max} = 1$ in Algorithm 4 or by solving the nonlinear equation (7.10) inexactly by means of a single semismooth Newton iteration. The result can be written as*

$$\left(\partial_{\mathbf{u}} \hat{\mathbf{F}}(\hat{\mathbf{z}}_d^{(k)}) + \hat{D}_d - \hat{K}_d \right) \delta \mathbf{z}_d^{(k)} = - \left(\hat{\mathbf{F}}(\hat{\mathbf{z}}_d^{(k)}) + \hat{D}_d \hat{\mathbf{z}}_d^{(k)} \right), \quad (7.11)$$

where the notation $\partial_{\mathbf{u}} \hat{\mathbf{F}}$ refers to the Schur system of the tangential matrices (7.2). Equation (7.11) can be interpreted as a semismooth quasi-Newton iteration to solve the nonlinear equation (7.9), where the tangential stiffness matrix $(\partial_{\mathbf{u}} \hat{\mathbf{F}}(\hat{\mathbf{z}}_d^{(k)}) + \hat{D}_d)$ is approximated by $(\partial_{\mathbf{u}} \hat{\mathbf{F}}(\hat{\mathbf{z}}_d^{(k)}) + \hat{D}_d - \hat{K}_d)$.

7.2. Coarse grid approximation. In this subsection, we present a possible definition of the coarse grid quantities $S_{\omega}^{H,(k)}$, $\bar{\mathbf{q}}_{\omega}^{H,(k)}$ needed in Algorithm 4. For material nonlinearities with a nonlinear stress tensor $\mathbf{s}(\mathbf{u})$, we construct $S_{\omega}^{H,(k)}$, $\bar{\mathbf{q}}_{\omega}^{H,(k)}$ during the same nonlinear assembly routine as $S_{\omega}^{h,(k)}$, $\bar{\mathbf{q}}_{\omega}^{h,(k)}$, with an auxiliary coarse displacement vector on ω determined by the solution of (7.4) on \mathbf{V}^H .

For the case of frictional contact, the approximation is a bit more involved. Numerical tests have shown that the convergence rate of the inner iteration in Algorithm 4 degrades if the Dirichlet contact conditions, i.e., the active nodes $\mathcal{A}_n^{h,(k)}$ in normal direction and the sticky nodes $\mathcal{I}_t^{h,(k)}$ in tangential direction, are not respected in the coarse approximation. Hence, we propose to construct $S_{\omega}^{H,(k)}$, $\bar{\mathbf{q}}_{\omega}^{H,(k)}$ by defining a set $\mathcal{A}_n^{H,(k)} \subset \mathcal{N}_{\gamma}^H$ of active coarse grid nodes approximating the fine contact zone. This coarse active set is constructed in terms of the finite element function $\chi_{\gamma,n}^{h,(k)} \in \mathbf{W}_{\gamma}^h$ given by

$$\chi_{\gamma,n}^{h,(k)}(p) = \begin{cases} \mathbf{1}, & p \in \mathcal{A}_n^{h,(k)}, \\ \mathbf{0}, & \text{otherwise.} \end{cases}$$

Introducing the mortar operator $P_{\gamma}^{Hh} : \mathbf{W}_{\gamma}^h \rightarrow \mathbf{W}_{\gamma}^H$ defined according to (2.10), we choose an appropriate threshold value $\tau_n \in [0, 1]$ and set

$$\mathcal{A}_n^{H,(k)}(\tau_n) := \left\{ p \in \mathcal{N}_{\gamma}^H : \left(P_{\gamma}^{Hh} \chi_{\gamma,n}^{h,(k)} \right)(p) > \tau_n \right\}. \quad (7.12)$$

The rest of the coarse nodes is set inactive, i.e., $\mathcal{I}_n^{H,(k)} := \mathcal{N}_\gamma^H \setminus \mathcal{A}_n^{H,(k)}$.

For the tangential part, we proceed similarly and define the set $\mathcal{I}_t^{H,(k)}$ of coarse sticky nodes by

$$\mathcal{I}_t^{H,(k)}(\tau_t) := \left\{ p \in \mathcal{N}_\gamma^H : \left(P_\gamma^{Hh} \chi_{\gamma,t}^{h,(k)} \right) (p) > \tau_t \right\}, \quad (7.13)$$

with

$$\chi_{\gamma,t}^{h,(k)}(p) = \begin{cases} \mathbf{1}, & p \in \mathcal{I}_t^{h,(k)}, \\ \mathbf{0}, & \text{otherwise.} \end{cases}$$

As the Robin condition for the slippery nodes are very difficult to model on the coarse grid, we free the remaining nodes $\mathcal{A}_t^{H,(k)} := \mathcal{N}_\gamma^H \setminus \mathcal{I}_t^{H,(k)}$ in tangential direction by enforcing $\lambda_t^{H,(k+1)} = \mathbf{0}$.

Using the sets (7.12), (7.13), we construct $S_\omega^{H,(k)}$ and $\mathbf{q}_\omega^{H,(k)}$ in the same way as the fine grid counterparts. We remark that smaller values of τ_n, τ_t generally lead to larger coarse contact sets $\mathcal{A}_n^{H,(k)}, \mathcal{I}_t^{H,(k)}$.

REMARK 7.2. *We have also tried to map the fine values $\mathbf{u}_\gamma^h, \lambda_\gamma^h$ onto the coarse discretization and then compute the coarse active sets from these projections. However, the coarse active sets are much smaller than those obtained from (7.12) for small threshold values, resulting in worse convergence rates.*

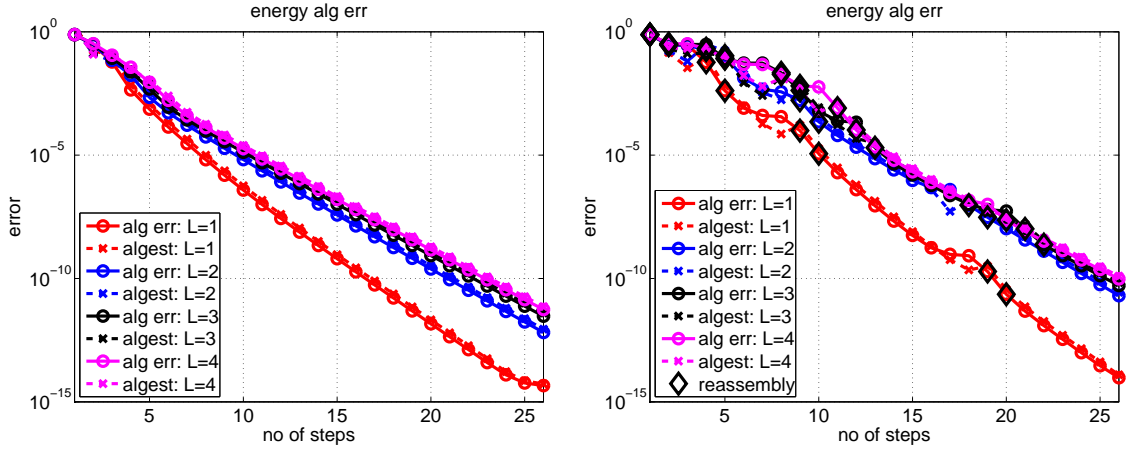


FIGURE 8.1. True e_{alg} and estimated η_{alg} relative algebraic energy error for Algorithm 4 with $L \in \{1, 2, 3, 4\}$ and $E_\Xi = E_\omega$ with respect to number of total iterations; left: $l_{max} = 1$; right: inner iteration stopped according to (8.2a).

8. Numerical tests.

8.1. Geometrically conforming setting in 2D. For the first set of nonlinear computations, we use a similar test setting as in Subsections 4.1 and 4.2 with nested finite element spaces $\mathbf{V}_\omega^H \subset \mathbf{V}^h$. There are only two differences to the setting described there: First, the Neumann boundary conditions on the lower boundary for $x_2 = 0$ are replaced by unilateral frictionless contact with the fixed obstacle $\Gamma_{\text{obs}}(x_1) = (x_1, 0.3 \cdot \max(0.25 - |x_1 - 1|, 0))$, and second, we employ the nonlinear static Mooney–Rivlin elasticity law with the second Piola–Kirchhoff stress tensor

$$\begin{aligned} \mathbf{s}(\mathbf{u}) &= \frac{\lambda}{2} ((\det \mathbf{C})^2 - 1) \mathbf{C}^{-1} \\ &+ \mu \left((1 - c_m) (\text{Id} - \mathbf{C}^{-1}) + c_m ((\text{tr} \mathbf{C}) \text{Id} - \mathbf{C} - (d - 1) \mathbf{C}^{-1}) \right), \end{aligned} \quad (8.1)$$

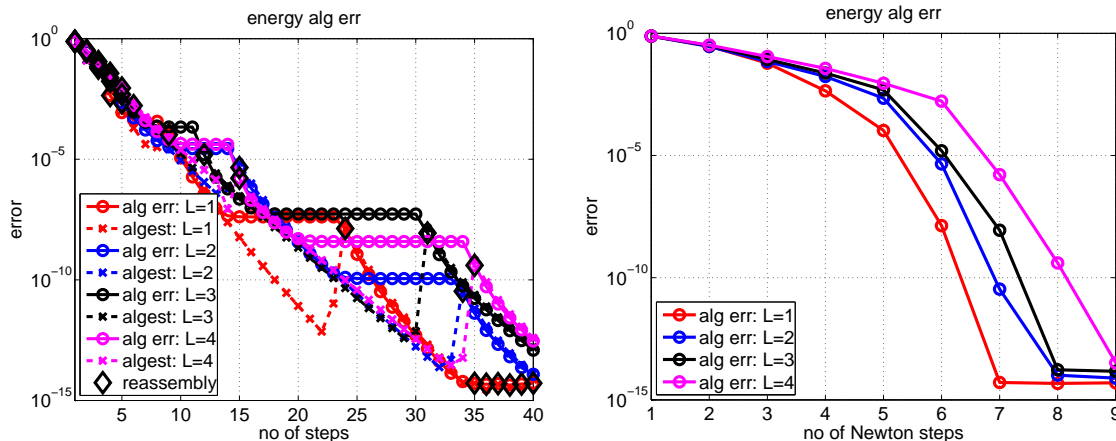


FIGURE 8.2. True e_{alg} and estimated η_{alg} rel. alg. error for Algorithm 4 for $L \in \{1, 2, 3, 4\}$ and $E_{\Xi} = E_{\omega}$ with inner iteration stopped according to (8.2b); left: wrt. total steps; right: wrt. Newton steps.

with $d \in \{2, 3\}$ denoting the number of spatial dimensions, the right Cauchy–Green tensor $\mathbf{C} := (\text{Id} + \nabla \mathbf{u})^T (\text{Id} + \nabla \mathbf{u})$ and the parameters $c_m = 0.5$, $E_{\Omega_0} = E_{\omega} = 100$, $\nu = 0.3$ and $\rho = 0$. The coarse grid approximation of the active set is chosen according to (7.12) with $\tau_n = 0.15$.

As before, we test the performance of Algorithm 4 by computing the relative algebraic error measure η_{alg} defined in (3.33) and comparing it with the algebraic energy error norm e_{alg} given in (4.1). The results for different grid sizes $H = 2^{-3}$, $h = 2^{-L} \cdot H$ and different strategies of stopping the inner iteration are shown in Figures 8.1 and 8.2. The quasi-Newton scheme obtained for $l_{\text{max}} = 1$ is depicted on the left of Figure 8.1; one can observe that the error decays linearly with respect to the number of iterations and that the error indicator η_{alg} predicts the actual algebraic error e_{alg} quite accurately. On the right side of Figure 8.1 and in Figure 8.2, we do not choose a fixed value of l_{max} but solve the inner iteration on l until one of the following conditions is satisfied (cf. (3.32) and (7.8)):

$$\left(\eta_{\text{abs}}^{(k+1,l)}\right)^2 := \left((S_{\Xi}^H + S_{\omega}^H)^{-1} \mathbf{r}_{\Xi}^{H,(k+1,l)}, \mathbf{r}_{\Xi}^{H,(k+1,l)} \right) \leq E_{\omega}^{-1} \|\mathbf{R}^{(k)}\|^2, \quad (8.2a)$$

$$\left(\eta_{\text{abs}}^{(k+1,l)}\right)^2 \leq E_{\omega} \|\mathbf{R}^{(k)}\|^4. \quad (8.2b)$$

The iterations where the stiffness matrix is reassembled are marked with the symbol \diamond . The picture on the right side of Figure 8.1 shows the computations obtained with the linear stopping condition (8.2a). Comparing it with the left picture where the stiffness matrix is reassembled in each step, one can observe that many of these assemblies can be avoided without losing too much accuracy.

Figure 8.2 displays the error decay per iteration if the inner fixpoint loop in Algorithm 4 is stopped according to (8.2b). One can see that sometimes during the iteration, the estimated algebraic error η_{alg} is decreased by the additional inner steps but e_{alg} stays constant until the Newton matrix is updated. This phenomenon is known as “oversolving” [22], implying that some of the inner fixpoint iterations do not ameliorate the error decay of the scheme. However, with the criterion (8.2b), we can guarantee that the local superlinear convergence of the outer Newton iteration is maintained, as can be seen on the right side of Figure 8.2 where the error decay is plotted with respect to the Newton steps. In addition, for some of the more challenging problems like the one shown in Subsection 8.4, additional inner steps can increase the robustness of the scheme.

In Figure 8.3, the decay of the relative energy algebraic error is depicted for the lk version stated in (b) and 2 or 4 iterations for the inner Newton loop, respectively. The additional Newton steps cause the algorithm to be more inefficient with respect to the total number of iterations, and the algebraic error is even larger than for the kl version with the same number of inner steps.

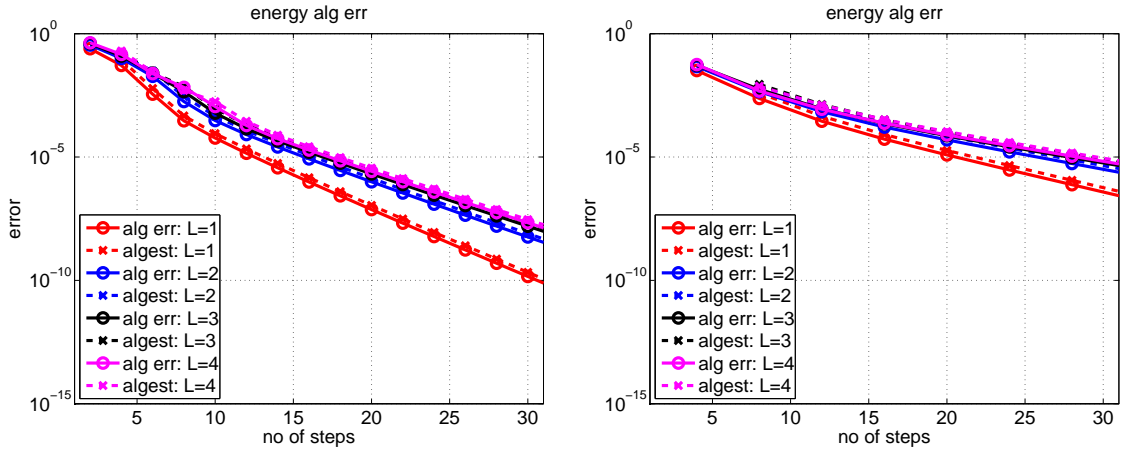


FIGURE 8.3. True e_{alg} and estimated η_{alg} relative algebraic error for lk version (b) for $L \in \{1, 2, 3, 4\}$ and $E_{\Omega_0} = E_\omega$ with respect to number of total steps; left: 2 inner iterations; right: 4 inner iterations.

Moreover, each inner step now implies the reassembly of the tangential stiffness matrix which renders it more expensive than a Gauß–Seidel step. Hence, the lk version seems to be the more inefficient one and will not be considered further in the numerical tests.

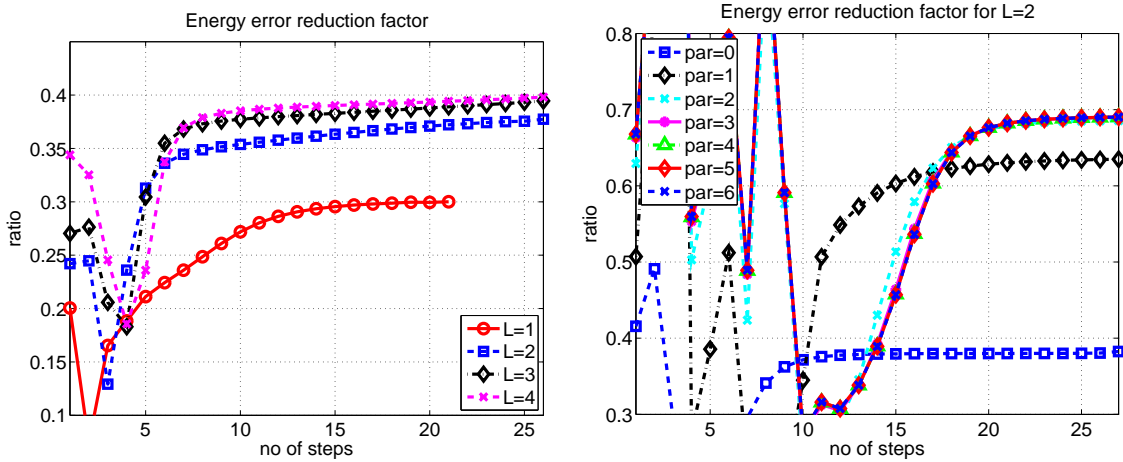


FIGURE 8.4. Mean algebraic error reduction factor for Algorithm 4 with respect to number of total iterations; left: $l_{\max} = 1$, $E_\Xi = E_\omega$ and $L \in \{1, 2, 3, 4\}$; right: $l_{\max} = 2$, $L = 2$ and $E_\omega = 10^{\text{par}} \cdot E_\Xi$, $\text{par} \in \{0, \dots, 6\}$.

As in Subsection 4.2, we shortly test the error reduction of Algorithm 4 for varying values of L as well as for discontinuous material parameters $E_\omega = 10^{\text{par}} E_\Xi$, $\text{par} \geq 0$. In Figure 8.4, the error reduction factor is depicted with respect to the number of total iterations; the left picture shows the results for $\text{par} = 0$, $l_{\max} = 1$ and different values of $L \in \{1, \dots, 4\}$, whereas the right picture displays the error reduction for $L = 2$, $l_{\max} = 2$ and $\text{par} \in \{0, \dots, 6\}$. Especially in the latter case, one can observe that the reduction factor is strongly varying in the pre-asymptotic range due to the changes in the active sets. However, the asymptotic behaviour confirms that Algorithm 4 is again robust with respect to the ratio E_ω/E_Ξ as well as the ratio H/h . We remark that the value $l_{\max} = 2$ has been chosen because we need more than one inner iteration in order for the algorithm to converge for $\text{par} \geq 1$. Further, the error reduction factors in Figure 8.4 are larger than those for the corresponding linear case given in Figure 4.4.

8.2. Geometrically nonconforming setting in 2D. As a second test setting, we consider a simplified two-dimensional geometry of a car tire. The domain Ω consists of a circular ring

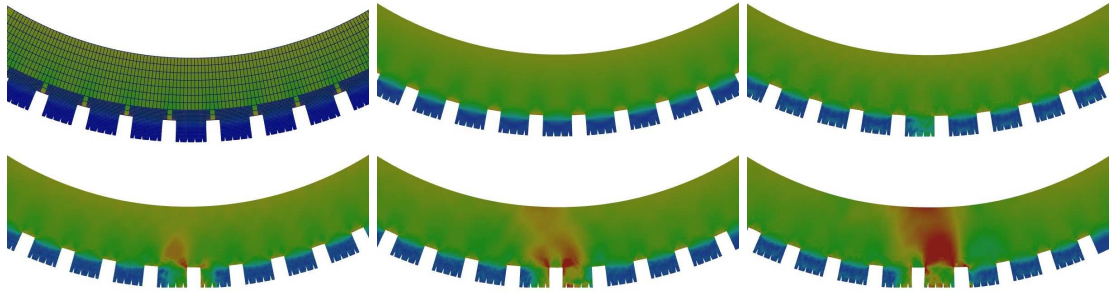


FIGURE 8.5. Geometrical nonconforming example; upper row: initial grid for $L = 2$ and effective stress at times t_0 and t_{50} ; lower row: effective stress at times t_{100} , t_{150} and t_{200} .

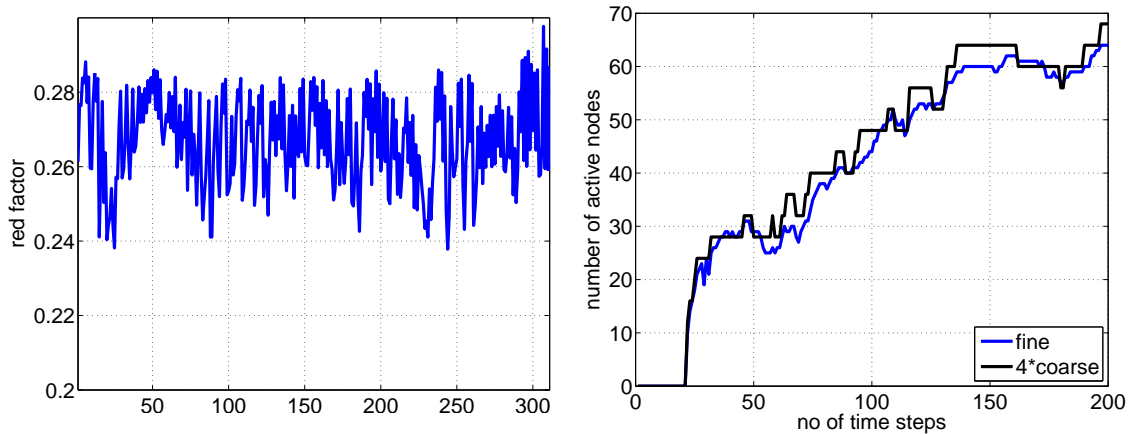


FIGURE 8.6. Geometrical nonconforming example; left: error reduction factor for intermediate steps of Algorithm 4 with $l_{max} = 1$; right: evolution of active sets $|\mathcal{A}_{n,j}^h|$ and $|\mathcal{A}_{n,j}^H(0)|$.

centered in the origin with the diameters $r_{inner} = 1.6$, $r_{outer} = 1.95$ with 60 additional salients of height 0.05; the geometry is sketched in Figure 1.1. The fine domain ω is built by 60 separate patches which are associated with the salients but have an extended T-like shape in order to include the corner singularities in the fine triangulation. On the potential contact boundary γ , each salient features four additional small sipes which are resolved by the fine grid \mathcal{T}^h but are not respected by the coarse grid \mathcal{T}^H . Hence, we have a geometrically nonconforming situation where the coarse triangulation defines an approximation $\Omega^H \neq \Omega$ of the actual domain, leading to $\mathbf{V}_\omega^H \not\subset \mathbf{V}_\omega^h$. On the upper left of Figure 8.5, the initial triangulation for $L = 2$ is shown which is constructed such that the trace spaces $\mathbf{W}_\Gamma^H \subset \mathbf{W}_\Gamma^h$ are nested.

For the dynamic computation with $\Delta t = 2.5 \cdot 10^{-6}$, we use the Mooney–Rivlin material law (8.1) with the parameters $E_\Xi = E_\omega = 4.4 \cdot 10^6$, $\varrho_\Xi = \varrho_\omega = 1$, $\nu = 0.33$ and $c_m = 0.5$. The tire has an initial velocity of

$$\mathbf{v}_0(\mathbf{x}) = 150 \begin{pmatrix} x_2 \\ -x_1 \end{pmatrix} - \begin{pmatrix} 0 \\ 20 \end{pmatrix}$$

and an initial displacement corresponding to stationary rolling. We have homogeneous Neumann boundary conditions everywhere, and a volume load of $(0, -19620)$ is applied. Contact occurs with a flat obstacle at $x_2 = -2.052$, and the coarse contact set is defined according to (7.12) with $\tau_n = 0$.

In order to obtain stable and energy consistent results, we use the persistency contact condition (6.12), assemble the contact conditions in an updated Lagrangian manner and employ a discrete gradient for the time discretization of the stress tensor \mathbf{u} based on the approach of [27].

Furthermore, in order to avoid spurious oscillations in the contact stresses λ_γ^h , we use the mass modification technique described in [28].

The resulting effective stress of the mortar solution at different time steps is depicted in Figure 8.5. Further, the left picture of Figure 8.6 illustrates the error reduction rate of the intermediate steps in Algorithm 4 for $l_{\max} = 1$ and $k \geq 1$. One can observe that the rates are about the same size as for the linear geometrically conforming setting in Subsection 4.3. On the right of Figure 8.6, the evolution of the number of fine active contact nodes and its coarse approximation (7.12) is shown.

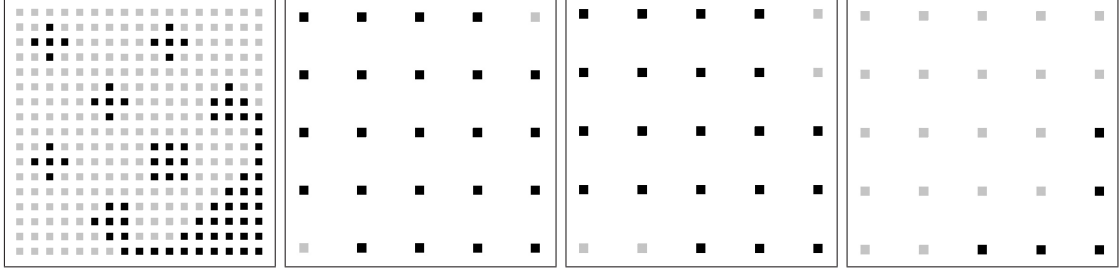


FIGURE 8.7. Fine normal active set \mathcal{A}_n^h (black nodes) for the frictionless test and approximations $\mathcal{A}_n^H(\tau_n)$ for $\tau_n \in \{0, 0.1, 0.4\}$.

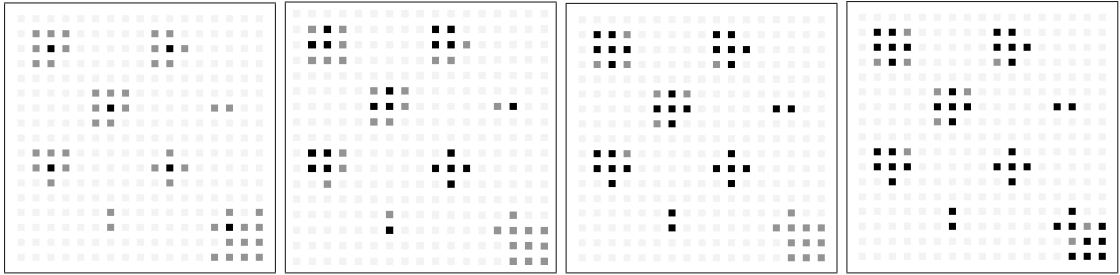


FIGURE 8.8. Fine tangential active sets \mathcal{I}_t^h (black nodes) and \mathcal{A}_t^h (grey nodes) for the frictional test with $\mathfrak{F} \in \{0.2, 0.35, 0.5, 1\}$.

8.3. Geometrically conforming setting in 3D. Before turning to applications with more complex geometries, we investigate the influence of the coarse grid approximations $\mathcal{A}_n^H(\tau_n)$, $\mathcal{I}_t^H(\tau_t)$ defined in (7.12), (7.13) on the convergence rate. For this, we consider the simple three-dimensional domain $\Omega = [0, 1] \times [0, 1] \times [0, 2]$ with the patch $\omega = [0, 1]^3$. We impose a fixed displacement of $(0, 0, -0.03)^T$ on the top, unilateral contact with the obstacle

$$\Gamma_{\text{obs}}(x_1, x_2) = \left(x_1, x_2, 0.25x_1 \cdot \sin(4\pi x_1) \cdot x_2 \cdot \sin(4\pi x_2) \right)$$

on the bottom and homogeneous Neumann conditions elsewhere. The material parameters for the linear elastic body are $E_\omega = E_\Xi = 100$, $\nu = 0.33$ and $\varrho = 0$, and we use uniform hexahedral grids of mesh size $H = \frac{1}{4}$ and $h = \frac{1}{16}$.

First, we consider frictionless contact with $\mathfrak{F} = g_t = 0$. In Figure 8.7, the corresponding fine active set \mathcal{A}_n^h at convergence is depicted, as well as the coarse grid approximations $\mathcal{A}_n^H(\tau_n)$ for $\tau_n \in \{0, 0.1, 0.4\}$.

Table 8.1 summarizes the error reduction rates for Algorithm 4 with $L = 2$ and $l_{\max} = 1$. The upper subtable corresponds to the frictionless case with $\tau_n \in \{-1, 0, 0.1, 0.2, 0.4, 2\}$, where the threshold values $\tau_n = -1$ and $\tau_n = 2$ correspond to the cases $\mathcal{A}_n^H = \emptyset$ and $\mathcal{I}_t^H = \emptyset$, respectively. We obtain a good convergence rate as long as $\tau_n \leq 0.2$, but for larger values of τ_n , the inner iteration of Algorithm 4 seems to become less effective.

$\mathfrak{F} \setminus \tau_n$	-1	0	0.1	0.2	0.4	2	$ \mathcal{A}_n^h $	
0	0.3041	0.3041	0.3041	0.3063	0.6245	0.8299	77	--
$\mathfrak{F} \setminus \tau_t$	-1	0	0.1	0.2	0.4	2	$ \mathcal{A}_n^h $	$ \mathcal{I}_t^h $
0.02	0.7411	0.3045	0.3045	0.3045	0.3045	0.3045	75	0
0.2	0.3712	0.3640	div	div	div	div	52	6
0.35	0.3046	0.3018	div	0.6988	div	div	51	21
0.5	0.3029	0.2991	0.3026	0.7299	div	div	51	32
1	0.3006	0.2994	0.2990	osc	osc	div	51	41
5	0.3018	0.3000	0.3010	0.3432	0.9429	div	49	46

TABLE 8.1

Asymptotic error reduction rates for Algorithm 4 and sizes of fine active sets for $L = 2$, $l_{\max} = 1$ and different values of \mathfrak{F} ; first row: $\mathfrak{F} = 0$, $\tau_n \in \{-1, 0, 0.1, 0.2, 0.4, 2\}$; other rows: $\mathfrak{F} > 0$, $\tau_n = 0$, $\tau_t \in \{-1, 0, 0.1, 0.2, 0.4, 2\}$.

The remaining rows of Table 8.1 refer to Coulomb friction with a friction coefficient $\mathfrak{F} \in \{0.02, 0.2, 0.35, 0.5, 1, 5\}$, where we approximate the normal active set by (7.12) with $\tau_n = 0$ and compare the error reduction rate for different values of τ_t . The notation div indicates that the method diverges, whereas osc refers to an oscillation of the active sets. One can observe that the convergence rate is best for the threshold value $\tau_t = 0$ which gives a good error reduction also for those problems with a complicated distribution of the active sets depicted in Figure 8.8. In general, it seems to be beneficial for the stability of the iteration to have a large set \mathcal{I}_t^H ; although the case $\mathcal{I}_t^H = \mathcal{A}_n^H$ corresponding to $\tau_t = -1$ is not the most efficient possibility, it is a lot more stable than the other extreme $\mathcal{I}_t^H = \emptyset$ obtained for $\tau_t = 2$.

REMARK 8.1. *The influence of the contact boundary conditions on the convergence rate diminishes if we include a mass term in the computation. For the frictionless contact problem with $\varrho = 10^{-2}$, $\Delta t = 10^{-3}$, we have obtained a convergence rate of 0.29 independent of the threshold value τ_n .*

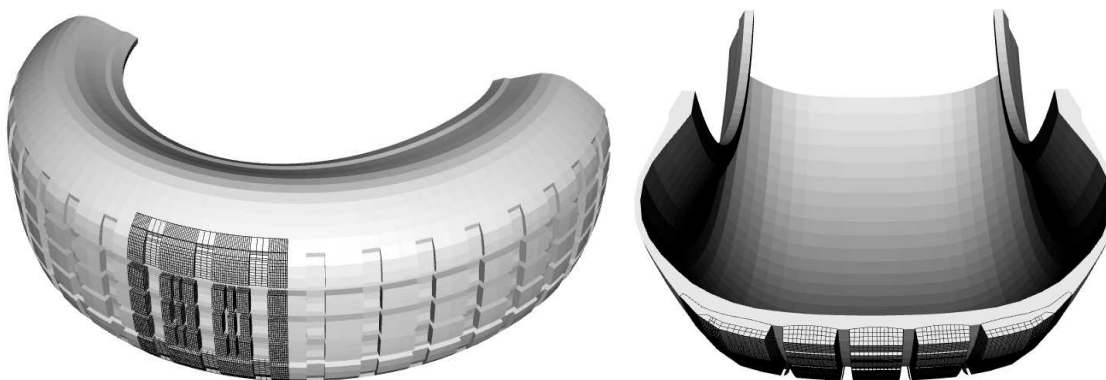


FIGURE 8.9. Geometry of the 3D nonconforming example.

8.4. Tire application. Finally, we apply our algorithm to a more complex 3D geometry consisting of the lower half of a car tire centering on the x_2 -axis and with an approximate radius of 318. In Figure 8.9, the outer domain Ω as well as the multiply connected fine patch ω are sketched, with a difference in the mesh sizes of about $4 \leq H/h \leq 8$. We emphasize that the geometry is nonconforming because the fine triangulation \mathcal{T}^h features some details at the potential contact boundary γ which are not resolved by the coarse grid \mathcal{T}^H (see Figure 8.10).

First, we restrict ourselves to the case of linear elasticity with normal contact and without friction. The contact plane is located at $x_3 = -320$, and the coarse approximation for the normal active set is done using (7.12). On the cutting faces of the tire (for $z = 0$), a fixed displacement of $(0, 0, -1)$ is prescribed, whereas all other boundaries are free. Further, a volume force of

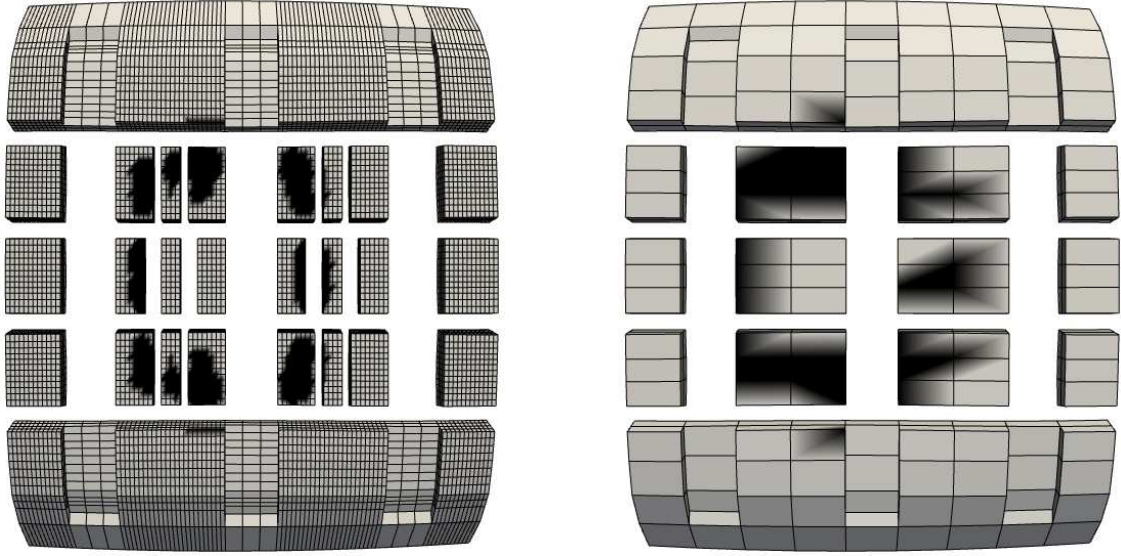


FIGURE 8.10. Fine contact set \mathcal{A}_n^h of exact solution with 555 nodes and approximation $\mathcal{A}_n^H(0.15)$ with 36 nodes.

$(0, 0, -1000)$ is applied to the tire, and the material parameters read $E_{\Xi} = E_{\omega} = 2.5 \cdot 10^7$ and $\nu = 0.33$. The active set \mathcal{A}_n^h of the corresponding mortar solution is sketched on the left of Figure 8.10; its coarse grid approximation $\mathcal{A}_n^H(0.15)$ can be seen on the right side.

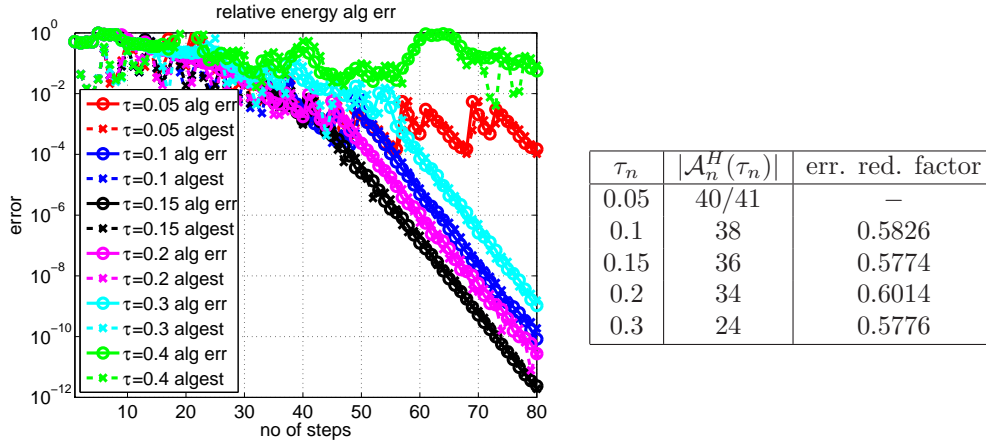


FIGURE 8.11. Performance of Algorithm 4 with $\alpha = 0.6$, $l_{\max} = 4$ wrt. number of total iterations for $\tau_n \in \{0.05, 0.1, 0.15, 0.2, 0.3, 0.4\}$; left: True e_{alg} and estimated η_{alg} relative algebraic energy error; right: Size of $\mathcal{A}_n^H(\tau_n)$ and mean error reduction factor after correct active set has been found.

Figure 8.11 displays the error decay and the mean error reduction factor of the damped version of Algorithm 4 with $\alpha = 0.6$, $l_{\max} = 4$ and different threshold values τ_n . One can observe that a too small threshold value can lead to oscillations in the coarse active set such that the algorithm does not converge. However, if τ_n is too large, the coarse contact set gets smaller which degrades or even disables the convergence, as already observed in the previous subsection.

From now on, we fix $\tau_n = 0.15$ and investigate the performance for different values of l_{\max} and damping parameters α . On the left side of Figure 8.12, the error decay for $l_{\max} = 4$ and $\alpha \in \{0.5, 0.6, 0.7, 0.8\}$ is shown. One can observe that for larger values of α , generally more Newton steps are necessary in order to detect the correct active set; for $\alpha = 0.8$, this has not been achieved within 80 iterations. But as soon as the correct active set has been found, the mean error

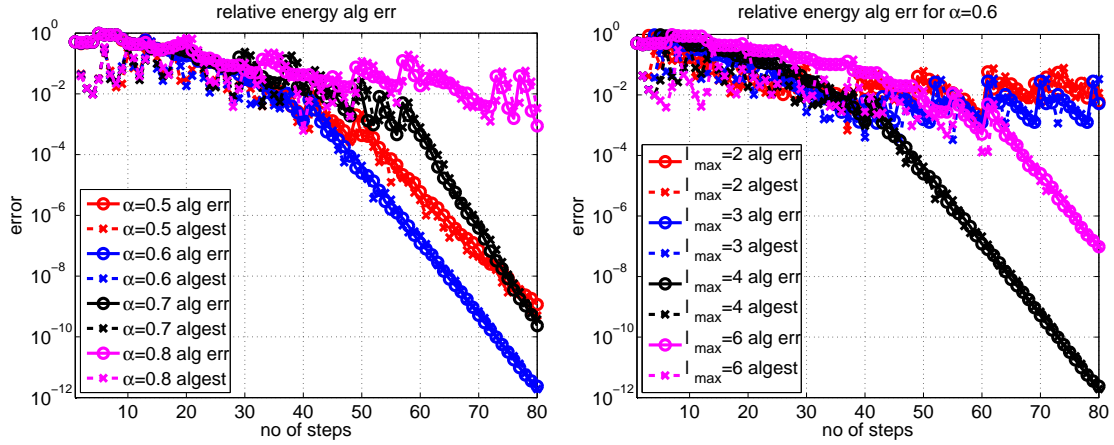


FIGURE 8.12. True e_{alg} and estimated η_{alg} relative alg. error for Algorithm 4 with $\tau_n = 0.15$ wrt. number of total iterations; left: $l_{max} = 4$, $\alpha \in \{0.5, 0.6, 0.7, 0.8\}$; right: $\alpha = 0.6$, $l_{max} \in \{2, 3, 4, 6\}$.

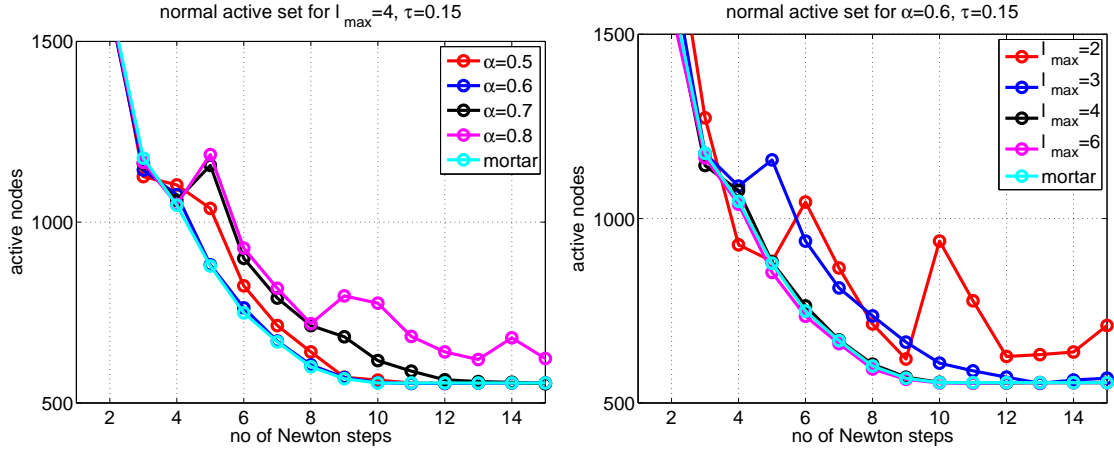


FIGURE 8.13. Evolution of normal active set for Algorithm 4 with $\tau_n = 0.15$ wrt. number of Newton iterations; left: $l_{max} = 4$, $\alpha \in \{0.5, 0.6, 0.7, 0.8\}$; right: $\alpha = 0.6$, $l_{max} \in \{2, 3, 4, 6\}$.

reduction factor is better for larger values of α – they vary between 0.49 for $\alpha = 0.7$ and 0.66 for $\alpha = 0.5$. This suggests an adaptive choice of α with respect to a change in the active sets.

On the right side of Figure 8.12, the error decay for $\alpha = 0.6$ and $l_{max} \in \{2, 3, 4, 6\}$ is plotted. Here, one can see that it can be beneficial to perform additional inner iterations even if the correct fine active set has not been found yet, because this improves the robustness of the algorithm. For $l_{max} \leq 3$, the algorithm has not been able to detect the correct active set within 80 iterations. However, performing too many inner iterations makes the algorithm more inefficient, as the error decay for $l_{max} = 6$ shows.

Figure 8.13 displays the size of the fine active set with respect to the number of Newton iterations for Algorithm 4 with different values of α and l_{max} , as well as for the reference mortar solution (2.33). One can see that the iterative solution with $\alpha = 0.6$ and $l_{max} \geq 4$ does not need more outer Newton steps than the mortar solution in order to detect the correct active set. However, the active set does not converge if α is chosen too large or l_{max} too small.

In order to decrease the number of total iterations further, we replace the condition $l \leq l_{max}$ by

$$\left(\eta_{abs}^{(k+1,l)}\right)^2 \leq E_{\omega}^{-1} \|\mathbf{R}^{(k)}\|^2 = E_{\omega}^{-1} \|\mathbf{C}_{\gamma}^h(\mathbf{u}_{\omega}^{h,(k)}, \zeta_{\gamma}^{h,(k)})\|^2, \quad (8.3)$$

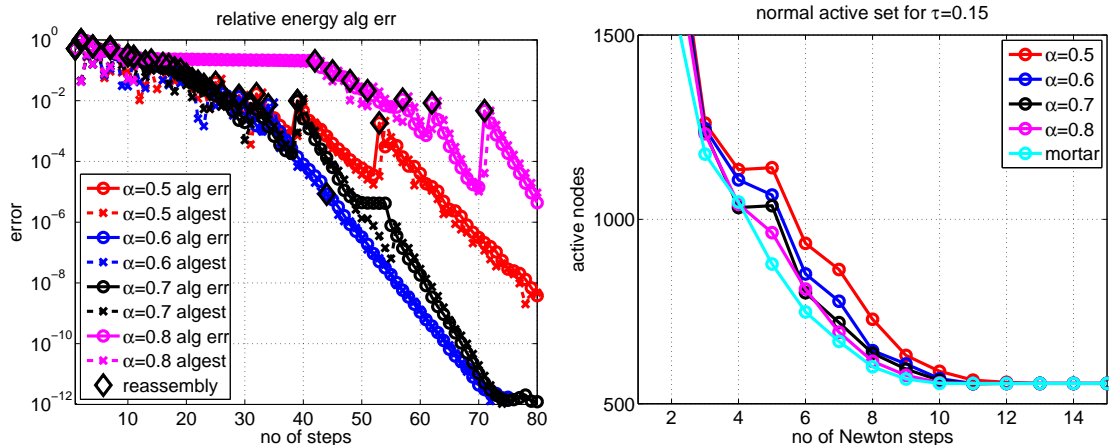


FIGURE 8.14. Performance of Algorithm 4 with $\tau_n = 0.15$ and inner iteration stopped according to (8.3) for $\alpha \in \{0.5, 0.6, 0.7, 0.8\}$; left: True e_{alg} and estimated η_{alg} relative alg. error; right: evolution of active set.

i.e., we measure the error in the nonlinear complementarity function \mathbf{C}_γ^h . The resulting error decay and evolution of the active set is depicted in Figure 8.14 for $\alpha \in \{0.5, 0.6, 0.7, 0.8\}$. Comparing these results with those in Figures 8.12 and 8.13, one can observe that the number of total iterations until convergence has been reduced by about 10 steps and that also the computation with $\alpha = 0.8$ is able to detect the correct active set within 15 Newton iterations.

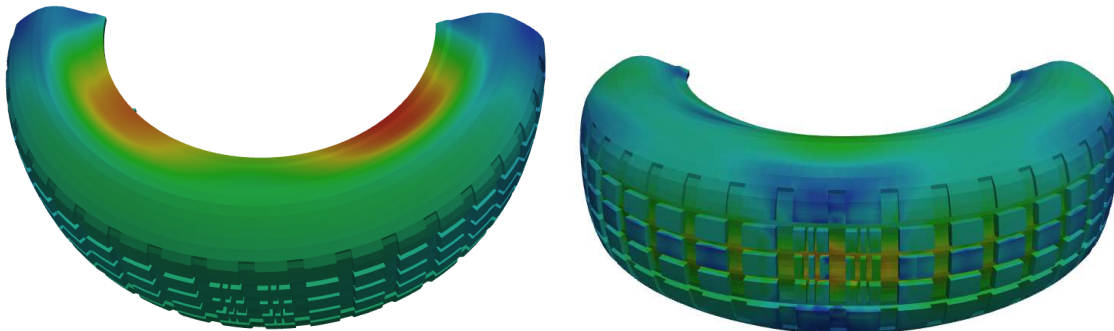


FIGURE 8.15. Effective stress of nonlinear problem on tire geometry with fine slave side \mathcal{E}_F^h ; left: without contact; right: with contact.

Finally, we show two 3D examples for the nonlinear Mooney–Rivlin material law (8.1). First, we choose the parameters $E_\Xi = E_\omega = 2.5 \cdot 10^7$, $\nu = 0.33$ and $c_m = 0.5$, apply no volume forces, omit the contact constraints and prescribe a fixed displacement of $(0, 0, -1.5 + 3 \text{sign}(x_1))$ on the top, whereas all other boundaries are free. The effective stresses of the corresponding mortar solution are depicted on the left of Figure 8.15. This problem is solved using Algorithm 4 with the following stopping criterion for the linear inner iteration (compare (8.2)):

$$\left(\eta_{\text{abs}}^{(k+1,l)}\right)^2 \leq 0.1 \|\mathbf{R}^{(k)}\|^4. \quad (8.4)$$

In Figure 8.16, the corresponding error decay is plotted, with the symbol \diamond marking those steps where the Newton matrix has been reassembled. The left picture shows the error decay with respect to the number of total iterations, whereas the right plot displays the error after each Newton step. One can see that the criterion (8.4) is suitable to obtain a superlinear convergence of the outer Newton iteration.

The final example has the material parameters $E_\Xi = E_\omega = 2.5 \cdot 10^7$, $\nu = 0.33$, $c_m = 0$ as well as the volume force $\mathbf{l} = (0, 0, -100)$. The boundary conditions are given by the surface load

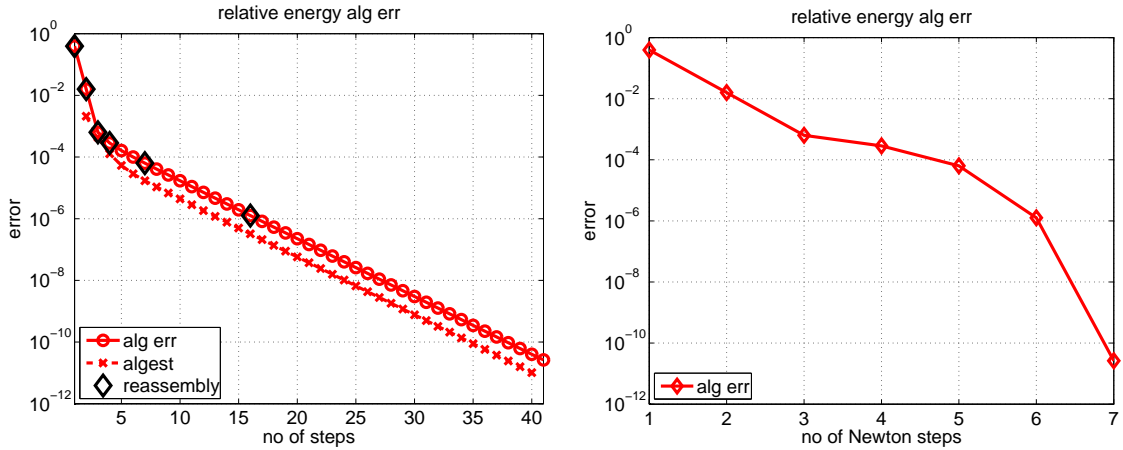


FIGURE 8.16. True e_{alg} and estimated η_{alg} algebraic energy error for Algorithm 4 with inexact solution of inner coupling loop according to (8.4). The asymptotic error reduction factor is 0.65. Left: error decay wrt total steps; right: error decay wrt Newton steps

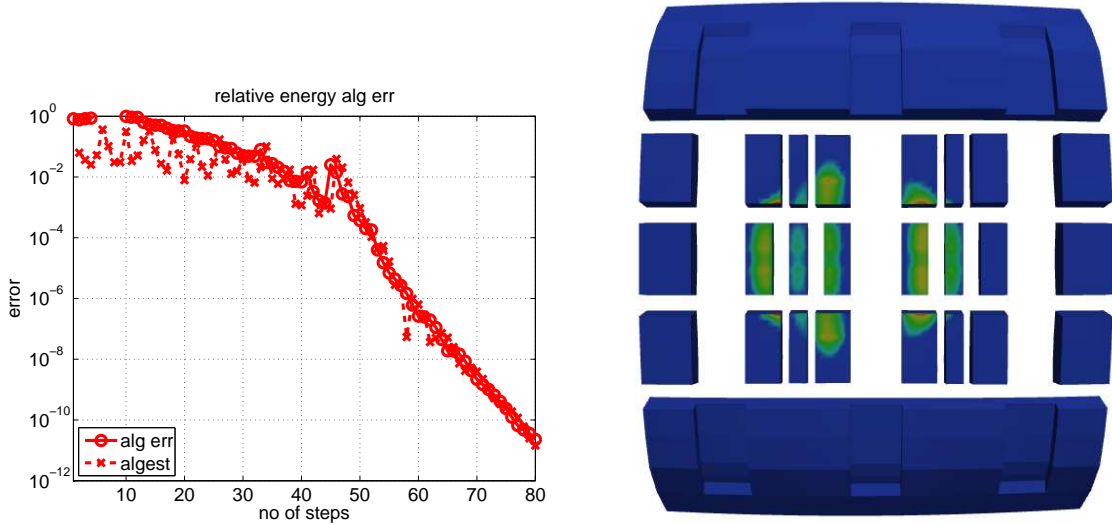


FIGURE 8.17. Performance of Algorithm 4 with $\alpha = 0.6$, $l_{max} = 4$, $\tau_n = 0.15$ for contact problem with nonlinear material. Left: error decay wrt total steps; right: contact stress

$\mathbf{g}_N = (0, 0, -10^5)$ at the points with $|x_2| < 65$ and the Dirichlet values $(0, 0, -1)$ on the top. The results of the iteration with the parameters $\alpha = 0.6$, $l_{max} = 4$ and $\tau_n = 0.15$, depicted on the right of Figure 8.15 and in Figure 8.17, show that Algorithm 4 is able to handle different types of nonlinearities within a single inexact Newton loop.

9. Nearly incompressible material law. The topic of the final section is the treatment of nearly incompressible elastic material, which corresponds to $\lambda \rightarrow \infty$ or equivalently $\nu \rightarrow 0.5$. The numerical simulation of such materials using lowest order conforming finite elements usually leads to volume locking (see, e.g., [7, 6, 14]). Hence, different discretizations are necessary, e.g., by introducing an additional variable for either the stress or the pressure [8, 9, 39, 40, 52]. In this section, we employ a numerical implementation based on a modified version of the Hu–Washizu formulation of the elasticity problem (2.1) described in [14, 46]. For convenience, we shortly sketch the approach in Subsection 9.1. After this, theoretical convergence results are obtained in Subsection 9.2 and tested numerically in Subsection 9.3.

As the challenges arising from incompressibility are not related to dynamic effects, we assume $\varrho = 0$ in this section and omit the time index.

9.1. Discrete Hu–Washizu formulation. The Hu–Washizu formulation considers the displacement, the strain and the stress as independent variables. Let \mathbf{V}^h , \mathbf{D}^h , \mathbf{S}^h be the discrete trial spaces for the displacements, strains and stresses, respectively, associated with a quadrilateral/hexahedral triangulation \mathcal{T}^h of $\omega \subset \mathbb{R}^d$. Further, we assume for simplicity that the material parameters λ , μ are constant on ω and introduce the notation $\kappa := 2\mu + d\lambda$. Then, the spatially discrete problem on the patch ω with prescribed Dirichlet values \mathbf{w}_Γ^h on Γ can be formulated as the following modified Hu–Washizu formulation depending on a scalar parameter $\alpha \neq -\frac{\mu}{\lambda}$ [46]: find $(\mathbf{u}^h, \mathbf{d}^h, \boldsymbol{\sigma}^h, \boldsymbol{\zeta}_\Gamma^h) \in \mathbf{V}^h \times \mathbf{D}^h \times \mathbf{S}^h \times \mathbf{M}_\Gamma^h$ such that for all test functions $(\mathbf{v}^h, \mathbf{e}^h, \boldsymbol{\tau}^h, \boldsymbol{\mu}_\Gamma^h) \in \mathbf{V}^h \times \mathbf{D}^h \times \mathbf{S}^h \times \mathbf{M}_\Gamma^h$

$$\begin{aligned} a_\omega^\alpha((\mathbf{u}^h, \mathbf{d}^h), (\mathbf{v}^h, \mathbf{e}^h)) + b_\omega^\alpha((\mathbf{v}^h, \mathbf{e}^h), \boldsymbol{\sigma}^h) + \langle \mathbf{v}^h, \boldsymbol{\zeta}_\Gamma^h \rangle_\Gamma &= f_\omega(\mathbf{v}^h), \\ b_\omega^\alpha((\mathbf{u}^h, \mathbf{d}^h), \boldsymbol{\tau}^h) - \frac{(1-\alpha)\lambda}{\kappa^2} (\text{tr } \boldsymbol{\sigma}^h, \text{tr } \boldsymbol{\tau}^h)_{0,\omega} &= 0, \\ \langle \mathbf{u}^h, \boldsymbol{\mu}_\Gamma^h \rangle_\Gamma &= \langle \mathbf{v}_\Gamma^h, \boldsymbol{\mu}_\Gamma^h \rangle_\Gamma. \end{aligned} \quad (9.1)$$

In (9.1), we have used the notation

$$\begin{aligned} a_\omega^\alpha((\mathbf{u}^h, \mathbf{d}^h), (\mathbf{v}^h, \mathbf{e}^h)) &:= 2\mu (\mathbf{d}^h, \mathbf{e}^h)_{0,\omega} + \alpha\lambda (\text{tr } \mathbf{d}^h, \text{tr } \mathbf{e}^h)_{0,\omega}, \\ b_\omega^\alpha((\mathbf{v}^h, \mathbf{e}^h), \boldsymbol{\sigma}^h) &:= (\boldsymbol{\varepsilon}(\mathbf{v}^h) - 2\mu(\mathbb{C}^{\text{el}})^{-1}\mathbf{e}^h, \boldsymbol{\sigma}^h)_{0,\omega} - \frac{\alpha\lambda}{\kappa} (\text{tr } \boldsymbol{\sigma}^h, \text{tr } \mathbf{e}^h)_{0,\omega}. \end{aligned}$$

The standard Hu–Washizu formulation is obtained for $\alpha = 1$. Furthermore, if the discrete trial spaces satisfy the requirements

$$\mathbf{S}^h \subset \mathbf{D}^h, \quad \text{tr}(\mathbf{D}^h)\text{Id} \subset \mathbf{D}^h, \quad (9.2)$$

the solution of (9.1) does not depend on α [46]. In this case, we obtain $\mathbf{d}^h = (\mathbb{C}^{\text{el}})^{-1}\boldsymbol{\sigma}^h$, and (9.1) is equivalent to the mixed formulation of Hellinger and Reissner (see, e.g., [7]).

The discrete spaces \mathbf{D}^h , \mathbf{S}^h are constructed elementwise as follows:

$$\begin{aligned} \mathbf{S}_0 &:= \left\{ \boldsymbol{\tau} \in [L_2(\omega)]^{d \times d} : \boldsymbol{\tau} = \boldsymbol{\tau}^T, (\text{tr } \boldsymbol{\tau}, 1)_{0,\omega} = 0 \right\}, \\ \mathbf{S}^h &:= \left\{ \boldsymbol{\tau} \in \mathbf{S}_0 : (\boldsymbol{\tau}|_K) = (\hat{\boldsymbol{\tau}}) \circ F_K^{-1}, \hat{\boldsymbol{\tau}} \in \mathbf{S}_\square, K \in \mathcal{T}^h \right\}, \\ \mathbf{D}^h &:= \left\{ \boldsymbol{\tau} \in \mathbf{S}_0 : (\boldsymbol{\tau}|_K) = (\hat{\boldsymbol{\tau}}) \circ F_K^{-1}, \hat{\boldsymbol{\tau}} \in \mathbf{D}_\square, K \in \mathcal{T}^h \right\}, \end{aligned}$$

where $F_K : \hat{K} \rightarrow K$ is assumed to be an isoparametric \mathbf{Q}_1 -map, and the spaces \mathbf{S}_\square , \mathbf{D}_\square are given polynomial spaces on the corresponding reference element $\hat{K} = (-1, 1)^d$. As discussed in [19], this general setting includes for example the methods of mixed enhanced strains [39, 40], enhanced assumed strains [6, 8, 54], or the classical \mathcal{Q}_1 – \mathcal{P}_0 pair [38]. For these methods (and some others described in [14]), the elementwise definition of the spaces \mathbf{D}^h , \mathbf{S}^h allows for a local static condensation of the corresponding degrees of freedom in (9.1), resulting in the following stabilized displacement-based problem (see [14, Lemma 4.2]): find $(\mathbf{u}^h, \boldsymbol{\zeta}_\Gamma^h) \in \mathbf{V}^h \times \mathbf{M}_\Gamma^h$ such that

$$\begin{aligned} (Q^h \boldsymbol{\varepsilon}(\mathbf{u}^h), \boldsymbol{\varepsilon}(\mathbf{v}^h))_{0,\omega} + \langle \mathbf{v}^h, \boldsymbol{\zeta}_\Gamma^h \rangle_\Gamma &= f_\omega(\mathbf{v}^h), \quad \mathbf{v}^h \in \mathbf{V}^h, \\ \langle \mathbf{u}^h, \boldsymbol{\mu}_\Gamma^h \rangle_\Gamma &= \langle \mathbf{w}_\Gamma^h, \boldsymbol{\mu}_\Gamma^h \rangle_\Gamma, \quad \boldsymbol{\mu}_\Gamma^h \in \mathbf{M}_\Gamma^h, \end{aligned} \quad (9.3)$$

with the projection operator

$$Q^h \boldsymbol{\varepsilon}(\mathbf{u}^h) := \mathbb{C}^{\text{el}} P_{\mathbf{S}_c^h} \boldsymbol{\varepsilon}(\mathbf{u}^h) + \varpi P_{\mathbf{S}_t^h} \boldsymbol{\varepsilon}(\mathbf{u}^h). \quad (9.4)$$

The orthogonal projections $P_{\mathbf{S}_c^h}$, $P_{\mathbf{S}_t^h}$ are given in terms of the decomposition

$$\mathbf{S}^h = \mathbf{S}_c^h \oplus \mathbf{S}_t^h \quad \text{with} \quad \mathbf{S}_c^h := \left\{ \boldsymbol{\tau} \in \mathbf{S}^h : \mathbb{C}^{\text{el}} \boldsymbol{\tau} \in \mathbf{S}^h \right\}.$$

The exact definition of the constant $\varpi = \varpi(\alpha, \lambda, \mu)$ is given in [46] for $d = 2$ and in [45] for $d = 3$; for our purpose, it is sufficient to know that $\varpi - 2\mu$ is positive and bounded from above independently of λ (see Assumption 9.1 below).

9.2. Condition number analysis. We define the trace spaces

$$R^h := \text{tr } \mathbf{S}^h, \quad R_c^h := \text{tr } \mathbf{S}_c^h, \quad R_t^h := \text{tr } \mathbf{S}_t^h.$$

The above displacement-based formulation (9.3) can be rewritten as a mixed formulation using the pressure-like variables $p_c^h \in R_c^h$, $p_t^h \in R_t^h$ (cf. [46, Lemma 5.11]): find $(\mathbf{u}^h, p_c^h, p_t^h, \boldsymbol{\zeta}_\Gamma^h) \in \mathbf{V}^h \times R_c^h \times R_t^h \times \mathbf{M}_\Gamma^h$ such that

$$\begin{aligned} a_\omega^h(\mathbf{u}^h, \mathbf{v}^h) + b_\omega^h(\mathbf{v}^h, p_c^h + p_t^h) + \langle \mathbf{v}^h, \boldsymbol{\zeta}_\Gamma^h \rangle_\Gamma &= f_\omega(\mathbf{v}^h), & \mathbf{v}^h &\in \mathbf{V}^h, \\ b_\omega^h(\mathbf{u}^h, q_c^h) - \frac{1}{\lambda} (p_c^h, q_c^h)_{0,\omega} &= 0, & q_c^h &\in R_c^h, \\ b_\omega^h(\mathbf{u}^h, q_t^h) - \frac{1}{\varpi - 2\mu} (p_t^h, q_t^h)_{0,\omega} &= 0, & q_t^h &\in R_t^h, \\ \langle \mathbf{u}^h, \boldsymbol{\mu}_\Gamma^h \rangle_\Gamma &= \langle \mathbf{w}_\Gamma^h, \boldsymbol{\mu}_\Gamma^h \rangle_\Gamma, & \boldsymbol{\mu}_\Gamma^h &\in \mathbf{M}_\Gamma^h, \end{aligned} \quad (9.5)$$

with the bilinear forms

$$a_\omega^h(\mathbf{u}^h, \mathbf{v}^h) := 2\mu (P_{\mathbf{S}^h} \boldsymbol{\varepsilon}(\mathbf{u}^h), P_{\mathbf{S}^h} \boldsymbol{\varepsilon}(\mathbf{v}^h))_{0,\omega}, \quad b_\omega^h(\mathbf{u}^h, q^h) := (\text{div } \mathbf{u}^h, q^h)_{0,\omega}.$$

Proof. By static condensation of (9.5)_{2,3}, we obtain

$$p_c^h = \lambda P_{R_c^h}(\text{div } \mathbf{u}^h), \quad p_t^h = (\varpi - 2\mu) P_{R_t^h}(\text{div } \mathbf{u}^h).$$

Substituting this into (9.5)₁ yields with the equation

$$(\boldsymbol{\tau}_t^h, \boldsymbol{\nu}_t^h)_{0,\omega} = (\text{tr } \boldsymbol{\tau}_t^h, \text{tr } \boldsymbol{\nu}_t^h)_{0,\omega}, \quad \boldsymbol{\tau}_t^h, \boldsymbol{\nu}_t^h \in \mathbf{S}_t^h,$$

discussed in [45] and the orthogonality of \mathbf{S}_c^h , \mathbf{S}_t^h

$$\begin{aligned} &a_\omega^h(\mathbf{u}^h, \mathbf{v}^h) + b_\omega^h(\mathbf{v}^h, p_c^h + p_t^h) \\ &= a_\omega^h(\mathbf{u}^h, \mathbf{v}^h) + \lambda (\text{div } \mathbf{v}^h, P_{R_c^h}(\text{div } \mathbf{u}^h))_{0,\omega} + (\varpi - 2\mu) (\text{div } \mathbf{v}^h, P_{R_t^h}(\text{div } \mathbf{u}^h))_{0,\omega} \\ &= 2\mu (P_{\mathbf{S}_c^h} \boldsymbol{\varepsilon}(\mathbf{u}^h), P_{\mathbf{S}_c^h} \boldsymbol{\varepsilon}(\mathbf{v}^h))_{0,\omega} + \lambda (P_{R_c^h}(\text{tr } \boldsymbol{\varepsilon}(\mathbf{v}^h)), P_{R_c^h}(\text{tr } \boldsymbol{\varepsilon}(\mathbf{u}^h)))_{0,\omega} \\ &\quad + 2\mu (P_{\mathbf{S}_t^h} \boldsymbol{\varepsilon}(\mathbf{u}^h), P_{\mathbf{S}_t^h}(\boldsymbol{\varepsilon}(\mathbf{v}^h)))_{0,\omega} + (\varpi - 2\mu) (P_{R_t^h}(\text{tr } \boldsymbol{\varepsilon}(\mathbf{v}^h)), P_{R_t^h}(\text{tr } \boldsymbol{\varepsilon}(\mathbf{u}^h)))_{0,\omega} \\ &= (Q^h \boldsymbol{\varepsilon}(\mathbf{u}^h), \boldsymbol{\varepsilon}(\mathbf{v}^h))_{0,\omega}. \end{aligned}$$

□ For the next estimate, we need the following assumptions:

ASSUMPTION 9.1. *There exist positive constants c , β , τ , not depending on h or the material parameters μ , λ such that*

- (i) $\|P_{\mathbf{S}^h} \boldsymbol{\varepsilon}(\mathbf{v}^h)\|_{0,\omega} \geq c \|\boldsymbol{\varepsilon}(\mathbf{v}^h)\|_{0,\omega}$ for all $\mathbf{v}^h \in \mathbf{V}^h$.
- (ii) The pairing \mathbf{V}^h , R_c^h satisfies an uniform inf-sup condition:

$$\sup_{\substack{\mathbf{v}^h \in \mathbf{V}^h \setminus \{\mathbf{0}\} \\ \mathbf{v}^h|_\Gamma = \mathbf{0}}} \frac{b_\omega^h(\mathbf{v}^h, q_c^h)}{\|\boldsymbol{\varepsilon}(\mathbf{v}^h)\|_{0,\omega}} \geq \beta \|q_c^h\|_{0,\omega}, \quad q_c^h \in R_c^h. \quad (9.6)$$

- (iii) $0 \leq \varpi(\alpha, \lambda, \mu) - 2\mu \leq \tau\mu$.

REMARK 9.2. *Assumption (i) is automatically satisfied as soon as the discrete spaces satisfy $\boldsymbol{\varepsilon}(\mathbf{V}^h) \subset \mathbf{S}^h$, which is the case for several established methods (see [19] for more details). Assumption (iii) automatically holds for the cases satisfying (9.2) with $\tau = \frac{2}{d-1}$, or for a wide range of α otherwise. In addition, Assumption (ii) is weaker than the inf-sup condition on the pairing \mathbf{V}^h , R^h because of $\dim(R_c^h) \leq \dim(R^h)$.*

Further, we introduce the discrete extension operator $\mathcal{H}_\omega^h : \mathbf{W}_\Gamma^h \rightarrow \mathbf{V}^h$ given by

$$(\boldsymbol{\varepsilon}(\mathcal{H}_\omega^h \mathbf{w}_\Gamma^h), \boldsymbol{\varepsilon}(\mathbf{v}^h))_{0,\omega} = 0, \quad \mathbf{v}^h \in \mathbf{V}^h, \mathbf{v}^h|_\Gamma = \mathbf{0},$$

as well as the discrete mixed extension $\mathcal{M}_\omega^h : \mathbf{W}_\Gamma^h \rightarrow \mathbf{V}^h$ given by $\mathcal{M}_\omega^h \mathbf{w}_\Gamma^h = \mathbf{u}^h$, with \mathbf{u}^h being the first component of the solution of (9.5) with $f_\omega = 0$ in (9.5)₁.

Then, we obtain the following lemma:

LEMMA 9.3. *Let Assumption 9.1 be satisfied. Then, there exist positive constants c, C not depending on the diameter of ω, h or μ, λ such that*

$$c|\mathbf{w}_\Gamma^h|_{\widetilde{\mathbf{W}}_\Gamma(\omega)}^2 \leq \|P_{\mathbf{S}^h} \varepsilon(\mathcal{M}_\omega^h \mathbf{w}_\Gamma^h)\|_{0,\omega}^2 \leq C|\mathbf{w}_\Gamma^h|_{\widetilde{\mathbf{W}}_\Gamma(\omega)}^2,$$

Proof. The idea of the proof is the same as in [9, Theorem 4.1]. The properties of the extension operator \mathcal{H}_ω^h yield the estimates [56]

$$c|\mathbf{w}_\Gamma^h|_{\widetilde{\mathbf{W}}_\Gamma(\omega)}^2 \leq \|\varepsilon(\mathcal{H}_\omega^h \mathbf{w}_\Gamma^h)\|_{0,\omega}^2 = \inf_{\substack{\mathbf{v}^h \in \mathbf{V}^h \\ \mathbf{v}^h|_\Gamma = \mathbf{w}_\Gamma^h}} \|\varepsilon(\mathbf{v}^h)\|_{0,\omega}^2 \leq C|\mathbf{w}_\Gamma^h|_{\widetilde{\mathbf{W}}_\Gamma(\omega)}^2.$$

Denoting $\mathbf{u}^h = \mathcal{M}_\omega^h \mathbf{w}_\Gamma^h$, we obtain with Assumption 9.1(i)

$$c|\mathbf{w}_\Gamma^h|_{\widetilde{\mathbf{W}}_\Gamma(\omega)}^2 \leq \|\varepsilon(\mathcal{H}_\omega^h \mathbf{w}_\Gamma^h)\|_{0,\omega}^2 \leq \|\varepsilon(\mathbf{u}^h)\|_{0,\omega}^2 \leq C \|P_{\mathbf{S}^h} \varepsilon(\mathbf{u}^h)\|_{0,\omega}^2.$$

Choosing $\mathbf{v}^h = \mathbf{u}^h - \mathcal{H}_\omega^h \mathbf{w}_\Gamma^h$, $q_c^h = p_c^h$, $q_t^h = p_t^h$ in (9.5) yields

$$a_\omega^h(\mathbf{u}^h, \mathbf{u}^h) = a_\omega^h(\mathbf{u}^h, \mathcal{H}_\omega^h \mathbf{w}_\Gamma^h) - b_\omega^h(\mathbf{u}^h - \mathcal{H}_\omega^h \mathbf{w}_\Gamma^h, p_c^h + p_t^h), \quad (9.7a)$$

$$b_\omega^h(\mathbf{u}^h, p_c^h) = \frac{1}{\lambda} \|p_c^h\|_{0,\omega}^2, \quad (9.7b)$$

$$b_\omega^h(\mathbf{u}^h, p_t^h) = \frac{1}{\varpi - 2\mu} \|p_t^h\|_{0,\omega}^2. \quad (9.7c)$$

From (9.7c) and Assumption 9.1(i, iii), we directly obtain

$$\|p_t^h\|_{0,\omega} \leq \tau\mu \|\varepsilon(\mathbf{u}^h)\|_{0,\omega} \leq \tau\mu \|P_{\mathbf{S}^h} \varepsilon(\mathbf{u}^h)\|_{0,\omega}, \quad (9.8)$$

whereas (9.7a) gives with $\lambda \geq 0, \varpi - 2\mu \geq 0$

$$\begin{aligned} & 2\mu \|P_{\mathbf{S}^h} \varepsilon(\mathbf{u}^h)\|_{0,\omega}^2 \\ &= a_\omega^h(\mathbf{u}^h, \mathcal{H}_\omega^h \mathbf{w}_\Gamma^h) + b_\omega^h(\mathcal{H}_\omega^h \mathbf{w}_\Gamma^h, p_c^h + p_t^h) - \frac{1}{\lambda} \|p_c^h\|_{0,\omega}^2 - \frac{1}{\varpi - 2\mu} \|p_t^h\|_{0,\omega}^2 \\ &\leq 2\mu \|P_{\mathbf{S}^h} \varepsilon(\mathbf{u}^h)\|_{0,\omega} \|\varepsilon(\mathcal{H}_\omega^h \mathbf{w}_\Gamma^h)\|_{0,\omega} + \|\varepsilon(\mathcal{H}_\omega^h \mathbf{w}_\Gamma^h)\|_{0,\omega} \left(\|p_c^h\|_{0,\omega} + \|p_t^h\|_{0,\omega} \right). \end{aligned}$$

With Assumption 9.1(ii) and (9.8), we get

$$\begin{aligned} \|p_c^h\|_{0,\omega} &\leq \beta^{-1} \sup_{\substack{\mathbf{v}^h \in \mathbf{V}^h \setminus \{\mathbf{0}\} \\ \mathbf{v}^h|_\Gamma = \mathbf{0}}} \frac{b_\omega^h(\mathbf{v}^h, p_c^h)}{\|\varepsilon(\mathbf{v}^h)\|_{0,\omega}} \\ &= \beta^{-1} \sup_{\substack{\mathbf{v}^h \in \mathbf{V}^h \setminus \{\mathbf{0}\} \\ \mathbf{v}^h|_\Gamma = \mathbf{0}}} \frac{a_\omega^h(\mathbf{u}^h, \mathbf{v}^h) + b_\omega^h(\mathbf{v}^h, p_t^h)}{\|\varepsilon(\mathbf{v}^h)\|_{0,\omega}} \leq C\mu \|P_{\mathbf{S}^h} \varepsilon(\mathbf{u}^h)\|_{0,\omega}, \end{aligned}$$

such that we arrive at

$$2\mu \|P_{\mathbf{S}^h} \varepsilon(\mathbf{u}^h)\|_{0,\omega} \leq C\mu \|\varepsilon(\mathcal{H}_\omega^h \mathbf{w}_\Gamma^h)\|_{0,\omega} \leq C\mu |\mathbf{w}_\Gamma^h|_{\widetilde{\mathbf{W}}_\Gamma(\omega)},$$

completing the proof. \square Let $S_{*,\omega}^h : \mathbf{W}_\Gamma^h \rightarrow (\mathbf{W}_\Gamma^h)'$ be given by

$$\langle S_{*,\omega}^h \mathbf{w}_\Gamma^h, \mathbf{v}^h \rangle_\Gamma = (Q^h \varepsilon(\mathbf{u}^h), \varepsilon(\mathbf{v}^h))_{0,\omega}, \quad \mathbf{v}^h \in \mathbf{V}^h, \quad (9.9)$$

and let $S_{*,\omega}^H$ be the corresponding coarse grid approximation on \mathcal{T}^H . Using Lemma 9.3, we directly obtain the following spectral equivalence result similar to Theorem 3.6:

THEOREM 9.4. *Assume that the material parameters E, ν satisfy the estimate $cE_\omega \leq E(\mathbf{x}) \leq CE_\omega$, $c\nu_\omega \leq \nu(\mathbf{x}) \leq C\nu_\omega$ for $\mathbf{x} \in \omega$. Let Assumptions 2.3 and 9.1 hold. Then, there exist constants c^*, C^* independent of the diameter of ω , h, H and the values E_ω, ν_ω (but c^* possibly dependent on c_p) such that the following estimates are satisfied for any function $\mathbf{w}_\Gamma^H \in \mathbf{W}_\Gamma^H$:*

$$c^* (\mathbf{w}_\Gamma^H, S_{*,\omega}^H \mathbf{w}_\Gamma^H) \leq (\mathbf{w}_\Gamma^H, (\Pi^{hH})^T S_{*,\omega}^h \Pi^{hH} \mathbf{w}_\Gamma^H) \leq C^* (\mathbf{w}_\Gamma^H, S_{*,\omega}^H \mathbf{w}_\Gamma^H).$$

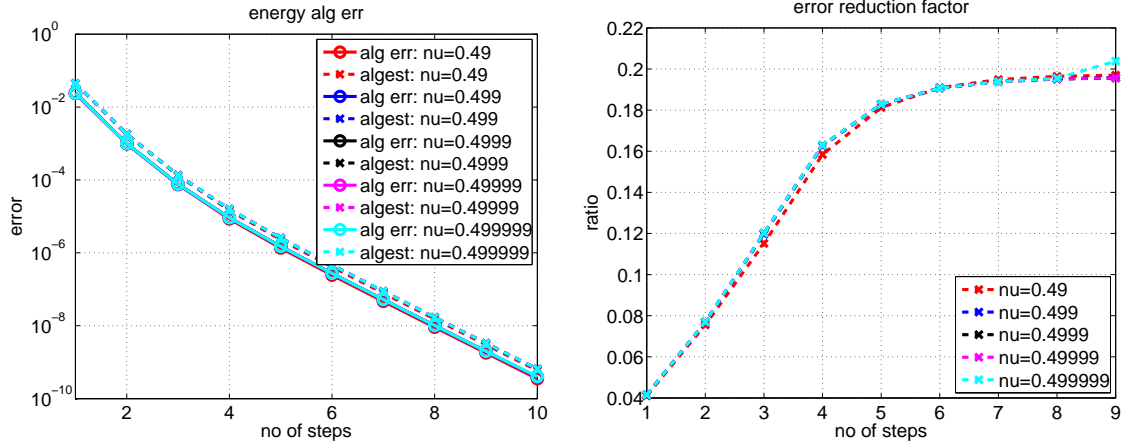


FIGURE 9.1. Performance of Algorithm 1 for $L = 2$, $E_\omega = E_\Xi$ and different values of ν_ω wrt l ; left: True $e_{alg}^{(l)}$ and estimated $\eta_{alg}^{(l)}$ relative alg. error; right: Error reduction factor $e_{alg}^{(l+1)}/e_{alg}^{(l)}$.

9.3. Numerical results. In order to test the convergence behaviour of Algorithm 1 applied to the nearly incompressible case, we consider the same test setting as in Subsection 8.3 with the domain $\Omega = [0, 1] \times [0, 1] \times [0, 2]$ and $\omega = [0, 1]^3$. We impose homogeneous Dirichlet boundary conditions on the top, the Neumann compression forces

$$\mathbf{g}_N = 1000 \cdot \max(0, 0.25 - r), \quad \text{with } r^2 = (0.5 - x_1)^2 + (0.5 - x_2)^2$$

on the bottom and homogeneous Neumann conditions elsewhere. We use uniform hexahedral grids of mesh size $H = \frac{1}{4}$ and $h = \frac{1}{16}$, and the parameters for the linear elastic material are chosen according to $E_\omega = E_\Xi = 100$, $\nu_\Xi = 0.33$ and $\nu_\omega \rightarrow 0.5$. The computation is done using the condensed displacement-based formulation (9.3) with the method of mixed enhanced strains.

In Figure 9.1, the error decay of Algorithm 1 for different values of ν_ω is depicted. One can see that the convergence rate is completely independent of ν_ω and hence also stable for $\nu_\omega \rightarrow 0.5$.

REFERENCES

- [1] P. ALART AND A. CURNIER, *A mixed formulation for frictional contact problems prone to Newton like solution methods*, Comput. Methods Appl. Mech. Engrg., 92 (1991), pp. 353–375.
- [2] F. BEN BELGACEM, *The mortar finite element method with Lagrange multipliers*, Numer. Math., 84 (1999), pp. 173–197.
- [3] C. BERNARDI, Y. MADAY, AND A. T. PATERA, *A new nonconforming approach to domain decomposition: The mortar element method*, in Nonlinear partial differential equations and their applications, H. Brezis and J.-L. Lions, eds., vol. XI of Collège de France Seminar, Pitman, 1994, pp. 13–51.
- [4] P. E. BJØRSTAD AND O. B. WIDLUND, *Iterative methods for the solution of elliptic problems on regions partitioned into substructures*, SIAM J. Numer. Anal., 23 (1986), pp. 1097–1120.
- [5] D. BRAESS, *Finite Elements*, Cambridge University Press, 1997.
- [6] ———, *Enhanced assumed strain elements and locking in membrane problems*, Comput. Methods Appl. Mech. Engrg., 165 (1998), pp. 155–174.

- [7] ———, *Finite Elemente*, Springer, Berlin, 3rd ed., 2003.
- [8] D. BRAESS, C. CARSTENSEN, AND B. D. REDDY, *Uniform convergence and a posteriori error estimators for the enhanced strain finite element method*, Numer. Math., 96 (2004), pp. 461–479.
- [9] J. H. BRAMBLE AND J. E. PASCIAK, *A domain decomposition technique for Stokes problems*, Appl. Numer. Math., 6 (1989), pp. 251–261.
- [10] J. H. BRAMBLE, J. E. PASCIAK, AND A. H. SCHATZ, *An iterative method for elliptic problems on regions partitioned into substructures*, Math. Comp., 46 (1986), pp. 361–369.
- [11] S. C. BRENNER, *Korn's inequalities for piecewise H^1 vector fields*, Math. Comp., 73 (2003), pp. 1067–1087.
- [12] S. C. BRENNER AND L. SCOTT, *The Mathematical Theory of Finite Element Methods*, Springer, New York, 1994.
- [13] F. BREZZI AND M. FORTIN, *Mixed and hybrid finite element methods*, Springer, New York, 1991.
- [14] K. S. CHAVAN, B. P. LAMICHHANE, AND B. I. WOHLMUTH, *Locking-free finite element methods for linear and nonlinear elasticity in 2D and 3D*, Comput. Meth. Appl. Mech. Engrg., 196 (2007), pp. 4075–4086.
- [15] V. CHAWLA AND T. A. LAURSEN, *Energy consistent algorithms for frictional contact problems*, Internat. J. Numer. Methods Engrg., 42 (1998), pp. 799–827.
- [16] P. W. CHRISTENSEN, A. KLARBRING, J. S. PANG, AND N. STRÖMBERG, *Formulation and comparison of algorithms for frictional contact problems*, Internat. J. Numer. Methods Engrg., 42 (1998), pp. 145–173.
- [17] R. S. DEMBO, S. C. EISENSTAT, AND T. STEINHAUG, *Inexact Newton methods*, SIAM J. Numer. Anal., 19 (1982), pp. 400–408.
- [18] P. DEUFLHARD, *Newton methods for nonlinear problems*, Springer, Berlin Heidelberg, 2004.
- [19] J. K. DJOKO, B. P. LAMICHHANE, B. D. REDDY, AND B. I. WOHLMUTH, *Conditions for equivalence between the Hu–Washizu and related formulations, and computational behavior in the incompressible limit*, Comput. Methods Appl. Mech. Engrg., 195 (2006), pp. 4161–4178.
- [20] C. ECK, J. JARUŠEK, AND M. KRBEČ, *Unilateral contact problems. Variational methods and existence theorems*, CRC Press Taylor & Francis Group, Boca Raton, 2005.
- [21] V. ELJKHOUT AND P. VASSILEVSKI, *The role of the strengthened Cauchy–Buniakowskii–Schwarz inequality in multilevel methods*, SIAM review, 33 (1991), pp. 405–419.
- [22] S. C. EISENSTAT AND H. F. WALKER, *Choosing the forcing terms in an inexact Newton method*, SIAM J. Sci. Comput., 17 (1996), pp. 16–32.
- [23] F. FACCHINEI AND J.-S. PANG, *Finite-dimensional variational inequalities and complementary problems*, vol. 1, Springer, New York, 2003.
- [24] ———, *Finite-dimensional variational inequalities and complementary problems*, Springer, New York, 2003.
- [25] C. FARHAT AND F.-X. ROUX, *A method of finite element tearing and interconnecting and its parallel solution algorithm*, Internat. J. Numer. Methods Engrg., 32 (1991), pp. 1205–1227.
- [26] P. GOLDFELD, L. F. PAVARINO, AND O. B. WIDLUND, *Balancing Neumann–Neumann preconditioners for mixed approximations of heterogeneous problems in linear elasticity*, Numer. Math., 95 (2003), pp. 283–324.
- [27] O. GONZALEZ, *Exact energy and momentum conserving algorithms for general models in nonlinear elasticity*, Comp. Methods Appl. Mech. Engrg., 190 (2000), pp. 1763–1783.
- [28] C. HAGER, S. HÜEBER, AND B. I. WOHLMUTH, *A stable energy conserving approach for frictional contact problems based on quadrature formulas*, Internat. J. Numer. Methods Engrg., 73 (2008), pp. 205–225.
- [29] C. HAGER AND B. I. WOHLMUTH, *Analysis of a space-time discretization for dynamic elasticity problems based on mass-free surface elements*, SIAM J. Numer. Anal., 47 (2009), pp. 1863–1885.
- [30] ———, *Nonlinear complementarity functions for plasticity problems with frictional contact*, Comput. Methods Appl. Mech. Engrg., 198 (2009), pp. 3411–3427.
- [31] E. HAIRER AND G. WANNER, *Solving ordinary differential equations II: Stiff and differential-algebraic problems*, Springer, Berlin Heidelberg, 1991.
- [32] P. HAURET AND P. LE TALLEC, *Energy-controlling time integration methods for nonlinear elastodynamics and low-velocity impact*, Comput. Methods Appl. Mech. Engrg., 195 (2006), pp. 4890–4916.
- [33] ———, *Two-scale Dirichlet–Neumann preconditioners for elastic problems with boundary refinements*, Comput. Methods Appl. Mech. Engrg., 196 (2007), pp. 1574–1588.
- [34] M. HINTERMÜLLER, K. ITO, AND K. KUNISCH, *The primal-dual active set strategy as a semi-smooth Newton method*, SIAM J. Optim., 13 (2003), pp. 865–888.
- [35] S. HÜEBER, G. STADLER, AND B. I. WOHLMUTH, *A primal-dual active set algorithm for three-dimensional contact problems with Coulomb friction*, SIAM J. Sci. Comput., 30 (2008), pp. 572–596.
- [36] S. HÜEBER AND B. I. WOHLMUTH, *An optimal a priori error estimate for non-linear multibody contact problems*, SIAM J. Numer. Anal., 43 (2005), pp. 157–173.
- [37] ———, *A primal-dual active set strategy for non-linear multibody contact problems*, Comput. Methods Appl. Mech. Engrg., 194 (2005), pp. 3147–3166.
- [38] T. J. R. HUGHES, *The finite element method: Linear, static and dynamic finite element analysis*, Prentice-Hall, 1987.
- [39] E. KASPER AND R. TAYLOR, *A mixed-enhanced strain method. part I: geometrically linear problems*, Comput. Struct., 75 (2000), pp. 237–250.
- [40] ———, *A mixed-enhanced strain method. part II: geometrically nonlinear problems*, Comput. Struct., 75 (2000), pp. 251–260.
- [41] H. B. KHENOUS, P. LABORDE, AND Y. RENARD, *Comparison of two approaches for the discretization of elastodynamic contact problems*, C. R. Akad. Sci. Paris, 342 (2006), pp. 791–796.

- [42] N. KIKUCHI AND J. T. ODEN, *Contact problems in elasticity: A study of variational inequalities and finite element methods*, SIAM Studies in Applied Mathematics 8, Philadelphia, 1988.
- [43] A. KLAWONN AND O. B. WIDLUND, *FETI and Neumann–Neumann iterative substructuring methods: Connections and new results*, Comm. on Pure Appl. Math., 54 (2001), pp. 57–90.
- [44] J. KRUIS, *Domain decomposition methods for distributed computing*, Saxe-Coburg Publications, Stirling, 2006.
- [45] B. P. LAMICHHANE, *Higher order mortar finite elements with dual Lagrange multiplier spaces and applications*, PhD thesis, Universität Stuttgart, 2006.
- [46] B. P. LAMICHHANE, B. D. REDDY, AND B. I. WOHLMUTH, *Convergence in the incompressible limit of finite element approximations based on the Hu–Washizu formulation*, Numer. Math., 104 (2006), pp. 151–175.
- [47] T. A. LAURSEN, *Computational contact and impact mechanics*, Springer, Berlin Heidelberg, 2002.
- [48] T. A. LAURSEN AND V. CHAWLA, *Design of energy conserving algorithms for frictionless dynamic contact problems*, Internat. J. Numer. Methods Engrg., 40 (1997), pp. 836–886.
- [49] T. A. LAURSEN AND G. R. LOVE, *Improved implicit integrators for transient impact problems – geometric admissibility within the conserving framework*, Internat. J. Numer. Methods Engrg., 53 (2002), pp. 245–274.
- [50] L. MARINI AND A. QUARTERONI, *A relaxation procedure for domain decomposition methods using finite elements*, Numer. Math., 55 (1989), pp. 575–598.
- [51] A. QUARTERONI AND A. VALLI, *Domain decomposition methods for partial differential equations*, Oxford University Press, 1999.
- [52] B. D. REDDY AND J. C. SIMO, *Stability and convergence of a class of enhanced strain methods*, SIAM J. Numer. Anal., 32 (1995), pp. 1705–1728.
- [53] L. R. SCOTT AND S. ZHANG, *Finite element interpolation of nonsmooth functions satisfying boundary conditions*, Math. Comput., 54 (1990), pp. 483–493.
- [54] J. C. SIMO AND M. S. RIFAI, *A class of mixed assumed strain methods and the method of incompatible modes*, Internat. J. Numer. Methods Engrg., 29 (1990), pp. 1595–1638.
- [55] B. SMITH, P. BJØRSTAD, AND W. GROPP, *Domain decomposition. Parallel multilevel methods for elliptic partial differential equations*, Cambridge Univ. Press, 1996.
- [56] A. TOSELLI AND O. B. WIDLUND, *Domain decomposition methods – algorithms and theory*, Springer Berlin Heidelberg, 2005.
- [57] K. WILLNER, *Kontinuums- und Kontaktmechanik*, Springer, Berlin Heidelberg, 2003.
- [58] B. I. WOHLMUTH, *A mortar finite element method using dual spaces for the Lagrange multiplier*, SIAM J. Numer. Anal., 38 (2000), pp. 989–1012.
- [59] ———, *Discretization methods and iterative solvers based on domain decomposition*, Springer, Berlin, 2001.
- [60] P. WRIGGERS, *Computational contact mechanics*, J. Wiley & Sons Ltd, 2002.
- [61] X. XU AND L. QIN, *Spectral analysis of Dirichlet–Neumann operators and optimized Schwarz methods with Robin transmission conditions*, SIAM J. Numer. Anal., 47 (2010), pp. 4540–4568.

Corinna Hager
Pfaffenwaldring 57
70569 Stuttgart
Germany
E-Mail: hager@ians.uni-stuttgart.de

Patrice Hauret
Mécanique Numérique, Manufacture Française des Pneumatiques Michelin
63040 Clermont-Ferrand, Cedex 9
France
E-Mail: patrice.hauret@fr.michelin.com

Patrick Le Tallec
Département de Mécanique, Ecole Polytechnique
91128 Palaiseau Cedex
France
E-Mail: patrick.letallec@polytechnique.fr

Barbara I. Wohlmuth
M2 - Zentrum Mathematik, Technische Universität München, Boltzmannstraße 3
85748 Garching
Germany
E-Mail: barbara.wohlmuth@ma.tum.de

Erschienenene Preprints ab Nummer 2010/001

Komplette Liste: <http://preprints.ians.uni-stuttgart.de>

- 2010/001 *Kaltenbacher, M., Shevchenko, I., Wohlmuth, B. I.:* Investigation of heat generation by acoustic waves
- 2010/002 *Surulescu, C., Surulescu, N.:* On two approaches to a multiscale model for bacterial chemotaxis
- 2010/003 *Kelkel, J., Surulescu, C.:* A multiscale approach to cell migration in tissue networks
- 2010/004 *Dressel, A., Rohde, C.:* A generalized Riemann problem for two-phase fluids with curvature-driven phase boundaries
- 2010/005 *Feistauer, M., Sändig, A.-M.:* Graded Mesh Refinement and Error Estimates of Higher Order for DGFE-solutions of Elliptic Boundary Value Problems in Polygons
- 2010/006 *Dihlmann, M., Haasdonk, B., Ohlberger, M.:* A Training Set and Multiple Bases Generation Approach for Parametrized Model Reduction Based on Adaptive Grids in Parameter Space
- 2010/007 *Hager, C., Hauret, P., Le Tallec, P., Wohlmuth, B. I.:* Overlapping domain decomposition for multiscale dynamic contact problems